NATIONAL AERONAUTICS AND SPACE ADMINISTRATION

Technical Memorandum 33-477

Part I

Mechanical Interaction of a Driven Roller (Wheel) on Soil Slopes

The Necessary Conditions for an Equilibrium-Velocity Solution

Isak Kloc

JET PROPULSION LABORATORY
CALIFORNIA INSTITUTE OF TECHNOLOGY
PASADENA, CALIFORNIA

June 15, 1971

Prepared Under Contract No. NAS 7-100
National Aeronautics and Space Administration

PREFACE

The investigation documented in this report constitutes part of the lunar roving vehicle (LRV) research conducted by the Advanced Lunar Studies Team at the Jet Propulsion Laboratory. This study was performed to develop and provide a better understanding of mobility concepts on soft sloping terrains as applied to LRVs.

ACKNOWLEDGMENT

The author wishes to express his appreciation to Mrs. Carolyn S. Level for developing and executing the soil-roller interaction computer program.

CONTENTS

I. Summary 1

II. Background — Lunar Mobility 3

III. Solution Approach 4

IV. Soil-Roller Kinematics 5

A. Problem Statement 5

B. Soil-Roller Velocity and Boundary Conditions 5

C. Velocity Fields 7

1. Active zones 7

2. Transition and passive zones 10

V. Soil-Roller Equilibrium 11

A. Limiting Soil Stress Field 11

B. Stresses Along Sliplines 11

1. Stress parameter $\bar{p}$ along straight sliplines 12

2. Stress parameter p along spiral sliplines 13

3. Transition and passive zones 15

C. Limiting Slipline Directions 15

1. Soil-roller interface — maximum stress obliquity 15

2. Free soil surface — singular points (LO) and (NO) 17

3. Summary of absolute admissible bounds for θ'_{LO}, θ'_{LL}, θ_{NN}, and θ_{NO} 17

D. Equilibrium Equations 18

E. Soil Reactions 18

F. Body Forces 22

G. Moments 23

1. Moments due to soil reactions 23

2. Moments due to body forces 23

H. Soil-Roller Interface Stresses 24

VI. Solution of Basic Equations 26

A. Basic Equations 26

B. Specific Energy Dissipation 27

C. Rigid Roller Sinkage 28

D. Mobility Safety Factors 28

E. Applications 29

VII. Conclusions 31

VIII. Recommendations 32

Appendix. Positive Rate of Dilation 33

A. Introduction 33

B. Trailing Zone ($\xi_i \leq \pi/2$) 33

C. Leading Zone ($\xi_i \geq \xi_M$) 34

Nomenclature 36

References 38

Tables

1.0. Soil-wheel input data for SWIP program application 40

1.1. Horizontal test for ξ_M = 99 and s_k = 0.75 (upper bound) 41

1.1a. Horizontal test for ξ_M = 99 and s_k = 0.75 (lower bound) 42

1.2. Horizontal test for ξ_M = 101 and s_k = 0.75 (upper bound) 43

1.2a. Horizontal test for ξ_M = 101 and s_k = 0.75 (lower bound) 44

1.3. Horizontal test for ξ_M = 102 and s_k = 0.75 (upper bound) 45

1.3a. Horizontal test for ξ_M = 102 and s_k = 0.75 (lower bound) 46

1.4. Horizontal test for ξ_M = 104 and s_k = 0.75 (upper bound) 47

1.4a. Horizontal test for ξ_M = 104 and s_k = 0.75 (lower bound) 48

2.1. Wheel performance on slope for ξ_M = 110 and s_k = 0.55 (upper bound) 49

2.1a. Wheel performance on slope for ξ_M = 110 and s_k = 0.55 (lower bound) 50

2.2. Wheel performance on slope for ξ_M = 110 and s_k = 0.65 (upper bound) 51

2.2a. Wheel performance on slope for ξ_M = 110 and s_k = 0.65 (lower bound) 52

2.3. Wheel performance on slope for ξ_M = 105 and s_k = 0.65 (upper bound) 53

2.3a.	Wheel performance on slope for $\xi_M = 105$ and $s_k = 0.65$ (lower bound).	54
2.4.	Wheel performance on slope for $\xi_M = 105$ and $s_k = 0.70$ (upper bound).	55
2.4a.	Wheel performance on slope for $\xi_M = 105$ and $s_k = 0.70$ (lower bound).	56
3.1.	Wheel performance for Apollo LRV for $\xi_M = 105$ and $s_k = 0.85$ (upper bound)	57
3.1a.	Wheel performance for Apollo LRV for $\xi_M = 105$ and $s_k = 0.85$ (lower bound)	58
3.2.	Wheel performance for Apollo LRV for $\xi_M = 105$ and $s_k = 0.90$ (upper bound)	59
3.2a.	Wheel performance for Apollo LRV for $\xi_M = 105$ and $s_k = 0.90$ (lower bound)	60
4.1.	Wheel performance for Lunokhod-1 for $\xi_M = 112$ and $s_k = 0.80$ (upper bound)	61
4.1a.	Wheel performance for Lunokhod-1 for $\xi_M = 112$ and $s_k = 0.80$ (lower bound)	62

Figures

1.	Typical failure pattern for driven rigid wheel on a pack of aluminum rolls	63
2.	Roller motion on sloping soil	63
3.	Driven rigid roller 100% slip ($s_k = 0$, $V_C = 0$) on a pack of aluminum rolls.	64
4.	Soil-roller plastic flow configuration	64
5.	Soil-roller rim-velocity boundary conditions (bifurcation of plastic zones)	65
6.	Limiting stress state	66
7.	Limit position of leading pole ($s_k = 0$).	67
8.	Locus of leading and trailing spiral poles	68
9.	Locus of trailing poles $\bar{I}_1$ for varying ξ_M and s_k	69
10.	Soil-roller interface velocities	70
11.	Soil-roller free body equilibrium	71
12.	Stresses along sliplines (active zones).	72
13.	Limiting slipline directions at leading and trailing zones	73
14.	Roller sinkage	73

ABSTRACT

A general solution is given to the mobility performance problem of a power-driven rigid cylindrical roller climbing a semi-infinite soft soil slope with uniform velocity. The roller axle is subjected to vertical and pull force components. A gravitating, cohesive-frictional soil is considered. Its application to lunar and planetary locomotion is emphasized. The mechanics of soil-roller interaction is described and solved, considering stresses and velocities, as a mixed boundary value problem. Kötter's quasi-static equilibrium equations are connected to a plastic stress configuration satisfying Shield's velocity conditions along the characteristic lines. Solutions of the equilibrium equations yield the driving torque, slip, sinkage, and soil-roller interface stresses. Driving power requirements and thrust efficiency are determined.

A general concept of safety factor against immobilization is introduced. A computer program for the soil-wheel interaction performance (SWIP) was developed and limited applications of this theory to rigid wheel tests on horizontal terrains indicate very reasonable agreement. The method is also applied to the Apollo and Lunokhod-1 lunar roving vehicle wheels. Part I, as published, presents the basic and necessary conditions satisfying the limiting equilibrium and velocity equations. Part II, to be published separately, will provide the concepts of sufficiency asserting the completeness of a given solution and the computer program.

I. SUMMARY

The use of wheeled roving vehicles in future lunar and planetary explorations will require consideration of two technical problems: (1) the expense and difficulty of performing lunar soil surface tests to derive experimental coefficients which define soil-wheel performance, and (2) the lack of the basic fundamentals and experimental background to predict either on a theoretical or empirical basis the mechanics of lightly loaded rolling devices on soft horizontal or sloping terrains.

This study presents a method of solution to the two-dimensional problem of a power-driven long and rigid cylindrical roller moving up a generally sloping soil surface with uniform velocity. The roller axle is subjected to the combined action of a driving torque, a vertical load, and a pull force parallel to the terrain slope. All practical ranges of soil mechanical properties are considered for either lunar or earth-based soils, including soil friction, cohesion, and gravitational effects.

In principle, the soil-roller interaction study, as would one for a wheel, points to two basic aspects. One corresponds to the operational conditions of a roller whose mobility is always guaranteed, particularly for low contact pressures and reduced sinkage. In this case, the design objective for mobility is mainly concerned with an efficiency optimization problem. The other aspect relates to the particular limiting state in which immobilization occurs when the soil thrust capacity has been reached due to the combined action of soil weight and applied roller loads. In this case, a margin of safety against immobilization, rather than efficiency, constitutes the constraint design factor.

This study indicates that the soil-roller solution represents, to a reasonable degree, a satisfactory basis for estimating the performance of rigid wheels under similar driving conditions. This is particularly true when the soil-wheel contact pressure level is low and the soil failure pattern develops mainly in the fore-aft direction rather than in a lateral mode. This characteristic is expected to occur predominantly for vehicle locomotion on the lunar surface, as evidenced from a photograph of wheel tracks left by the Soviet Lunokhod-1 (Fig. 3 of Ref. 1). Obviously, the soil-roller solution does not entail the solution of the wheel problem "per se" since the wheel is a finite representation of a roller. However, the roller approach is a necessary step which will permit the elucidation and disclosure of some important aspects applicable to the soil-wheel interaction problem. In particular, these aspects refer to:

(1) The mechanics of slope climbing under various types of soil materials, and loading conditions of self-propulsion or pull forces.

(2) The role of slip as a kinematic factor affecting the wheel mechanical performance and locomotion efficiency.

(3) The basic principles concerning how soil thrust is generated and motion sustained as a continuous mechanical process.

If all these factors can be derived for a roller, the conclusions may be directly extended to wheels or otherwise approximated by appropriate modeling techniques. In this context, the roller analogy is more akin to the soil-wheel interaction problem than to using flat plate tests since in the former the mechanics of rolling is reflected at all slip levels as it actually occurs for a wheel.

The solution approach consists of selecting a soil-roller failure configuration in accordance with experimental evidence on horizontal terrains. This failure pattern is generalized to sloping surfaces. A compatible velocity field is defined that satisfies all velocity requirements. Then the governing stress equilibrium equations are solved along the velocity characteristics (sliplines) in connection with the remnant stress boundary conditions. The method of solution is implemented by a computer program which evaluates the basic soil-roller performance parameters as given by the torque, slip, sinkage, and interface stress. The concept of specific rolling energy dissipation is generalized to slopes, and the driving power requirement is determined under quite general conditions of load combinations and terrain slope. A general mobility safety factor definition is introduced and calculated for a soil-roller system. This definition applies also to wheels and covers the whole spectrum of rolling with slip up to and including immobilization.

The current status of soil-wheel interaction as a design tool for planetary vehicle exploration is rather unsuitable due to the lack of pertinent quantitative tests and design information that is normally available for on-earth vehicles. New theoretical concepts are required to predict vehicle performance requirements, especially with regard to safety and power needs when traversing lunar soft terrain and steep slopes. In this context, a pertinent survey of the state-of-the-art on off-the-road vehicle design was made and has led to the following conclusions:

(1) The present status of the theory of soil-wheel interaction applies exclusively to horizontal or gently sloping terrains. Wheel design parameters and vehicle performance are definitely connected with the soil mechanical properties and the nature of lunar topography. Consequently, lunar vehicle slope climbing and traversing capabilities are bound to constitute a controlling design factor in terms of mobility safety and locomotion energy requirements.

(2) Current on-earth vehicle mobility experience refers mainly to high soil-wheel contact pressures and dictates that heavily loaded vehicles cannot practically negotiate soft slopes higher than approximately 25 deg. Instead, lunar roving vehicles will operate under comparatively low soil contact pressures (approximately 6.9×10^3 N/m^2, 1 psi) and may require climbing slopes steeper than 25 deg. It is not known, using present mobility concepts, if a vehicle can safely operate under conditions of low pressure and reduced gravity on lunar crater slopes near limiting equilibrium where excessive sinkage and loss of soil stability support may be imminent.

(3) Present approaches to derive basic performance parameters of soil-wheel interaction resort to separate sinkage and horizontal shear deformation plate tests performed on potential terrains of vehicle operation. On this basis, a comprehensive semi-empirical theory for off-the-road mobility was developed by Bekker (Ref. 2). The inherent uncertainty of this approach relates to the fact that the character and distribution of soil-wheel interface stresses derived from flat plate tests cannot be reliably translated into a roll on a sloping surface.

(4) There is insufficient evidence to what extent the combined or independent action of friction, cohesion, and gravitation influences soil-rolling thrust performance. Experiments and analysis by Costes, et al. (Ref. 3), indicate that the lunar soil surface mechanical properties relate to a frictional-cohesive behavior.

The use of wheeled roving vehicles in future lunar and planetary explorations will require consideration of two technical problems: (1) the expense and difficulty of performing lunar soil surface tests to derive experimental coefficients which define soil-wheel performance, and (2) the lack of the basic fundamentals and experimental background to predict either on a theoretical or empirical basis the mechanics of lightly loaded rolling devices on soft horizontal or sloping terrains.

The broad objective of this study is to establish a basis for a consistent and unified approach to the soil-wheel interaction problem to estimate the performance of lunar roving vehicles traversing generally sloping soft surfaces. To this end, basic soil mechanical concepts, applicable to the lunar environment, are incorporated in analytical expressions to derive torque, energy, interface stresses, operating slip, and sinkage values as may be applicable to lunar mobility requirements.

These analytical expressions can then be compared with the results of controlled experiments either on earth (Ref. 4) or on the moon (Refs. 1 and 5), using, for example, the Soviet Lunokhod-1 lunar roving vehicle mobility system.

III. SOLUTION APPROACH

The solution approach to the soil-roller interaction problem is based on the application of the theory of plasticity to soil mechanical problems. The governing differential equations of equilibrium (Ref. 6) and velocity compatibility along the sliplines (Ref. 7) are solved as a mixed boundary value problem connecting stresses and velocities. This problem is concerned with a quasi-static, steady-state, two-dimensional plastic flow with soil assumed to behave as a rigid perfectly plastic material. The soil is granular in character with strength properties defined by the Mohr-Coulomb theory of failure, which depends on the soil angle of internal friction ϕ and cohesion c. The soil strength properties are isotropic and homogeneous throughout the plastic domain up to and including the soil-roller interface.[1] Soil self-weight is specifically considered.

The problem of rolling contact between a rigid towed cylinder on a plastic deforming horizontal half space was investigated theoretically by Marshall (Ref. 8) for a Tresca material, applying a perturbation method of solution. Dagan and Tulin (Ref. 9) studied the steady flow of a rigid plastic clay beneath a driven cylindrical roller on a horizontal half space, using the method of sliplines. Experimentally, Boucherie (Ref. 10) obtained photographic flow patterns produced by towed and driven rigid wheels on a supporting bed of packed metal rolls (Fig. 1). Wong and Reece (Ref. 11) performed a series of tests on level sand surfaces, acted upon by rigid rollers and wheels for various loads, slip, and skid combinations. Using photographic techniques, they presented and commented in detail on the character and patterns associated with soil failure due to rolling loads.

To date, all known complete solutions of uncontained rigid perfectly plastic flow problems consist of selecting an appropriate slipline stress field and then verifying whether or not the boundary and the field velocities are also satisfied throughout. If not, a new stress slipline pattern has to be tried (Ref. 12). Obviously, this procedure is rather limited regarding the boundary velocity functions which can be considered other than simple uniform ones.

Here, instead, an inverse procedure has been adopted. First, a compatible soil-roller velocity field of characteristic lines is generated which satisfies the roller boundary velocity conditions, then to this field is adjoined a stress domain that satisfies all the remnant boundary conditions. That this is possible is based on the fact that velocities and stress characteristic lines are coincident (Ref. 7) if the former derive from the theory of plastic potential (Ref. 13). To the author's knowledge, this is the first time a problem of mixed boundary values in the theory of plasticity is solved for both stresses and velocities by satisfying first the velocities rather than the stress conditions.

This method considerably facilitates the search for a complete solution. Also, this approach may be found useful in the study of metal forming and tooling operations and other soil mechanical problems which are accompanied by variable interface friction and complex moving plastic boundaries. There exist infinite stress field patterns which can satisfy equilibrium. In addition, completeness of a solution is defined only when (1) the kinematic compatibility conditions are also satisfied, (2) the dilation rate is positive throughout the plastic domain, and (3) at no point of the rigid domain do the stresses exceed yield. It is reasonable to expect that if the problem is well posed and a solution is found, the results obtained will coincide with a possible matching experiment.

The sequence of the study reported here is as follows: In Section IV, a velocity flow field pattern is selected and validated in accordance with experimental evidence of rolling tests on horizontal soil surfaces. These results are generalized to slopes. The kinematics of slip and velocity boundary conditions are analyzed as they relate to the soil-roller interface. These velocities are then propagated throughout the plastic domain. In Section V, a summary of the plane strain theory for rigid plastic solids is given. The slipline fields defined in Section IV are used to determine soil limiting stresses. Soil reactions and moments are calculated by considering soil weight. The quasi-static equilibrium equations are defined and the soil-roller interface stresses are evaluated.

In Section VI, the results of Section V are synthesized into a system of equations whose solution is the basis for the complete solution of the soil-roller problem. The total torque, energy, and roller sinkage equations are formulated. A general definition of the factor of safety against immobilization is introduced. The computer program is applied to soil-rigid wheel test results which are numerically compared to illustrate the use of the method and to verify its prediction capabilities.

Finally, the theory is applied to the Apollo lunar roving vehicle (LRV) and the Soviet Lunokhod-1 wheels operating on the lunar surface to estimate their mobility performance.

[1] If the soil-roller interface constitutes a material strength discontinuity, particularly if the interface friction and/or adhesion properties are different than the corresponding soil-properties, then the local orientation of the sliplines is dictated by the relative soil-roller interface mechanical properties. There is no theoretical difficulty in accounting for this fact in the analysis in terms of either one or both factors, adhesion or friction, as long as the strength discontinuity is represented by a Mohr-Coulomb relationship.

A. Problem Statement

The roller moves with uniform velocity V_C parallel to the original undisturbed soil surface (Fig. 2). The surface slope angle α is measured positive in a counterclockwise sense from the positive x-axis. The rotational velocity ω (rad/s) is positive clockwise. An orthogonal Cartesian coordinate reference system (x, z) is adopted with origin at the roller axle center C. The positive z-axis is oriented down, parallel to the local gravity vector. As a steady-state process, the kinematics of the roller is described by the position of its center of instantaneous rotation $I(\bar{x}, \bar{z})$, located along a line passing through C and normal to the original surface.

$$\bar{x} = -Rs_k \sin \alpha \qquad (1)$$

$$\bar{z} = Rs_k \cos \alpha \qquad (2)$$

The translational velocity of the roller center C is

$$V_C = \omega R s_k \qquad (3)$$

where s_k = slip factor and Rs_k defines the position of point I with respect to C. In terms of displacement, s_k is an index number which, for a full wheel turn (2π rad), indicates the axle displacement as a fraction of the developed wheel perimeter length. For a driven roller, $0 \leq s_k \leq 1.0$. Limiting conditions are:

(1) Pure rotation, $s_k = 0$ and $V_C = 0$.

(2) Pure translation, $s_k = 1.0$ and $V_C = \omega R$.

The roller kinematics may also be evaluated, based on the knowledge of the rotational velocity ω and the translation velocity V_C, by following the definition of slip,

$$s = \frac{V - V_C}{V} 100 \qquad (4)$$

where $V = \omega R$ = roller peripheral velocity. It is verified from Eq. (4) that, for driven rollers $s > 0$, the roller slips. For towed rollers, $s < 0$ and it is said that the roller skids. Based on Eq. (4), $s = 100\%$ slip for pure rotation and $s = 0\%$ slip for pure translation.

This type of motion description was used by Poletayev (Ref. 14) and by Onafeko and Reece (Ref. 15) in the study of rigid wheels on level terrain ($\alpha = 0$). Here, this motion concept is generalized to slopes where $\alpha \geq 0$. The problem is now posed as follows: Given a semifinite soil surface slope α, possessing the unit volume weight γ and strength properties defined by the cohesion c and the friction angle ϕ, loaded by an infinitely long rigid roller of radius R, carrying an axial weight W and pulling a load P* per unit roller width b parallel to the original slope, determine the

(1) Operational slip factor s_k which defines the limiting equilibrium condition that permits the roller center C to move with uniform velocity V_C (Eq. 3).

(2) Driving torque M capable of sustaining the velocity V_C.

(3) Plastic failure pattern and state of stress that satisfy the kinematic, stress, and geometric boundary conditions.

(4) Roller sinkage z measured normal to the original surface.

(5) Specific rolling energy required per unit surface normal load and unit distance of travel.

(6) Safety factor with respect to roller immobilization, which occurs when the slip factor $s_k = 0$, for a given slope α.

This study does not apply to the initial stages of rolling motion, and to conditions following roller immobilization. In the former case, inertial forces predominate and in the latter case, continued sinkage takes place. Both cases are associated with unsteady conditions. This study considers the problem of soil-roller interaction only under uniform operating velocity conditions up to and including immobilization.

B. Soil-Roller Velocity and Boundary Conditions

As mentioned, Wong and Reece (Ref. 11) and Boucherie (Ref. 10) have revealed the general nature of the soil failure pattern associated with rigid driven rollers and wheels moving on level soft surfaces at various slip and loading conditions. This photographic evidence indicates (Fig. 1):

(1) Typical leading and trailing plastic regions are formed, each, respectively, moving fore and aft of the advancing roller.

(2) Both flow regions tend to meet at a common point M on the roller rim surface.

(3) Soil sinkage increases with increasing loads and slip.

(4) The roller leaves no rut due to local sinkage. This means, after the passage of the roller, the soil surface fully recovers due to backward soil transport produced by the advancing roller.

(5) The relative sizes and pattern of the soil leading and trailing plastic regions depend on the kinematics of soil-roller interaction. At 100% slip, the leading plastic region disappears, leaving only the trailing plastic zone (Fig. 3).

In the following, the theory of sliplines is applied to soils for rolling with plastic flow. The leading and trailing plastic regions are identified by M(ML)EFL and M(MN)ABN, respectively (Fig. 4). The corresponding lines M(ML)EF and M(MN) AB are considered to be first and second characteristic velocity discontinuity lines, respectively, separating the lower stationary rigid region from the plastic deforming one. These two characteristic lines meet the soil-roller interface point M at an angle $(\pi/2) - \phi$. It is assumed that the soil point M is at rest relative to the roller and that it pertains to the rigid stationary domain.

The coordinates of a point i on the roller rim are given by (Fig. 5)

$$x_i = R \cos (\alpha + \xi_i) \tag{5}$$

$$z_i = R \sin (\alpha + \xi_i) \tag{6}$$

The corresponding absolute velocity components parallel to the coordinate axes x, z are, respectively,

$$u_{x,i} = \omega(z_i - \bar{z}) \tag{7}$$

$$u_{z,i} = \omega(\bar{x} - x_i) \tag{8}$$

The resultant velocity is

$$V_i = \sqrt{u_{x,i}^2 + u_{z,i}^2} \tag{9}$$

The angular orientation of V_i is

$$\bar{\rho}_i = \tan^{-1}\left(\frac{u_{z,i}}{u_{x,i}}\right) \tag{10}$$

Next, the rim boundary velocities will be related to the soil flow in terms of the slipline velocity components along the soil-roller interface.

When the soil stress-strain law is derived, applying the concept of plastic potential, Drucker and Prager (Ref. 13) show that the relative particle velocity along a velocity discontinuity line is oriented at an angle ϕ to the line. This concept will be used here to construct the plastic configuration.

At the bifurcation point M, the corresponding trailing soil particle is subjected to a velocity <u>component</u> V_M' tangent at M to the discontinuity slipline M(MN) and equal in magnitude and direction to the roller rim velocity V_M. From Eqs. (9) and (10), for rim point i = M (Fig. 5),

$$V_M = \left(u_{x,M}^2 + u_{z,M}^2\right)^{1/2} = -V_M' \tag{11}$$

$$\bar{\rho}_M = \tan^{-1}\left(\frac{u_{z,M}}{u_{x,M}}\right) = \theta_M' \tag{12}$$

The negative sign in Eq. (11) is consistent with the sign convention that a positive velocity component along the *first slipline*, when rotated through an angle $(\pi/2) + \phi$, produces a positive velocity component along the second slipline (Ref. 7) (Fig. 6b). It is of interest to note that Wong (Ref. 16) postulated that the trajectory of the trailing soil particle at the bifurcation point M coincides with the direction θ_M' of the trailing slipline at M. Here, the adoption of a velocity <u>component</u> V_M', instead of a resultant velocity as referred to by Wong, is due to the fact that the latter must be oriented at an angle ϕ to the discontinuity line to comply with the requirements of the theory of plastic potential. Consequently, the trailing soil particle velocity resultant at M is

$$V_M^T = \frac{V_M'}{\cos \phi} \tag{13}$$

Continuity conditions at the soil-roller interface dictate that the radial velocity component of the leading soil particle at M must be equal to the radial velocity of the roller rim point M. Then, the leading soil particle radial velocity component (Fig. 5) is

$$V_{M,R} = V_M \cos (\alpha + \xi_M - \bar{\rho}_M) = V_M \cos \Delta_M \tag{14}$$

where

$$\Delta_M = \alpha + \xi_M - \bar{\rho}_M \tag{15}$$

and the corresponding velocity resultant is

$$V_M^L = V_{M,R} \sec \left[\theta_M - (\alpha + \xi_M) + \phi\right] \tag{16}$$

The velocity component along the first slipline at M is

$$V_M^* = V_M^L \cos \phi \tag{17}$$

The angular orientation of the first slipline M(ML) at M is

$$\theta_M = \theta_M' + \frac{\pi}{2} - \phi \tag{18}$$

Equations (11) to (18) represent the soil velocity boundary conditions at the plastic bifurcation point M.

The validity of the theory of plastic potential to define the soil strain rates and the assumption regarding the boundary velocity condition (Eqs. 11 and 12) have to be properly justified on an experimental basis. The former was adopted because of its rather simple application, and the latter appears to represent a reasonable fact.

C. Velocity Fields

The plastic failure pattern configuration is further postulated as follows (Fig. 4): The trailing region is divided into three plastic zones, M(MN)N, N(MN)A, and NAB, identified as the active, transition, and passive zones, respectively. The same applies to the leading plastic region for zones M(ML)L, L(ML)E, and LEF, respectively.

1. Active zones. As mentioned previously, the sliplines M(MN)AB and M(ML)EF separate the rigid stationary boundary from the plastic deforming one. Since a boundary at rest must have a zero local normal velocity component, the velocity must be inclined at an angle ϕ to the discontinuity line. Along M(ML)EF, the first slipline discontinuity, $V' = 0$, and along M(MN)AB, the second slipline discontinuity, $V^* = 0$. Since both these discontinuity lines start at rim point M, the resultant soil particle velocity at point M (trailing zone) is (Fig. 5)

$$V_M^T = \frac{V_M}{\cos\phi} = \omega\frac{a_M}{\cos\phi} = \omega r_M \tag{19}$$

where

$$r_M = \frac{a_M}{\cos\phi} \tag{20}$$

and

$$a_M = \left[(x_M - \overline{x})^2 + (z_M - \overline{z})^2\right]^{1/2} \tag{21}$$

From Eq. (20), when $\phi = 0$, $r_M = a_M$ and $\overline{I}_1$ coincides with I and the trailing spiral slipline transforms into circles centered at I.

The resultant velocity of the leading soil particle at M, based on Eqs. (14) and (15), is

$$V_M^L = V_M \cos\Delta_M = \omega a_M \cot\Delta_M = \omega\overline{r}_M \tag{22}$$

where, as shown in Fig. 5,

$$\overline{r}_M = a_M \cot\Delta_M \tag{23}$$

Expressions (19) and (22) indicate the transformation of the rim velocity V_M into the corresponding soil particle velocity at the roller interface point M. Particularly when

$$s_k = 0, \qquad \Delta_M = \alpha + \xi_M - \overline{\rho}_M = \frac{\pi}{2}$$

then, from Eq. (23), $\overline{r}_M = 0$, indicating that there is no leading failure zone, which is verified from tests (Fig. 3) and is schematically shown in Fig. 7. These velocity criteria produce, in general, a tangential soil velocity "jump" at M, which may be obtained by projecting the velocities, Eqs. (19) and (22), along the roller tangential direction at M.

Next, we discuss the nature of the remaining soil-roller interface velocity conditions and the plastic domain. The governing velocity equations that refer to the first and second characteristic lines, as determined by Shield (Ref. 7), are

$$dV^* - (V^* \tan\phi + V' \sec\phi)\, d\theta = 0 \tag{24}$$

$$dV' + (V' \tan\phi + V^* \sec\phi)\, d\theta' = 0 \tag{25}$$

Applying Eq. (25) to the trailing zone discontinuity line, with $V^* = 0$, yields

$$dV' + V' \tan\phi\, d\theta' = 0$$

$$\int_{V'_M}^{V'} \frac{dV'}{V'} = -\tan\phi \int_{\theta'_M}^{\theta'} d\theta'$$

$$V' = V'_M \exp\left[(\theta'_M - \theta')\tan\phi\right] \tag{26}$$

which, with Eq. (19), reduces to

$$V' = \omega\cos\phi\, r_M \exp\left[(\theta'_M - \theta')\tan\phi\right] \tag{27}$$

Equations (26) and (27) indicate that the velocities along the discontinuity line M(MN) vary exponentially and that they relate to a logarithmic spiral function

$$r = r_M \exp\left[\tan\phi\,(\theta_M - \theta)\right] \tag{28}$$

The coordinate positions of the trailing spiral pole $\overline{I}_1$ $(\overline{x}_1, \overline{z}_1)$ are (Fig. 5)

$$\overline{x}_1 = x_M - r_M \cos\theta_M \tag{29}$$

$$\overline{z}_1 = z_M - r_M \sin\theta_M \tag{30}$$

with (x_M, z_M) given by Eqs. (5) and (6) for $i = M$ and θ_M given by Eq. (18). Also, for the leading zone along the spiral velocity discontinuity line, M(ML) is from Eq. (24),

$$V^* = V^*_M \exp\left[(\theta - \theta_M)\tan\phi\right] \tag{31}$$

From Eqs. (17) and (22), Eq. (31) reduces to

$$V^* = \omega \cos \phi \; \bar{r}_M \exp \left[(\theta - \theta_M) \tan \phi\right] \qquad (32)$$

which applies along

$$\bar{r} = \bar{r}_M \exp \left[(\theta - \theta_M) \tan \phi\right] \qquad (33)$$

The coordinate positions of the leading spiral pole $\bar{I}_2(\bar{x}_2, \bar{z}_2)$ are

$$\bar{x}_2 = x_M - \bar{r}_M \cos \theta'_M \qquad (34)$$

$$\bar{z}_2 = z_M - \bar{r}_M \sin \theta'_M \qquad (35)$$

Equations (26) to (35) yield the geometry of the velocity distribution along the trailing and leading discontinuity lines. They indicate also that the velocities along these discontinuities correspond to rotations about the poles I_1 and I_2, respectively.

The geometrical character of the poles $\bar{I}_1$ and $\bar{I}_2$, in terms of the relative variations of s_k and ξ_M, may be graphically described with reference to Fig. 8 as follows:

(1) Given a point M on the roller rim with $\xi_M > \pi/2$ and $0 \leq s_k \leq 1.0$, the locus of all corresponding trailing spiral poles $\bar{I}_1$ (Eqs. 29 and 30) defines a straight segment T_0T_1 oriented at an angle $(\pi/2) - \phi$ to the x-axis. The extreme points T_0 and T_1 of this segment correspond to $s_k = 0$ and $s_k = 1$, respectively. Any intermediate point between T_0 and T_1 pertains to an s_k such as $0 < s_k < 1$. For $\xi_M > \pi/2$, the poles $\bar{I}_1$ and $\bar{I}_2$ are always located inside the roller periphery. The quadrant position of $\bar{I}_1$ is given by

$$\bar{\beta}_T = \cos^{-1}\left(\frac{\bar{x}_1}{\sqrt{\bar{x}_1^2 + \bar{z}_1^2}}\right) \qquad (36)$$

A similar expression applies to $\bar{I}_2$ for $\bar{\beta}_L$ (Fig. 5). In general, it may be verified that, for $s_k \lesseqgtr R \sin \xi_M$,

$$\bar{\beta}_T \lesseqgtr \frac{\pi}{2} \qquad (37)$$

(2) On the same basis as in (1) above, Fig. 8 indicates that the locus of all corresponding leading spiral poles $\bar{I}_2$ (Eqs. 33 and 34) defines a curve MM_1 where M and M_1 relate to $s_k = 0$ and $s_k = 1.0$, respectively. In general, points M and M_1 are always located on the roller rim. Any intermediate point between M and M_1 corresponds to s_k such as $0 < s_k < 1.0$. Point M_1 at $\xi_{M1} = 3\pi/4$ remains fixed under all conditions of rolling without slip ($s_k = 1.0$).

(3) There is a conformal geometric relationship of ξ_M and the T_0T_1 lines. When point M shifts along the roller periphery, the segment T_0T_1 moves parallel to itself. Thus, for increasing (or decreasing) ξ_M, the segment T_0T_1 moves closer to (or further away from) the roller center C.

The locus of poles $\bar{I}_1$ for s_k = constant describes a series of circles with radius $R_k = R \tan \phi$ (Fig. 9). The center of these circles are located along a line $C_0C_{1.0}$ oriented at an angle $(\pi/2) - \phi$ to the x-axis. Along this line, the center marked $C_{1.0}$ corresponds to the circle with $s_k = 1.0$ and the center $C_0 = C$ to the circle for which $s_k = 0$. The center of a generic circle corresponding to any $0 < s_k < 1.0$ will be located proportionally between points $C_0C_{1.0}$ as shown in Fig. 9.

(4) Given a fixed slip-factor s_k, an increase (or reduction) of ξ_M correspondingly produces an increase (or reduction) of both spiral radial vectors r_M and $\bar{r}_M$.

(5) When ξ_M is fixed, an increase of s_k produces a reduction of r_M and $\bar{r}_M$.

The geometrical implication of the above statements relates to the basic fact that the limiting soil stress and spiral orientations (characteristics) are controlled by the relative position of poles $\bar{I}_1$ and $\bar{I}_2$, as defined by the parametric set ξ_M and s_k. In Section V, it will be shown that once the equilibrium equations and stress boundary conditions are satisfied, the final magnitude of the soil stress will also relate directly to ξ_M and s_k in terms of r_M (Eq. 20) and $\bar{r}_M$ (Eq. 23).

Next, consider the active plastic domains between the soil-roller interface and the discontinuity lines M(MN) and M(ML), which are fully described by a set of radial and logarithmic spiral characteristics with poles $\bar{I}_1$ and $\bar{I}_2$, respectively. First, it will be shown that the soil-roller velocity boundary conditions are also satisfied.

As mentioned at the beginning of this section, $V^* = 0$ along the trailing velocity discontinuity slipline spiral M(MN). The corresponding intersecting first sliplines are radial lines through the spiral pole $\bar{I}_1$; based on Eq. (25), $V^* = 0$ throughout the active trailing zone. This implies that at a point i on the soil-roller rim interface (Fig. 10), the resultant soil particle velocity V_i^T must be normal to the radial sliplines. Then, the velocity component along the spiral second slipline through point i is

$$V'_i = -\frac{V_i}{\cos \beta_i} \cos \phi \qquad (38)$$

and

$$V^*_i = 0 \qquad (39)$$

$$\beta_i = \bar{\rho}_i - \theta_i' + \phi = \bar{\rho}_i - \theta_i + \frac{\pi}{2} \tag{40}$$

with V_i obtained from Eq. (9) and $\bar{\rho}_i$ from Eq. (10) and

$$\theta_i = \tan^{-1}\left(\frac{z_i - \bar{z}_1}{x_i - \bar{x}_1}\right) \tag{41}$$

The velocity of any soil particle (ij) located at a point j along a generic spiral slipline passing through rim point i within the trailing plastic domain (Fig. 10) is

$$V_{ij}' = V_i' \exp\left[(\theta_i - \theta_{ij}) \tan\phi\right] \tag{42}$$

and

$$V_{ij}^{*} = 0 \tag{43}$$

Following the same continuity criteria set as for the leading soil particle at the bifurcation point M (Eq. 14), the radial velocity component of the soil particle at any point i along the leading soil-roller interface (ML), Fig. 10, is

$$V_{i,R} = V_i \cos(\alpha + \xi_i - \bar{\rho}_i) \tag{44}$$

where

$$V_i^{*} = \frac{V_{i,R} \cos\phi}{\cos\left[\theta_i - (\alpha + \xi_i) + \phi\right]} \tag{45}$$

Using Eq. (44) and $\theta_i + \phi = \theta' + \pi/2$, Eq. (45) reduces to

$$V_i^{*} = V_i \frac{\cos(\alpha + \xi_i - \bar{\rho}_i)}{\sin(\alpha + \xi_i - \theta_i')} \cos\phi \tag{46}$$

also,

$$V_i' = 0 \tag{47}$$

For a soil particle (ij) located at point j along a spiral slipline passing through rim point i,

$$V_{ij}^{*} = V_i^{*} \exp\left[\tan\phi\,(\theta_{ij} - \theta_i)\right] \tag{48}$$

and

$$V_{ij}' = 0 \tag{49}$$

The active zone velocity expressions (42), (43), (48), and (49) extend up to and including the points along the radial lines N(MN) and L(ML). Thus far, the characteristic lines and velocities pertaining to the active leading and trailing zones have been completely defined. It has also been established that the velocity of each point on the roller rim can be transformed into an equivalent admissible velocity along the corresponding sliplines that intersect the point. In particular, the velocity orientation of any point on the soil-roller rim interface, with respect to its center of instantaneous rotation I, may also be defined in terms of the spiral pole positions $\bar{I}_1(\bar{x}_1, \bar{z}_1)$ and $\bar{I}_2(\bar{x}_2, \bar{z}_2)$ for points along the arcs MN and ML, respectively.

The locations of poles $\bar{I}_1$ and $\bar{I}_2$ are functions of the velocity boundary conditions, described by s_k and ξ_M. Instead the location of rim points N and L can only be obtained in connection with the solution of the stress equilibrium equations. These equations allow the determination of the extent and configuration of the plastic domain by specifying a final set of slipline directions consisting of (Fig. 4)

$$\left\{\theta_{LO}', \theta_{LL}', \theta_M', \theta_{NN}, \theta_{NO}\right\}$$

which will be calculated in Section VI-A.

The velocity field determined thus far satisfies the soil-roller velocity boundary conditions and the velocity field equations (Eqs. 24 and 25). Their detailed numerical evaluation is not a prerequisite for the solution of the limiting stress equations, but their existence is important to the correct statement of a "complete solution" within the context of the theory of plasticity (Ref. 12). Furthermore, the existence of an admissible velocity field must also satisfy the postulate of positive rate of dilation (Appendix).

Points N and L are singular points on which the velocities are multivalued. At these points, the soil-roller rim interface separates itself from the trailing and leading traction-free soil surfaces.

Rim points (NN) and (LL) correspond to sliplines N(MN) and L(ML), respectively, and as such both pertain to the soil-roller interface. Points (NO) and (LO) correspond to the characteristic lines NA and LE separating the transition from the passive zones and belong to the traction-free trailing and leading soil surfaces, respectively.

The geometry of the characteristic lines M(MN) and L(ML) are determined by

$$r_N = \frac{x_{MN} - x_N}{\cos\theta_{NN}} \tag{50}$$

and

$$r_L = \frac{x_{ML} - x_L}{\cos\theta_{LO}'} \tag{51}$$

where

$$x_{MN} = x_N + r_M \exp\left[(\theta_M - \theta_{NN}) \tan\phi\right] \cos\theta_{NN} \tag{52}$$

$$x_{ML} = x_L + \bar{r}_M \exp\left[(\theta'_{LL} - \theta'_M)\tan\phi\right]\cos\theta'_{LL} \tag{53}$$

and

$$\theta_{NN} = \tan^{-1}\left(\frac{z_N - \bar{z}_1}{x_N - \bar{x}_1}\right) \tag{54}$$

and

$$\theta'_{LL} = \tan^{-1}\left(\frac{z_L - \bar{z}_2}{x_L - \bar{x}_2}\right) \tag{55}$$

with coordinates x, z obtained from Eqs. (5) and (6) for i = N and i = L.

2. Transition and passive zones. The characteristics of the transition and passive zones (*Fig. 4*) are calculated after the soil-roller equilibrium conditions corresponding to the active zones are satisfied. This will be referred to again in Section V-B-3 and in Part II.

A. Limiting Soil Stress Field

An admissible velocity characteristic field has been defined that satisfies both the velocity boundary conditions and the governing differential equations for the velocities. When the velocities are derived from the yield stress condition according to the concept of plastic potential, the stress characteristics coincide with the characteristics of the velocity (Ref. 7). The problem now is to associate an admissible stress field that satisfies the equilibrium conditions along the velocity characteristics.

The limiting state of stress at a point occurs when the Mohr circle of stress becomes tangent to the soil strength envelope line defined by the Coulomb formula $\tau = c + \sigma \cot \phi$, where c is the cohesion and ϕ the soil angle of internal friction. In terms of the point stresses σ_x, σ_z, and τ_{xz}, considering compression stress as positive, the Coulomb yield criterion for soils is (Ref. 17) (Fig. 6a)

$$\left[\frac{1}{4}(\sigma_x - \sigma_z)^2 + \tau_{xz}^2\right]^{1/2} - \frac{1}{2}(\sigma_x + \sigma_z) \sin \phi = c \cos \phi \tag{56}$$

Neglecting inertia forces, the stress equilibrium equations in Cartesian coordinates x, z satisfy the condition

$$\frac{\partial \sigma_x}{\partial x} + \frac{\partial \tau_{xz}}{\partial z} = 0 \tag{57}$$

$$\frac{\partial \sigma_z}{\partial z} + \frac{\partial \tau_{xz}}{\partial x} = \gamma \tag{58}$$

Equations (56 - 58) represent a statically determined problem and constitute a hyperbolic system having two families of characteristics as sliplines. Any point in the physical plane is crossed by a set of two sliplines, each inclined at an angle $\mu = \pi/4 - \phi/2$ to the directions of the major principal stress σ_1 (Fig. 6). The first slipline is conventionally identified by a counterclockwise rotation μ from the σ_1 principal stress direction. The angular direction of the first and second sliplines are defined by θ and θ' measured positive in a counterclockwise sense from the x and σ axis in the physical and stress planes, respectively. The yield condition (Eq. 56) is satisfied if the state of stress is expressed by

$$\sigma_x = p\left[1 + \sin \phi \sin (2\theta + \phi)\right] - c \cot \phi \tag{59}$$

$$\sigma_z = p\left[1 - \sin \phi \sin (2\theta + \phi)\right] - c \cot \phi \tag{60}$$

$$\tau_{xz} = p \sin \phi \cos (2\theta + \phi) \tag{61}$$

where p is the reduced mean stress parameter defined by

$$p = \frac{\sigma_1 - \sigma_2}{2 \sin \phi} = \frac{1}{2}(\sigma_x + \sigma_z) + c \cot \phi \geq 0 \tag{62}$$

To completely define a limiting state of stress at a point (x, z), it is sufficient to know the stress parameters p and θ. Substituting Eqs. (59 - 61) in Eqs. (57) and (58) and adopting s and s', first and second sliplines, respectively, as a new set of curvilinear coordinates, the partial differential equations of limiting equilibrium are obtained along the characteristics (Refs. 6 and 19):

$$\frac{\partial p}{\partial s} + 2p \tan \phi \frac{\partial \theta}{\partial s} = \gamma \sin (\theta + \phi) \tag{63}$$

$$\frac{\partial p}{\partial s'} - 2p \tan \phi \frac{\partial \theta}{\partial s'} = \gamma \sin (\theta - \phi) \tag{64}$$

Although during plastic deformation the soil density decreases (Appendix), it is assumed in Eqs. (63) and (64) that γ remains constant.

B. Stresses Along Sliplines

Using the Mohr limiting stress circle, the normal stress σ and shear stress τ at any point along a slipline may be expressed by

$$\sigma = p\left[1 + \sin \phi \sin (2\theta - 2\Omega + \phi)\right] - c \cot \phi \tag{65}$$

$$\tau = p \sin \phi \cos (2\theta - 2\Omega + \phi) \tag{66}$$

where Ω is the direction of the slipline normal through the point under consideration. In particular, along a first slipline

$$\Omega = \theta' - \phi \tag{67}$$

and along a second slipline

$$\Omega = \theta + \phi \tag{68}$$

Substituting Eq. (67) or (68) in Eqs. (65) and (66), the general state of stress along both families of characteristics are defined by

$$\sigma = p \cos^2 \phi - c \cot \phi \tag{69}$$

$$\tau = \pm p \sin \phi \cos \phi \tag{70}$$

The plus sign in Eq. (70) indicates that the stress resultant at the point is rotated counterclockwise with reference to the local normal. In what follows, the corresponding p values in Eqs. (69) and (70) will be defined along the sliplines L(ML), (ML)M, M(MN), and (MN)N, and the stress along these sliplines will be used to evaluate the corresponding soil reaction forces.

1. Stress parameter p along straight sliplines. Alternate equilibrium equations are obtained setting $ds = dx/\cos\theta$ and $ds' = dx/\cos\theta'$ in Eqs. (63) and (64):

$$p + 2p \tan\phi \, d\theta = \gamma \, dx \, (\tan\theta + \tan\phi) \tag{71}$$

$$p - 2p \tan\phi \, d\theta = \gamma \, dx \, (\tan\theta' - \tan\phi) \tag{72}$$

Expressions (71) and (72) will be used to determine the stresses along the straight sliplines N(MN) and L(ML), respectively. Since θ_{LL} and θ_{NN} are constant, $d\theta = d\theta' = 0$, and Eqs. (71) and (72) reduce to

$$dp = \gamma \, dx \, (\tan\theta + \tan\phi) \tag{73}$$

$$dp = \gamma \, dx \, (\tan\theta' - \tan\phi) \tag{74}$$

Integration of Eqs. (73) and (74) gives, respectively,

$$p = \gamma(\tan\theta + \tan\phi)x + C \tag{75}$$

$$p = \gamma(\tan\theta' - \tan\phi)x + C' \tag{76}$$

To determine the constant of integration at rim point (LL), $x = x_L$, $\theta' = \theta'_{LL}$, and $p = p_{LL}$, then

$$C' = p_{LL} - \gamma(\tan\theta'_{NN} - \tan\phi)x_L$$

For rim point (NN), $x = x_N$, $\theta = \theta_{NN}$, and $p = p_{NN}$, then

$$C = p_{NN} + \gamma(\tan\theta_{NN} + \tan\phi)x_N$$

For point (ML) along L(ML), $x = x_{ML}$ and

$$p_{ML} = p_{LL} + \gamma(\tan\theta'_{LL} - \tan\phi)(x_{ML} - x_L)$$

$$= p_{LL} + \Delta p_{ML} \tag{77}$$

where

$$\Delta p_{ML} = \gamma(\tan\theta'_{LL} - \tan\phi)(x_{ML} - x_L) \geq 0 \tag{78}$$

Similarly, for trailing point (MN) along the slipline N(MN), $x = x_{MN}$ and

$$p_{MN} = p_{NN} + \gamma(\tan\theta_{NN} + \tan\phi)(x_{MN} - x_N)$$

$$= p_{NN} + \Delta p_{MN} \tag{79}$$

where

$$\Delta p_{MN} = \gamma(\tan\theta_{NN} + \tan\phi)(x_{MN} - x_N) \geq 0 \tag{80}$$

Both points L and N constitute singular stress points around which the stress are multivalued, each representing geometrically a limiting first and second characteristic lines, respectively, having zero radius of curvature. When points L and N belong to the soil-rim interface side, they are identified as (LL) and (NN). If these points belong to the traction-free soil surface, they are identified as points (LO) and (NO). To completely determine Eqs. (77) and (79), it is required to define the value of p_{LL} and p_{NN}. Applying Eq. (71) to point L,

$$dp = -2p \tan\phi \, d\theta$$

$$\ln p = -2 \tan\phi\theta + C'_O$$

For point (LO), with $\theta = \theta_{LO}$ and $p = p_{LO}$, we obtain

$$C'_O = \ln p_{LO} + 2 \tan\phi\theta_{LO}$$

and

$$\ln \frac{p}{p_{LO}} = 2 \tan\phi(\theta_{LO} - \theta)$$

For rim point (LL), with $\theta = \theta_{LL}$, $p = p_{LL}$, and

$$p_{LL} = p_{LO} \exp\left[(\theta_{LO} - \theta_{LL}) \tan\phi\right] \tag{81}$$

Similarly for rim point (NN),

$$p_{NN} = p_{NO} \exp\left[(\theta_{NN} - \theta_{NO}) \tan\phi\right] \tag{82}$$

The stress parameters p_{LO} and p_{NO} are determined, considering a passive failure condition. Since the soil surface is free of stresses, $\sigma_0 = \tau_0 = 0$, then from the Mohr circle of stress,

$$p_{LO} = p_{NO} = \frac{c \cot\phi}{1 - \sin\phi} = p_0 \tag{83}$$

According to Eqs. (77) and (79), the stress parameter p varies linearly with depth; consequently, we can operate with average stresses along L(ML) and N(MN) sliplines. The average stress parameter $\bar{p}_L$ along the leading slipline segment L(ML), using Eq. (77), is

$$\bar{p}_L = p_{LL} + \frac{\Delta p_{ML}}{2} \tag{84}$$

where Δp_{ML} is given by Eq. (78). The corresponding average normal and shear stresses within the second slipline segment L(ML), using Eqs. (69) and (70), are (Fig. 13)

$$\bar{\sigma}_L = \bar{p}_L \cos^2 \phi - c \cot \phi \tag{85}$$

$$\bar{\tau}_L = \bar{p}_L \sin \phi \cos \phi \tag{86}$$

The stress parameters p_{MN} at (MN) must be the same when approaching point (MN) either along the slipline M(MN) or along the spiral M(MN). Thus, the average value of the stress parameter p_N corresponding to the slipline segment N(MN) is

$$\bar{p}_N = p_{MN} - \frac{\Delta p_{MN}}{2} \tag{87}$$

with p_{MN} given by Eq. (79) and Δp_{MN} by Eq. (80).

The corresponding average normal and shear stresses within the second slipline segment N(MN) are (Fig. 13)

$$\bar{\sigma}_N = \bar{p}_N \cos^2 \phi - c \cot \phi \tag{88}$$

$$\bar{\tau}_N = -\bar{p}_N \sin \phi \cos \phi \tag{89}$$

2. Stress parameter p along spiral sliplines. To determine the stresses along the spiral sliplines, multiply Eq. (63) by $\exp[\theta \tan \phi]$ and Eq. (64) by $\exp[-\theta \tan \phi]$ and express p in integral form along the first and second characteristic lines, respectively (Ref. 6):

$$p = \gamma \exp(-2 \tan \phi\theta) \times \int \exp\left[(2 \tan \phi\theta)\right] \frac{\sin(\theta + \phi)}{\cos \phi} ds + C \tag{90}$$

$$p = \gamma \exp\left[(2 \tan \phi\theta)\right] \times \int \exp\left[(-2 \tan \phi\theta)\right] \frac{\cos \theta}{\cos \phi} ds' + C' \tag{91}$$

where ds and ds' are the elemental arc lengths along a first and second slipline, respectively. To determine the state of stress along the spiral sliplines, adopt as positive directions of the characteristic spirals the ones which relate to decreasing values of θ and θ' (Fig. 11). Expressing ds and ds' in terms of its radius of curvatures ρ and ρ', for the trailing M(MN) spiral, we get

$$ds = -\rho\, d\theta = -\frac{r_M \exp\left[(\theta_M - \theta) \tan \phi\right]}{\cos \phi} d\theta \tag{92}$$

and, for the leading (ML)M spiral,

$$ds' = -\rho'\, d\theta' = -\frac{\bar{r}_M \exp\left[(\theta_M - \theta) \tan \phi\right]}{\cos \phi} d\theta' \tag{93}$$

Replacing Eq. (92) in Eq. (90) yields the stress parameter p_s^L along the leading spiral as a function of θ:

$$p_s^L = -\frac{\gamma \bar{r}_M}{\cos^2 \phi} \exp\left[-(2\theta' + \theta'_M) \tan \phi\right] \int \exp\left[(3\theta' \tan \phi)\right] \cos \theta'\, d\theta' + C$$

Integrating,

$$p_s^L = -\frac{\gamma \bar{r}_M}{(9 \tan^2 \phi + 1) \cos^2 \phi} \exp\left[-(2\theta' + \theta'_M) \tan \phi\right] \left\{\exp\left[(3\theta' \tan \phi)\right](3 \tan \phi \cos \theta' + \sin \theta')\right\} + C \tag{94}$$

When $\theta' = \theta'_{LL}$, $p_s^L = p_{ML}$, and the constant of integration is

$$C = p_{ML} + C_s^L \exp\left[(2\theta'_{LL} - \theta'_M) \tan \phi\right](3 \tan \phi \cos \theta'_{LL} + \sin \theta'_{LL}) = p_{ML} + C_1^L \tag{95}$$

where

$$C_s^L = \frac{\gamma \bar{r}_M}{(9 \tan^2 \phi + 1) \cos^2 \phi} \tag{96}$$

Replacing Eq. (95) in Eq. (94) results in

$$p_s^L = p_{ML} + C_1^L - C_s^L \exp\left[(\theta' - \theta_M') \tan\phi\right](3 \tan\phi \cos\theta' + \sin\theta') \tag{97}$$

To obtain p_M, setting in Eq. (97) $\theta' = \theta_M'$ gives

$$p_M = p_{ML} + C_1^L - C_s^L (3 \tan\phi \cos\theta_M' + \sin\theta_M') \tag{98}$$

with

$$C_M^L = 3 \tan\phi \cos\theta_M' + \sin\theta_M' \tag{99}$$

and

$$F_3 = C_1^L - C_s^L C_M^L \tag{100}$$

Equation (98) reduces to

$$p_M = p_{ML} + F_3 \tag{101}$$

Also, with Eq. (77),

$$p_M = p_{LL} + \Delta p_{ML} + F_3 = p_{LL} + F_4 \tag{102}$$

where

$$F_4 = \Delta p_{ML} + F_3 \tag{103}$$

Similarly, replacing Eq. (93) in Eq. (91), the stress parameter p_s^T along the trailing spiral is

$$p_s^T = \frac{\gamma r_M}{\cos^2\phi} \exp\left[(2\theta + \theta_M) \tan\phi\right] \int \exp\left[-3\theta \tan\phi\right] \cos\theta \, d\theta + C \tag{104}$$

Integrating,

$$p_s^T = \frac{\gamma r_M}{(9 \tan^2\phi + 1) \cos^2\phi} \exp\left[(2\theta + \theta_M) \tan\phi\right] \left\{\exp\left[(-3\theta \tan\phi)\right](-3 \tan\phi \cos\theta + \sin\theta)\right\} + C \tag{105}$$

When $\theta = \theta_M$, $p_s^T = p_M$, and the constant of integration is

$$C = p_M - C_s^T(-3 \tan\phi \cos\theta_M + \sin\theta_M) = p_M - C_1^T \tag{106}$$

where

$$C_s^T = \frac{\gamma r_M}{(9 \tan^2\phi + 1) \cos^2\phi} \tag{107}$$

and

$$C_1^T = C_s^T(-3 \tan\phi \cos\theta_M + \sin\theta_M) \tag{108}$$

Replacing Eq. (106) in Eq. (105) results in

$$p_s^T = p_M - C_1^T + C_s^T \exp\left[(\theta_M - \theta) \tan\phi\right](-3 \tan\phi \cos\theta + \sin\theta) \tag{109}$$

To obtain p_{MN}, set $\theta = \theta_{NN}$ in Eq. (108):

$$p_{MN} = p_M - C_1^T + C_s^T \exp\left[(\theta_M - \theta_{NN}) \tan\phi\right](-3 \tan\phi \cos\theta_{NN} + \sin\theta_{NN}) = p_M + \bar{\Delta}p_{MN} \quad (110)$$

where

$$\bar{\Delta}p_{MN} = -C_1^T + C_s^T \exp\left[(\theta_M - \theta_{NN}) \tan\phi\right](-3 \tan\phi \cos\theta_{NN} + \sin\theta_{NN}) \quad (111)$$

With Eq. (102) and based on Eq. (109),

$$p_{MN} = p_{LL} + F_4 + \bar{\Delta}p_{MN} = p_{LL} + F_{11} \geq p_0 \quad (112)$$

where F_4 is given by Eq. (103), and

$$F_{11} = F_4 + \bar{\Delta}p_{MN} \quad (113)$$

The last condition in Expression (112) insures that point (MN) is at or below the ground surface.

The equations derived in this section will be utilized to determine the soil stresses and reactions that are considered in Sections V-C and E, and VI-A.

3. Transition and passive zones (Fig. 4). The stress characteristic lines corresponding to both the transition and passive zones are determined by solving numerically the finite difference form of Eqs. (63) and (64), subject to their corresponding boundary stress conditions.

The boundary conditions of the transition zones relate to: (1) the stress along the characteristic lines L(ML) and N(MN), respectively, and (2) the state of stress around the singular points L and N as defined in Section V-B-1. These stresses are known from the solution of the soil-roller active zones equilibrium equations in connection with the stress compatibility conditions, described in Section VI-A. For the passive zones, the solution is obtained by extending the transition stress characteristics into the passive zones, considering the traction-free leading and trailing soil surfaçes LF and NB. This solution also yields the final deformed and statically correct configuration of the soil surfaces LF and NB (Fig. 4).

The solution procedure and corresponding applications will be described in detail in Part II of this study.

C. Limiting Slipline Directions

There exist definite limitations regarding the values that the θ parameters may acquire along the soil-roller interface. It will be shown that the solution of the soil-roller problem entails, to a large extent, calculation of an admissible set of characteristic directions at points L, M, and N defined by

$$\left\{\theta'_{LO}, \theta'_{LL}, \theta'_M, \theta_{NN}, \theta_{NO}\right\} \quad (114)$$

For any solution to a given soil-roller problem, it must be verified that the values corresponding to Expression (114) are within acceptable bounds. Determination of these bounds is necessary not only to validate the solution itself, but also to systematically initiate and objectively search for solutions utilizing only admissible θ values. Obviously, the final set of Expression (114) is obtained only after satisfying equilibrium and boundary conditions. In general, the absolute bounds to Expression (114) result from considering the envelope of values originating from (1) the maximum obliquity of the stress resultant as related to the radial direction at the soil-roller interface, (2) the maximum free surface slope as dictated by either the local roller rim surface tangent or the soil natural angle of repose, and (3) the stress compatibility requirements along the transition slipline zone. Each of these cases are considered next.

1. Soil-roller interface — maximum stress obliquity. At any point along the soil-roller interface, the shear stress τ and the reduced stress $\sigma + c \cot\phi$ define a stress resultant

$$q_r = \left[\tau^2 + (\sigma + c \cot\phi)^2\right]^{1/2} \quad (115)$$

The obliquity angle δ of q_r is measured positive for a clockwise rotation relative to the rim surface normal (radial direction) and is defined by

$$\delta = \tan^{-1}\left(\frac{\tau}{\sigma + c \cot\phi}\right) \leq \phi \quad (116)$$

When $\delta = \phi$, Eq. (116) indicates that one of the sliplines becomes tangent to the roller rim surface at the point under consideration. In this case, for the trailing point (NN), with

$$\xi_N < \frac{\pi}{2} \quad (117)$$

$$\theta_{NN} = \alpha + \xi_N - \phi \quad (118)$$

For the leading rim point (LL), with

$$\xi_L > \xi_M > \frac{\pi}{2} \quad (119)$$

$$\theta'_{LL} = \alpha + \xi_L + \phi \quad (120)$$

The corresponding slipline directions for points (NN) and (LL) are defined by

$$\tan \theta_{NN} = \frac{R \sin(\alpha + \xi_N) - \bar{z}_1}{R \cos(\alpha + \xi_N) - \bar{x}_1} \quad (121)$$

or

$$\theta_{NN} = \xi_N + \alpha - \sin^{-1}\left[\frac{1}{R}(\bar{z}_1 \cos \theta_{NN} - \bar{x}_1 \sin \theta_{NN})\right] \quad (122)$$

and

$$\tan \theta'_{LL} = \frac{R \sin(\alpha + \xi_L) - \bar{z}_2}{R \cos(\alpha + \xi_L) - \bar{x}_2} \quad (123)$$

or

$$\theta'_{LL} = \xi_L + \alpha - \sin^{-1}\left[\frac{1}{R}(\bar{z}_2 \cos \theta'_{LL} - \bar{x}_2 \sin \theta'_{LL})\right] \quad (124)$$

Adopting Eq. (118) in connection with Eq. (121) and Eq. (120) with Eq. (123), the limiting θ_{NN} and θ'_{LL} values for $\delta = \phi$ are obtained from the following quadratic equations:

$$\left(\bar{x}_1^2 + \bar{z}_1^2\right) \cos^2 \theta_{NN} + 2R\bar{z}_1 \sin \phi \cos \theta_{NN} + \left(R^2 \sin^2 \phi - \bar{x}_1^2\right) = 0 \quad (125a)$$

$$\left(\bar{x}_2^2 + \bar{z}_2^2\right) \cos^2 \theta'_{LL} + 2R\bar{z}_2 \sin \phi \cos \theta'_{LL} + \left(R^2 \sin^2 \phi - \bar{x}_2^2\right) = 0 \quad (125b)$$

When the discriminant of Eqs. (125a, b)

$$\left.\begin{matrix} \bar{x}_1^2 + \bar{z}_1^2 \\ \\ \bar{x}_2^2 + \bar{z}_2^2 \end{matrix}\right\} \geq R \sin \phi = R_\phi \quad (126)$$

then each of the Eqs. (125a, b) yields two roots θ_1, θ_2, which relate to two distinct rim points ξ_1, ξ_2, respectively, as derived either from Eq. (118) or (120) as required. At these two rim points the sliplines are tangent to the roller surface. The decision on which root to adopt is based on the condition that at no point along the rim surface will the spirals cross into the rigid roller body. Consequently the problem is to verify if between these two rim-slipline tangency points, the sliplines diverge inward to or outward from the roller center. The condition precluding the spiral sliplines to cross into the rigid roller body depends on the relative dimensions of the spiral radius of curvature to the roller radius R. To this effect the radius of curvature at point N must be

$$\rho_{NN} = \frac{r_M \exp\left[(\theta_M - \theta_{NN}) \tan \phi\right]}{\cos \phi} \geq R \quad (127)$$

With roots $\theta_{N,1}$ and $\theta_{N,2}$, such that considering $\theta_{N,1} > \theta_{N,2}$, it can be shown that if $\rho_{N,1} < R$, then $\theta_{N,1}$ is the limiting direction. Thus, $\theta_{NN} = \theta_{N,1}$. But if $\rho_{N,1} > R$, there is no geometrical limitation to the position of point N along the rim since all sliplines diverge outwards from the roller rim. Similar criteria are exercised to determine the limiting position of rim point L when the spiral pole position satisfies Eq. (120). Here, in order to prevent the spiral from crossing into the roller, the spiral radius of curvature must be

$$\rho_{LL} = \frac{\bar{r}_M \exp\left[(\theta_{LL} - \theta_M) \tan \phi\right]}{\cos \phi} \geq R \quad (128)$$

When $s_k = 0$, from Eq. (21), $a_M = R$ and, from Eq. (20),

$$r_M = \frac{R}{\cos \phi}$$

In this case, Condition (127) is always satisfied in the sense that the trailing spiral never diverges into the roller body.

Graphically, Conditions (118) and (120) are defined when the pole coordinates of $\bar{I}_1$ and $\bar{I}_2$ (Fig. 13) are located at or outside a circle with center C and radius R sin ϕ, herein called the "ϕ circle." Tangent lines are drawn from poles $\bar{I}_1$ and $\bar{I}_2$ which intersects the ϕ circle at points T_1, T_2 for pole $\bar{I}_1$ and at points $\bar{T}_1$, $\bar{T}_2$ for $\bar{I}_2$. Intersection of these lines with the roller rim defines the leading points L_1, L_2 and trailing points N_1, N_2 whose angles ξ_L, ξ_N satisfy, respectively, Conditions (118) and (120). When $\bar{I}_1$ or $\bar{I}_2$ coincides with the ϕ circle, $\xi_{L1} = \xi_{L2}$ and $\xi_{N1} = \xi_{N2}$, then Eqs. (127) and (128) apply.

When the discriminant of Eqs. (125a, b) is negative, then the spirals will not cross into the roller body. This corresponds to pole $\bar{I}_1$ or $\bar{I}_2$ being at or inside the "ϕ circle."

An admissible value of θ'_{LL} must also satisfy the conditions of Eq. (78):

$$\Delta p_{ML} = \gamma(x_{ML} - x_L)(\tan \theta'_{LL} - \tan \phi) \geq 0 \tag{129}$$

When $\theta'_{LL} < \pi/2$, $(x_{ML} - x_L) > 0$; therefore,

$$\min \theta'_{LL} \geq \phi \tag{130}$$

When $s_k = 0$, $\xi_M = \xi_L$ and $x_{ML} = x_L$; then there is no leading plastic zone (Figs. 3 and 7). In this case, Eq. (78) reduces to $\Delta p_{ML} = 0$, and the spiral M(MN) is tangent to the roller rim at M:

$$\theta'_{LO} = \theta'_{LL} = \theta'_M - \alpha + \xi_M - \frac{\pi}{2} \tag{131}$$

Also, Eq. (81) defines $p_{LL} = p_M = p_0$ as given by Eq. (83).

A similar analysis with reference to Eq. (83) yields, for $c \geq 0$,

$$\max \theta_{NN} \leq \pi - \phi \tag{132}$$

In general, $\xi_N \leq \pi/2$, which, from Eq. (121), corresponds to

$$\theta_{NN} = \tan^{-1}\left(\frac{R \cos \alpha - \bar{z}_1}{-R \sin \alpha - \bar{x}_1}\right) \tag{133}$$

2. Free soil surface — singular points (LO) and (NO). The limits of θ_{LO} and θ_{NO} are dictated by the condition that the free surface slopes at points L and N defined by α_{LO} and α_{NO} can at most be tangent to the roller rim surface. Thus,

$$\alpha_{LO} \leq \alpha + \xi_L + \frac{\pi}{2} \tag{134}$$

$$\alpha_{NO} \geq \alpha + \xi_N - \frac{\pi}{2} \tag{135}$$

Also when dealing with cohesionless soils ($c = 0$), the free surface maximum slope cannot exceed the soil natural angle of repose. Therefore,

$$\left|\alpha_{LO}\right| \leq \phi \tag{136}$$

$$\left|\alpha_{NO}\right| \leq \phi \tag{137}$$

Obviously, if $c > 0$, the angle of repose has no significance since the soil is stable up to and including vertical slopes as long as the critical height is not exceeded (Ref. 17, p. 152).

The transition plastic zone separating the active from the passive zones may, in the limit, disappear and allow the latter two zones to merge side by side; therefore,

$$\theta'_{LO} \geq \theta'_{LL} \tag{138}$$

$$\theta_{NO} \leq \theta_{NN} \tag{139}$$

In terms of slipline parameters in general, with $\mu = \pi/4 - \phi/2$, Eqs. (134) and (135) reduce to

$$\alpha_{LO} = \theta'_{LO} + \mu \tag{140}$$

$$\alpha_{NO} = \theta_{NO} - \mu \tag{141}$$

Based on Eq. (141), Conditions (134) through (139) reduce, for cohesive soils ($c > 0$), to

$$\alpha + \xi_L + \frac{\pi}{2} - \mu \geq \theta'_{LO} \geq \theta'_{LL} \tag{142}$$

$$\alpha + \xi_N - \frac{\pi}{2} + \mu \leq \theta_{NO} \leq \theta_{NN} \tag{143}$$

and, for cohesionless soils ($c = 0$), with Conditions (136) and (137),

$$\pi + \phi - \mu \geq \theta'_{LO} \geq \pi - (\mu + \phi) \tag{144}$$

$$\mu - \phi \leq \theta_{NO} \leq \phi + \mu \tag{145}$$

3. Summary of absolute admissible bounds for θ'_{LO}, θ'_{LL}, θ_{NN}, and θ_{NO}. Recapitulating Subsections C-1 and C-2, the limiting slipline directions at points L and M are as follows: For $c \geq 0$, from Expressions (118) and (130),

$$\phi \leq \theta'_{LL} \leq \alpha + \xi_L + \phi \tag{146}$$

Based on Expressions (120), (132), and (133), we obtain

$$\alpha + \xi_N - \phi \leq \theta_{NN} \leq \begin{cases} \pi - \phi & (147) \\ \tan^{-1}\left(\dfrac{R \cos \alpha - \bar{z}_1}{-R \sin \alpha - \bar{x}_1}\right) & (148) \end{cases}$$

Between Conditions (147) and (148), the lower of the two upper limits shown is selected.

Expressions (146) to (148) apply to both cohesive and purely frictional soils.

Admissible values of θ'_{LO} and θ_{NO} also depend on the soil characteristics. For $c > 0$,

$$\alpha + \xi_L + \frac{\pi}{2} - \mu \geq \theta'_{LO} \geq \theta'_{LL} \qquad (149)$$

and

$$\alpha + \xi_L - \frac{\pi}{2} + \mu \leq \theta_{NO} \leq \theta_{NN} \qquad (150)$$

And for $c = 0$, it can be proved that Conditions (149) and (150) also apply but subject to the following limitations:

$$\pi + \phi - \mu \geq \theta'_{LO} \geq \pi - (\mu + \phi) \qquad (151)$$

and

$$\mu - \phi \leq \theta_{NO} \leq \phi + \mu \qquad (152)$$

For lunar locomotion ($c > 0$), then Expressions (149) and (150) will generally apply.

Expressions (146) to (152) are incorporated in the computer program to operate within a compatible range of stress parameters p and θ.

D. Equilibrium Equations

With the positive direction of forces the same as the positive x, z coordinate directions, and with applied vertical axle loads W and pull force P parallel to the terrain slope, horizontal equilibrium conditions require (Fig. 11)

$$\sum X = H_k^L + H_k^T + P \cos \alpha = 0 \qquad (153)$$

and, for vertical equilibrium,

$$\sum Z = W_k^L + W_k^T + W + P \sin \alpha = 0 \qquad (154)$$

where H_k^L, H_k^T, W_k^L, W_k^T are horizontal and vertical forces corresponding to leading (L) and trailing (T) plastic active zones adjoining the soil-roller interface arc LN. Sub-index k (=1, 2, $\cdots$) identifies the possible existence of more than one soil-roller solution for a fixed slip value s_k and various ξ_M.

A driven roller moving over horizontal or sloping terrains operates under self-propulsion conditions when it transports only its axle weight W (pull force $P = 0$). Under self-propulsion there is no net soil thrust development nor soil resistance to motion since the leading and trailing forces balance each other ($H_k^L + H_k^T = 0$). The net effect of the interplay of these self-equilibrated internal forces is to offset the position of the vertical soil reaction to accommodate the rolling torque $M = M_k$; instead, when $P > 0$ in Eq. (153), the leading and trailing forces make up for the difference in allowing for P to become equilibrated.

Taking moments with respect to roller axle center C, with positive torques measured counterclockwise, moment equilibrium requires

$$\sum M = M_k^L + M_k^T - M_k = 0 \qquad (155)$$

where M_k is the applied axle torque, and M_k^L and M_k^T correspond to leading (L) and trailing (T) moments produced by the mobilized soil strength and corresponding soil weight. The above forces and moments relate exclusively to the active zones L(ML)M and M(MN)N. Expressions (153), (154), and (155) are further developed as follows:

$$\sum X = H_{k,s}^L + H_{k,s}^T + H_{k,p}^L + H_{k,p}^T$$

$$+ P \cos \alpha = 0 \qquad (156)$$

$$\sum Z = W_{k,s}^L + W_{k,p}^L + W_{k,\gamma}^L + W_{k,s}^T + W_{k,p}^T$$

$$+ W_{k,\gamma}^T + W + P \sin \alpha = 0 \qquad (157)$$

$$\sum M = M_{k,s}^L + M_{k,p}^L + M_{k,\gamma}^L + M_{k,s}^T + M_{k,p}^T$$

$$+ M_{k,\gamma}^T - M_k = 0 \qquad (158)$$

The sub-index s corresponds to forces (or moments) due to stresses along the spiral slipline M(ML) and M(MN). The sub-index p indicates forces (or moments) due to stresses along the straight slipline L(ML) and M(MN) as derived from both the transition and passive zones. $W_{k,\gamma}^L$ and $W_{k,\gamma}^T$ are soil weights within the confines of the leading and trailing active zones M(ML)L and M(MN)N, respectively. $M_{k,\gamma}^L$ and $M_{k,\gamma}^T$ are moments due to $W_{k,\gamma}^L$ and $W_{k,\gamma}^T$, respectively. To evaluate these forces and moments it is necessary to determine the nature and extent of both active plastic domains (Fig. 11), their associated stresses and corresponding soil weight participating with the roller motion.

E. Soil Reactions

The horizontal and vertical force components due to stresses acting along slipline L(ML) are (Figs. 11 and 12)

$$H^L_{k,p} = (\bar{\sigma}_L \sin \theta'_{LL} - \bar{\tau}_L \cos \theta'_{LL}) \frac{x_{ML} - x_L}{\cos \theta'_{LL}} b \tag{159}$$

$$W^L_{k,p} = -(\bar{\sigma}_L \cos \theta'_{LL} + \bar{\tau}_L \sin \theta'_{LL}) \frac{x_{ML} - x_L}{\cos \theta'_{LL}} b \tag{160}$$

where b is the roller width, and

$$x_{ML} = \bar{x}_2 + r_M \exp\left[(\theta'_{LL} - \theta'_M) \tan \phi\right] \cos \theta'_{LL} \tag{161}$$

$$x_L = R \cos (\alpha + \xi_L) \tag{162}$$

Replacing Eqs. (161) and (162) in Eqs. (159) and (160) and ordering terms results in

$$H^L_{k,p} = C_{14} p_{LL} \sin (\theta'_{LL} - \phi) + F_{12}(\theta'_{LL}) \tag{163}$$

$$W^L_{k,p} = -C_{14}\left[\bar{p}_L \cos (\theta'_{LL} - \phi) - \frac{c}{\sin \phi} \cos \theta'_{LL}\right] \tag{164}$$

where

$$C_{14} = b \frac{\cos \phi}{\cos \theta'_{LL}} (x_{ML} - x_L) \tag{165}$$

$$F_{12}(\theta'_{LL}) = C_{14}\left[\frac{\Delta p_{ML}}{2} \sin (\theta'_{LL} - \phi) - \frac{c}{\sin \phi} \sin \theta'_{LL}\right] \tag{166}$$

Derivation of the force components $H^T_{k,p}$, $W^T_{k,p}$ on the trailing first slipline N(MN) is basically similar to the procedure adopted for the leading slipline L(ML). The horizontal and vertical force components from stress acting along N(MN) are (Fig. 12)

$$H^T_{k,p} = (\bar{\sigma}_T \sin \theta_{NN} + \bar{\tau} \cos \theta_{NN}) \frac{x_{MN} - x_N}{\cos \theta_{NN}} b \tag{167}$$

$$W^T_{k,p} = (\bar{\sigma}_T \cos \theta_{NN} - \bar{\tau} \sin \theta_{NN}) \frac{x_{MN} - x_N}{\cos \theta_{NN}} b \tag{168}$$

where

$$x_{MN} = \bar{x}_1 + r_M \exp\left[(\theta_M - \theta_{NN}) \tan \phi\right] \cos \theta_{NN} \tag{169}$$

$$x_N = R \cos (\alpha + \xi_N) \tag{170}$$

Substituting Eqs. (169) and (170) in Eqs. (167) and (168) and ordering terms results in

$$H^T_{k,p} = C_{15} p_{LL} \sin (\theta_{NN} + \phi) + F_{13}(\theta_{NN}) \tag{171}$$

$$W^T_{k,p} = -C_{15}\left[\bar{p}_N \cos (\theta_{NN} + \phi) - \frac{c}{\sin \phi} \cos \theta_{NN}\right] \tag{172}$$

where

$$C_{15} = -b \frac{\cos \phi}{\cos \theta_{NN}} (x_{MN} - x_N) \tag{173}$$

$$F_{13}(\theta_{NN}) = C_{15}\left[\left(F_{11} - \frac{\Delta p_{MN}}{2}\right) \sin (\theta_{NN} + \phi) - \frac{c}{\sin \phi} \sin \theta_{NN}\right] \tag{174}$$

Expressions (163), (164), (171), and (172) will be incorporated in equilibrium Eqs. (156), (157), and (158). The horizontal and vertical force components on the elemental arc ds along the spiral (ML)M are (Fig. 11)

$$dH^L_{k,s} = -b\left[\sigma^L_s \cos (\theta' - \phi) - \tau^L_s \sin (\theta' - \phi)\right] ds \tag{175}$$

$$dW^L_{k,s} = -b\left[\sigma^L_s \sin (\theta' - \phi) + \tau^L_s \cos (\theta' - \phi)\right] ds \tag{176}$$

where σ^L_s and τ^L_s correspond to σ and τ as given by Eqs. (69) and (70) respectively, with $p = p^L_s$ (Eq. 97).

Similarly, the horizontal and vertical components on the elemental arc ds' along the spiral M(MN) are

$$dH^T_{k,s} = b(\sigma^T_s \sin\theta' - \tau^T_s \cos\theta')\, ds' \tag{177}$$

$$dW^T_{k,s} = -b(\sigma^T_s \cos\theta' + \tau^T_s \sin\theta')\, ds' \tag{178}$$

where σ^T_s and τ^T_s correspond to σ and τ as given by Eqs. (69) and (70), respectively, with $p = p^T_s$ (Eq. 108).

The total force components are derived by replacing the σ, τ stresses in Eqs. (175) to (178) and integrating within the corresponding spiral limits. Thus,

$$H^L_{k,s} = b\bar{r}_M \int_{\theta'_{LL}}^{\theta'_M} \left[p^L_s \cos(\theta' - 2\phi) - \frac{c}{\sin\phi}\cos(\theta' - \phi)\right] \exp\left[(\theta' - \theta_M)\tan\phi\right] d\theta' \tag{179}$$

$$W^L_{k,s} = b\bar{r}_M \int_{\theta'_{LL}}^{\theta'_M} \left[p^L_s \sin(\theta' - 2\phi) - \frac{c}{\sin\phi}\sin(\theta' - \phi)\right] \exp\left[(\theta' - \theta_M)\tan\phi\right] d\theta' \tag{180}$$

$$H^T_{k,s} = br_M \int_{\theta_M}^{\theta_{NN}} \left[p^T_s \cos\theta - \frac{c}{\sin\phi}\cos(\theta + \phi)\right] \exp\left[(\theta_M - \theta)\tan\phi\right] d\theta \tag{181}$$

$$W^T_{k,s} = br_M \int_{\theta_M}^{\theta_{NN}} \left[p^T_s \sin\theta - \frac{c}{\sin\phi}\sin(\theta + \phi)\right] \exp\left[(\theta_M - \theta)\tan\phi\right] d\theta \tag{182}$$

Replacing Eq. (97) in Eqs. (179) and (180) and Eq. (108) in Eqs. (181) and (182), integrating, and arranging terms, the soil reactions $H_{k,s}$ and $W_{k,s}$ along the sliplines are obtained. For the leading zone, the solutions are

$$H^L_{k,s} = C_8\left[p_{ML} \cdot F_2(\theta'_{LL}, \theta'_M) + F_1(\theta'_{LL}, \theta'_M)\right] \tag{183}$$

and

$$W^L_{k,s} = C_8\left[-p_{ML} \cdot F_7(\theta'_{LL}, \theta'_M) + F_8(\theta'_{LL}, \theta'_M)\right] \tag{184}$$

where

$$C_8 = b\bar{r}_M \cos\phi \tag{185}$$

$$\begin{aligned}
F_1 = & -\frac{c}{\sin\phi}\left\{\sin\theta'_M - \exp\left[(\theta'_{LL} - \theta'_M)\tan\phi\right]\sin\theta'_{LL}\right\} \\
& + C^L_1\left\{\sin(\theta'_M + \phi) - \exp\left[(\theta'_{LL} - \theta'_M)\tan\phi\right]\sin(\theta'_{LL} + \phi)\right\} \\
& - \frac{3}{4}\tan\phi\, C^L_s\left[\frac{1}{\sin\phi} + \sin(2\theta'_M + \phi)\right] + \frac{3}{4}\tan\phi\, C^L_s \exp\left[2(\theta'_{LL} - \theta'_M)\tan\phi\right] \\
& \times \left[\frac{1}{\sin\phi} + \sin(2\theta'_{LL} + \phi)\right] + \frac{C^L_s}{4}\left\{\cos(2\theta'_M + \phi) - \exp\left[2(\theta'_{LL} - \theta'_M)\tan\phi\right]\right. \\
& \left. \times \cos(2\theta'_{LL} + \phi)\right\}
\end{aligned} \tag{186}$$

$$F_2 = \sin(\theta'_M + \phi) - \exp\left[(\theta'_{LL} - \theta'_M)\tan\phi\right] \sin(\theta'_{LL} + \phi) \tag{187}$$

$$F_7 = \cos(\theta'_M + \phi) - \exp\left[(\theta'_{LL} - \theta'_M)\tan\phi\right] \cos(\theta'_{LL} + \phi) \tag{188}$$

$$\begin{aligned} F_8 = {} & \frac{c}{\sin\phi}\left\{\cos\theta'_M - \exp\left[(\theta'_{LL} - \theta'_M)\tan\phi\right]\cos\theta'_{LL}\right\} - C_l^L\left\{\cos(\theta'_M + \phi)\right. \\ & \left. - \exp\left[(\theta'_{LL} - \theta'_M)\tan\phi\right]\cos(\theta'_{LL} + \phi)\right\} + \frac{3}{4}\tan\phi\, C_s^L\left\{\cos(2\theta'_M + \phi)\right. \\ & \left. - \exp\left[2(\theta'_{LL} - \theta'_M)\tan\phi\right]\cos(2\theta'_{LL} + \phi)\right\} - \frac{C_s^L}{4}\left[\frac{1}{\sin\phi} - \sin(2\theta'_M + \phi)\right] \\ & + \frac{C_s^L}{4}\exp\left[2(\theta'_{LL} - \theta'_M)\tan\phi\right]\left[\frac{1}{\sin\phi} - \sin(2\theta'_{LL} + \phi)\right] \end{aligned} \tag{189}$$

For the trailing zone,

$$H^T_{k,s} = C_7\left[p_M \cdot F_5(\theta_{NN}, \theta_M) + F_6(\theta_{NN}, \theta_M)\right] \tag{190}$$

and

$$W^T_{k,s} = C_7\left[-p_M \cdot F_9(\theta_{NN}, \theta_M) + F_{10}(\theta_{NN}, \theta_M)\right] \tag{191}$$

where

$$C_7 = br_M \cos\phi \tag{192}$$

$$F_5 = \exp\left[(\theta_M - \theta_{NN})\tan\phi\right]\sin(\theta_{NN} - \phi) - \sin(\theta_M - \phi) \tag{193}$$

$$\begin{aligned} F_6 = {} & -\frac{c}{\sin\phi}\left\{\exp\left[(\theta_M - \theta_{NN})\tan\phi\right]\sin\theta_{NN} - \sin\theta_M\right\} \\ & - C_l^T\left\{\exp\left[(\theta_M - \theta_{NN})\tan\phi\right]\sin(\theta_{NN} - \phi) - \sin(\theta_M - \phi)\right\} \\ & - \frac{1}{4}C_s^T\exp\left[2(\theta_M - \theta_{NN})\tan\phi\right]\left\{3\tan\phi\left[-\frac{1}{\sin\phi} + \sin(2\theta_{NN} - \phi)\right] + \cos(2\theta_{NN} - \phi)\right\} \\ & + \frac{1}{4}C_s^T\left\{3\tan\phi\left[-\frac{1}{\sin\phi} + \sin(2\theta_M - \phi)\right] + \cos(2\theta_M - \phi)\right\} \end{aligned} \tag{194}$$

$$F_9 = \exp\left[(\theta_M - \theta_{NN})\tan\phi\right]\cos(\theta_{NN} - \phi) - \cos(\theta_M - \phi) \tag{195}$$

$$\begin{aligned} F_{10} = {} & \frac{c}{\sin\phi}\left\{\exp\left[(\theta_M - \theta_{NN})\tan\phi\right]\cos\theta_{NN} - \cos\theta_M\right\} \\ & + C_l^T\left\{\exp\left[(\theta_M - \theta_{NN})\tan\phi\right]\cos(\theta_{NN} - \phi) - \cos(\theta_M - \phi)\right\} \\ & + \frac{1}{4}C_s^T\exp\left[2(\theta_M - \theta_{NN})\tan\phi\right]\left[3\tan\phi\cos(2\theta_{NN} - \phi) - \frac{1}{\sin\phi} + \sin(2\theta_{NN} - \phi)\right] \\ & - \frac{1}{4}C_s^T\left[3\tan\phi\cos(2\theta_M - \phi) - \frac{1}{\sin\phi} + \sin(2\theta_M - \phi)\right] \end{aligned} \tag{196}$$

Expressions (183) to (196) will be incorporated in Eqs. (156), (157), and (158) for the detailed study of equilibrium in Section VI-A.

F. Body Forces

Soil body forces $W_{k,\gamma}$ are obtained by integrating the soil volume contained within the leading and trailing active zone L(ML)M and M(MN)N as shown in Fig. 11.

For the leading zone,

$$W^L_{k,\gamma} = \gamma b \Big[\text{area } \overline{I}_2(ML)M$$

$$- \text{ area circular sector } \overline{I}_2 LM \Big] \quad (197)$$

$$\text{Area } \overline{I}_2(ML)M = \int_{\theta'_M}^{\theta'_{LL}} \frac{1}{2} \overline{r}^2 d\theta' \quad (198)$$

where $\overline{r}$ is given by Eq. (33).

Area $\overline{I}_2LM$ = (area triangle $\overline{I}_2LM$ + area circular segment with arc LM) = C^L_γ or

$$C^L_\gamma = \frac{1}{2} \overline{r}_M \overline{r}_c \sin(\theta_{LL} - \theta_M) + \overline{A}_c \quad (199)$$

where

$$\overline{A}_c = \frac{1}{2} R^2 \Big[\xi_L - \xi_M - \sin(\xi_L - \xi_M) \Big] \quad (200)$$

and

$$\overline{r}_c = \overline{I}_2 L - -R \cos(\alpha + \xi_L - \theta'_{LL})$$

$$+ \overline{a}_L \cos(\overline{\beta}_L - \theta'_{LL}) \quad (201)$$

$$\overline{\beta}_L = \tan^{-1}\left(\frac{\overline{z}_2}{\overline{x}_2}\right) \quad (202)$$

$$\overline{a}_L = \sqrt{\overline{x}_2^2 + \overline{z}_2^2} \quad (203)$$

Integrating Eq. (198), and with Eq. (199), Eq. (197) becomes

$$W^L_{k,\gamma} =$$

$$b\gamma \left\{ \frac{\overline{r}^2_M}{4 \tan\phi} \left\{ \exp\left[2(\theta'_{LL} - \theta'_M) \tan\phi\right] - 1 \right\} - C^L_\gamma \right\} \quad (204)$$

with C^L_γ given by Eq. (199).

For the trailing zone M(MN)N, the soil weight is (Fig. 11)

$$W^T_{k,\gamma} = \gamma b \Big[\text{area } I_1 M(MN)$$

$$- \text{ area circular sector } I_1 MN \Big] \quad (205)$$

$$\text{Area } \overline{I}_1 M(MN) = \int_{\theta_{NN}}^{\theta_M} \frac{1}{2} r^2 d\theta \quad (206)$$

where r is given by Eq. (28).

Area $\overline{I}_1MN$ = (area triangle $\overline{I}_1MN$ + area circular segment with arc MN) = C^T_γ or

$$C^T_\gamma = \frac{1}{2} r_M r_c \sin(\theta_M - \theta_{NN}) + A_c \quad (207)$$

where

$$A_c = \frac{1}{2} R^2 \Big[\xi_M - \xi_N - \sin(\xi_M - \xi_N) \Big] \quad (208)$$

and

$$r_c = \overline{I}_1 N - R \cos(\alpha + \xi_N - \theta_{NN})$$

$$- \overline{a}_T \cos(\theta_{NN} - \overline{\beta}_T) \quad (209)$$

$$\overline{\beta}_T = \cos^{-1}\left(\frac{\overline{x}_1}{\overline{a}_T}\right) \quad (210)$$

$$\overline{a}_T = \sqrt{\overline{x}_1^2 + \overline{z}_1^2} \quad (211)$$

$$\xi_N = \theta_{NN} - \alpha + \sin^{-1}\left[\frac{1}{R}(\overline{z}_1 \cos\theta_{NN} - \overline{x}_1 \sin\theta_{NN})\right] \quad (212)$$

Integrating Eq. (206), and with Eq. (207), Eq. (205) becomes

$$W^T_{k,\gamma} =$$

$$b\gamma \left\{ \frac{r^2_M}{4 \tan\phi} \left\{ \exp\left[2(\theta_M - \theta_{NN}) \tan\phi\right] - 1 \right\} - C^T_\gamma \right\} \quad (213)$$

where C^T_γ is given by Eq. (207).

Equations (204) and (213) will be used in Eqs. (156), (157), and (158) for the detailed study of soil-roller equilibrium in Section VI-A and also to determine the driving torque M in Section V-G.

G. Moments

1. Moments due to soil reactions. The resultant force originating from reduced stresses along a spiral slipline intercepts the spiral pole (Fig. 12). The moments due to these spiral stresses relative to the roller axes $C(x = z = 0)$ depend exclusively on the position of the spiral poles $\overline{I}_1$ $(\overline{x}_1, \overline{z}_1)$; $\overline{I}_2(\overline{x}_2, \overline{z}_2)$. Positive moments tend to produce a counterclockwise rotation. The trailing (T) and leading (L) moments due to stresses along the spirals M(MN) and M(ML), respectively, are

$$M^T_{k,s} = W^T_{k,s}\overline{x}_1 - H^T_{k,s}\overline{z}_1 + M^T_c \qquad (214)$$

$$M^L_{k,s} = W^L_{k,s}\overline{x}_2 - H^L_{k,s}\overline{z}_2 + M^L_c \qquad (215)$$

with $W_{k,s}$ and $H_{k,s}$ forces given by Eqs. (183) to (196). M^T_c and M^L_c are the moments due to cohesion stresses along the spirals M(MN) and M(ML) with respect to poles I_1 and I_2, respectively:

$$M^T_c = -\frac{r^2_M\left\{\exp\left[2(\theta_{NN} - \theta_M)\tan\phi\right] - 1\right\}}{2\tan\phi}c$$

$$M^L_c = \frac{\overline{r}^2_M\left\{\exp\left[2(\theta_{LL} - \theta_M)\tan\phi\right] - 1\right\}}{2\tan\phi}c$$

Regarding the moments produced by the stresses along the sliplines L(ML) and N(MN),

$$M^L_{k,p} = W^L_{k,p}x^L_p - H^L_{k,p}z^L_p \qquad (216)$$

$$M^T_{k,p} = W^T_{k,p}x^T_p - H^T_{k,p}z^T_p \qquad (217)$$

where $W_{k,p}$ and $H_{k,p}$ are forces given by Eqs. (163), (164), (171), and (172), and

$$x^L_p = x_L + \frac{(x_{ML} - x_L)(2p_{ML} + p_{LL})}{3(p_{ML} + p_{LL})} \qquad (218)$$

$$z^L_p = z_L + \frac{(z_{ML} - z_L)(2p_{ML} + p_{LL})}{3(p_{ML} + p_{LL})} \qquad (219)$$

$$x^T_p = x_N + \frac{(x_{MN} - x_N)(2p_{MN} + p_{NN})}{3(p_{MN} + p_{NN})} \qquad (220)$$

$$z^T_p = z_N + \frac{(z_{MN} - z_N)(2p_{MN} + p_{NN})}{3(p_{MN} + p_{NN})} \qquad (221)$$

2. Moments due to body forces. Moments due to soil body forces relate also to the roller axle at C. Following the same procedure used to generate the body forces, the moments due to soil weight contained within the active zones are:

For the leading zone L(ML)M,

$$M^L_{k,\gamma} = \gamma b\left\{\int_{\theta'_M}^{\theta'_{LL}}\frac{1}{2}\overline{r}^2(\overline{x}_2 + \frac{2}{3}\overline{r}\cos\theta')\,d\theta' - \overline{M}_c\right\} \qquad (222)$$

where $\overline{r}$ is given by Eq. (33), and

$$\overline{M}_c = \frac{1}{6}\overline{r}_M\overline{r}_c\sin(\theta_L - \theta_M)(x_M + x_L + \overline{x}_2) + \overline{A}_c\overline{x}_c$$

with $\overline{A}_c$ given by Eq. (200) and

$$\overline{x}_c = \frac{4}{3}R\frac{\sin^3\left(\frac{\xi_L - \xi_M}{2}\right)\cos\left(\frac{\xi_L + \xi_M}{2}\right)}{\xi_L - \xi_M - \sin(\xi_L - \xi_M)}$$

Integrating Eq. (222) results in

$$M^L_{k,\gamma} = \gamma b\left[\frac{\overline{r}^2_M\overline{x}_2}{4\tan\phi}\left\{\exp\left[2(\theta'_{LL} - \theta'_M)\tan\phi\right] - 1\right\} - \overline{M}_c - \frac{\overline{r}^3_M}{3(9\tan^2\phi + 1)}\left\{\exp\left[3(\theta'_{LL} - \theta'_M)\tan\phi\right](3\tan\phi\cos\theta'_{LL} + \sin\theta'_{LL}) - (3\tan\phi\cos\theta'_M + \sin\theta'_M)\right\}\right] \qquad (223)$$

For the trailing zone M(MN)N,

$$M_{k,\gamma}^{T} = \gamma b \left\{ \int_{\theta_{NN}}^{\theta_M} \frac{1}{2} r^2 \left(\bar{x}_1 + \frac{2}{3} r \cos \theta \right) d\theta - M_c \right\} \tag{224}$$

where r is given by Eq. (28), and

$$M_c = \frac{1}{6} r_M r_c \sin (\theta_M - \theta_{NN}) (x_M + x_N + \bar{x}_1) + A_c x_c$$

A_c is given by Eq. (208), and

$$x_c = \frac{4}{3} R \frac{\sin^3 \left(\frac{\xi_M - \xi_N}{2} \right) \cos \left(\frac{\xi_M + \xi_N}{2} \right)}{\xi_M - \xi_N - \sin (\xi_M - \xi_N)}$$

Integrating Eq. (224),

$$M_{k,\gamma}^{T} = \gamma b \left[\frac{r_M^2 \bar{x}_1}{4 \tan \phi} \left\{ \exp \left[2(\theta_M - \theta_{NN}) \tan \phi \right] - 1 \right\} - M_c \right.$$

$$\left. - \frac{r_M^3}{\left[3(9 \tan^2 \phi + 1) \right]} \left\{ \exp \left[3(\theta_M - \theta_{NN}) \tan \phi \right] (3 \tan \phi \cos \theta_{NN} - \sin \theta_{NN}) + (\sin \theta_M - 3 \tan \phi \cos \theta_M) \right\} \right] \tag{225}$$

The driving torque will be used in Section VI-B to determine the roller driving power requirements.

H. Soil-Roller Interface Stresses

Once the pattern and extent of the active plastic domain zone are derived, the soil-roller interface stress at a generic rim point i are (Eqs. 65 and 66)

$$\sigma_i = p_i \left[1 + \sin \phi \sin \psi_i \right] - c \cot \phi \tag{226}$$

$$\tau_i = p_i \sin \phi \cos \psi_i \tag{227}$$

where

$$\psi_i = 2\theta_i - 2\Omega_i + \phi \tag{228}$$

with

$$\Omega_i = \alpha + \xi_i \tag{229}$$

For the leading zone,

$$\theta_i = \alpha + \xi_i - \sin^{-1} \left[\frac{1}{R} \left(\bar{z}_2 \cos \theta_i' - \bar{x}_2 \sin \theta_i' \right) \right] + \frac{\pi}{2} - \phi$$

and for the trailing zone,

$$\theta_i = \alpha + \xi_i - \sin^{-1} \left[\frac{1}{R} (\bar{z}_1 \cos \theta_i - \bar{x}_1 \sin \theta_i) \right]$$

which results in

$$\psi_i^L = -\sin^{-1} \left[\frac{1}{R} (\bar{z}_2 \cos \theta_i' - \bar{x}_2 \sin \theta_i') \right] + \pi - \phi \tag{230}$$

and

$$\psi_i^T = -\sin^{-1} \left[\frac{1}{R} (\bar{z}_1 \cos \theta_i - \bar{x}_1 \sin \theta_i) \right] + \phi \tag{231}$$

The parameter p along the slipline M(ML) is derived from Eq. (97), and for the slipline M(MN) from Eq. (108). On the leading zone, along a radial slipline which intersects the roller rim at a point i ($\xi_i \geq \xi_M$) and also the slipline M(ML) at point (M_i) is

$$p_i^L = p_{Mi}^L + \Delta p_i^L \tag{232}$$

where p_{Mi}^L corresponds to Eq. (97) for $\theta' = \theta_i'$, and

$$\Delta p_i^L = \gamma (x_i - x_{Mi}) (\tan \theta_i' + \tan \phi) \tag{233}$$

with

$$x_{Mi} = \bar{x}_2 + \bar{r}_M \exp\left[(\theta_i' - \theta_M') \tan\phi\right] \cos\theta_i' \quad (234)$$

and x_i from Eq. (5) and $\bar{r}_M$ from Eq. (23).

Similar criteria apply to the trailing zone ($\xi_i < \pi/2$). Along the radial slipline intersecting the roller rim at point i and the slipline M(MN) at point (iM),

$$p_i^T = p_{iM}^T + \Delta p_i^T \quad (235)$$

where p_{iM}^T corresponds to Eq. (108) for $\theta = \theta_i$, and

$$\Delta p_i^T = \gamma(x_i - x_{iM})(\tan\theta_i - \tan\phi) \quad (236)$$

with

$$x_{iM} = \bar{x}_1 + r_M \exp\left[(\theta_M - \theta_i) \tan\phi\right] \cos\theta_i \quad (237)$$

and x_i from Eq. (5) and r_M from Eq. (20).

The orientation δ_i of the soil-roller interface stress resultant q_r is given by Eq. (122) in connection with Eqs. (226) and (227).

A. Basic Equations

It was shown in Section IV-C that the geometry and extent of the active and transition zones relate exclusively to the slipline directions at points L, M, and N, as defined by Expression (114) (Fig. 4). Also, if the set (Expression (114) is known, a velocity slipline pattern can be unambiguously built that satisfies the roller velocity conditions. To initiate a solution of a given soil-roller problem, as postulated in Section IV-A, a set of parameters s_k and ξ_M is selected first. These parameters define unique values of θ'_M (Eq. 12) and θ_M (Eq. 18) and also determine the position of poles $\bar{I}_1$ (Eqs. 29 and 30) and $\bar{I}_2$ (Eqs. 34 and 35).

To evaluate the four remaining unknown parameters of Expression (114), there are available four basic simultaneous equations. Two of them originate from satisfying the horizontal and vertical equilibrium conditions, as given by Eqs. (156) and (157). For completeness, Eqs. (156) and (157) are repeated as Eqs. (238) and (239):

$$\Sigma X = H^L_{k,s} + H^T_{k,s} + H^L_{k,p} + H^T_{k,p} + P\cos\alpha$$

$$= F_H(\theta'_{LO}, \theta'_{LL}, \theta'_M, \theta_{NN}) = 0 \tag{238}$$

$$\Sigma Z = W^L_{k,s} + W^L_{k,p} + W^L_{k,\gamma} + W^T_{k,s} + W^T_{k,p}$$

$$+ W^T_{k,\gamma} + W + P\sin\alpha$$

$$= F_W(\theta'_{LO}, \theta'_{LL}, \theta'_M, \theta_{NN}) = 0 \tag{239}$$

Substituting in Eq. (238) the corresponding H_k force components given by Eqs. (163), (171), (183), and (190), after a short transformation, results in

$$p_{LL} = \frac{G_2}{G_1} = F_L(\theta'_{LL}, \theta_{NN}) \geq p_0 \tag{240a}$$

where

$$G_1 = -C_8(F_2 \cdot \Delta p_{ML} + F_1) - F_{12}$$

$$- C_7(F_4 \cdot F_5 + F_6) - F_{13} - P\cos\alpha$$

and

$$G_2 = C_8 \cdot F_2 + C_{14}\sin(\theta'_{LL} - \phi) + C_7 \cdot F_5$$

$$+ C_{15}\sin(\theta_{NN} + \phi)$$

Since, in Eq. (240a), $p_{LL} > p_0 > 0$, G_1 and G_2 must have the same sign.

From Eqs. (81) and (83),

$$p_{LL} = p_0 \exp\left[(\theta'_{LO} - \theta'_{LL})\tan\phi\right] \tag{240b}$$

After equating (240a) and (240b),

$$\theta'_{LO} = \theta'_{LL} + \frac{1}{2\tan\phi}\ln\frac{G_1}{p_0 G_2} \tag{241}$$

Also, it is known from Eqs. (82) and (83) that

$$p_{NN} = p_0 \exp\left[(\theta_{NN} - \theta_{NO})\tan\phi\right] \tag{242}$$

According to Eq. (79),

$$p_{NN} = p_{MN} - \Delta p_{MN} \tag{243}$$

After equating (242) and (243),

$$\theta_{NO} = \theta_{NN} - \frac{1}{2\tan\phi}\ln\frac{p_{MN} - \Delta p_{MN}}{p_0} \tag{244}$$

Thus, we arrive at a system of four equations (Eqs. 239, 240a, 241, and 244) in the unknown parameters θ'_{LO}, θ'_{LL}, θ_{NN}, θ_{NO}. These equations are solved by iteration using a computer program. Admissible values of θ'_{LL} are first selected within the corresponding bounds stated in Section V-C. Subsequently, θ_{NN} is determined from Eq. (239). Substituting θ'_{LL} and θ_{NN} in Eq. (241), a unique θ'_{LO} value is determined which satisfies simultaneously the horizontal and vertical equilibrium equations. With θ'_{LL}, θ'_{LO}, and θ_{NN} known, θ_{NO} is determined from Eq. (244). During the solution process, the computer program verifies the fact that the determined angular parameters θ comprise only admissible values; otherwise, a new θ'_{LL} is selected or a new case (s_k, ξ_M) is initiated, as required. Equations (238) and (239) express the necessary conditions under which an

Equilibrium solution is admissible with regard to the soil-roller active plastic domain. It is of significance to point out that the existence of the set of values, Expression (114), which satisfies the equilibrium and the stress compatibility equations, does not necessarily imply that a solution to the problem has been found, unless the following conditions are also simultaneously met:

(1) The rate of dilation, as mentioned in Section IV-C must be positive throughout the plastic domain. (This is verified in the Appendix.)

(2) At no point outside the plastic regions shall the stress exceed yield.

(3) The free-surface points F and B (Fig. 4), which belong to both the rigid and plastic domains, must also be aligned with the original surface slope α; thus,

$$\tan \alpha = \frac{z_F - z_B}{x_F - x_B} \tag{245}$$

which assumes that, after the roller passage, the original trailing surface slope is not significantly altered. This was verified experimentally by Wong and Reece (Ref. 11) for roller tests on level surfaces. Here, this condition is assumed to prevail also for slopes.

Although conditions (1) and (2) do not bear directly on the solution process of the equations, they are fundamental to describing the requirements for the completeness of a solution. Condition (2) is not specifically verified, but may be considered satisfied if no sharp corners of rigid material develop within the rigid plastic boundary. In fact, it may be proved that the soil state of stress at point M does not exceed yield and, in general, it may be assumed that the rigid material can support the plastic deforming body. The method of extending the plastic stress field into the rigid domain, as studied by Shield (Ref. 20) and by Cox, et al. (Ref. 21), can also be applied to this problem.

Regarding Eq. (245), the coordinates of F and B are obtained, satisfying the boundary conditions on the leading and trailing traction-free surface slope. The positions of points F and B are satisfactorily approximated based on the following analysis. It was noted in Sections V-D and V-E that the horizontal and vertical stresses along L(ML) (Fig. 11) determine the reaction forces $H^L_{k,p}$ and $W^L_{k,p}$, respectively. Similarly, the stresses along M(MN) define the force components $H^T_{k,p}$ and $W^T_{k,p}$. These leading and trailing forces have a special significance with regard to the validity of any solution of Eqs. (238) and (239). If a solution is found, it has to be verified that the mentioned forces $H_{k,p}$ and $W_{k,p}$ can be sustained at the corresponding transition and passive plastic domains. In other words, it must be verified that all plastic zones satisfy simultaneously the basic requirements of local and overall equilibrium. In this context, a solution to Eqs. (238) and (239) represents only a necessary condition. Sufficiency is proven when, in addition, the solution of the two active zones can be appropriately coupled to the neighboring transition and passive fields, which satisfy Eqs. (63) and (64) and the remaining boundary conditions. Here, we advance the fact that the active plastic field solution can be extended up to and including the traction-free surfaces LF and NB (Fig. 4), if the input data is consistent. In Part II it will be shown that the completion of the plastic field also yields the statically correct deformed free surface and that Condition (245) can, in general, be satisfied.

B. Specific Energy Dissipation

The roller moves parallel to the original soil surface with uniform velocity $V_c = \omega R_e s_k$ where R_e is the effective rolling radius. For a rigid cylindrical roller $R_e = R$. The axle traverses a distance L per unit time,

$$L = \omega R_e s_k \tag{246}$$

The total soil thrust parallel to the original surface is

$$T = P + W \sin \alpha \tag{247}$$

with P = the drawbar pull force and W = the applied axle load. The load component normal to the original surface is

$$N = W \cos \alpha \tag{248}$$

The total energy input $\overline{E}_M$ per unit time due to an applied torque M at the roller axle is consumed by the thrust force energy output $\overline{E}_T$ and the soil-roller energy dissipation $E_{S/R}$:

$$\overline{E}_M = \overline{E}_T + E_{S/R} \tag{249}$$

where

$$\overline{E}_M = M\omega \tag{250}$$

and

$$\overline{E}_T = TL \tag{251}$$

In general, the soil energy dissipation per unit travel length Eq. (246) and per unit normal load Eq. (248) will be defined as the soil-roller specific energy dissipation coefficient:

$$E = \frac{E_{S/R}}{NL} = \frac{M}{WR_e s_k \cos \alpha} - \left(\frac{P}{W \cos \alpha} + \tan \alpha\right) \tag{252}$$

Equation (252) accounts for the soil and tire deformation and soil-wheel interface friction energy losses due to slip. It represents a general energy expression and defines the performance of any rolling, power-driven device; the equation applies to both rigid and flexible rollers or wheels. If the roller is flexible, E will express the specific energy dissipation produced by both the soil and the rolling device. Care must be taken to properly measure or calculate the effective turning radius R_e. For the rigid roller, the values of M and s_k in Eq. (252) are determined from the problem solution (Section VI-A).

When $\alpha = 0$, Eq. (252) reduces to

$$E_0 = \frac{M}{WR_e s_k} - \frac{P}{W} \tag{253}$$

Equation (253) was used by Leflaive (Ref. 22) to analyze test results of driven rigid and flexible wheels on horizontal soil surfaces. The specific energy (Eq. 252) shows two terms. One is the specific torque energy input at the axle per unit normal load and unit travel distance.

$$E_M = \frac{M}{WR_e s_k \cos\alpha} \tag{254}$$

The other is the specific thrust energy output per unit normal load and unit travel distance.

$$E_T = \frac{P}{W \cos\alpha} + \tan\alpha \tag{255}$$

Only when $\alpha = 0$ does the specific thrust energy equal the pull/load ratio $E_T = P/W$; otherwise, for $\alpha > 0$, Eq. (255) refers to the specific thrust energy. Equations (254) and (255) can be used to evaluate the performance of power-driven vehicles, providing the relative wheel slip factors and axle load distribution are known. The wheel thrust efficiency is given in general by

$$n\% = \frac{\frac{P}{W} + \sin\alpha}{\frac{M}{WR_e}} s_k \times 100 \tag{256}$$

In practice, the specific power consumption per kilometer of travel along a straight line on a slope $\alpha \geq 0$ is given by

$$P_w = E_M \times W \times \left(\frac{1}{3.6}\right)\left(\frac{\text{watt-hour}}{\text{km}}\right) \tag{256a}$$

where E_M is defined by Eq. (254) for $s_k > 0$ and W is the applied axle load in Newtons.

C. Rigid Roller Sinkage

The roller sinkage z is measured perpendicular to the original surface. Once the leading and trailing points F and B are determined, satisfying the basic equilibrium equations, it is verified if points F and B are aligned on a slope α (Fig. 14). To this effect, the coordinates of F and B yield

$$\tan\alpha' = \frac{z_B - z_F}{x_B - x_F}$$

where α' is the direction BF for a trial solution. Only when $\alpha' = \alpha$ does the solution found correspond to the given problem. Then, with

$$t = z_B + x_B \tan\alpha$$

and

$$n = t \cos\alpha$$

the sinkage is

$$z = R - n \tag{257}$$

The derivation of Eq. (257) presumes the condition stated in connection with Eq. (245).

D. Mobility Safety Factors

It was shown in Section VI-A that the soil-roller mobility problem can be solved satisfying the velocity and limiting equilibrium equations that are subjected to the corresponding boundary conditions. The solution determines the operational slip factor s_k and torque M for a given axle loading P and W. It was also shown (Section I) that, when $s_k = 0$, the roller becomes immobilized ($V_C = 0$). From a mobility safety standpoint, given the soil conditions (c, ϕ, γ, α) and a fixed set of operational loads, pull P_0 and weight W_0, it is required to determine the corresponding maximum load W_{max} (or P_{max}) which, in combination with P_0 and W_0, produces immobilization of the roller. Thus, there exist two basic loading conditions capable of immobilizing the roller: (1) increasing only the pull force from P_0 to P_{max}, and (2) increasing only the axle weight from W_0 to W_{max}. Consequently, two types of mobility safety factors (*SF*) can be defined, depending on the ultimate cause that stops the roller.

The first definition of SF is

$$SF = \frac{P_{max} + W_0 \sin\alpha}{P_0 + W_0 \sin\alpha} = \frac{T_{max}}{T_0} \tag{258}$$

where the numerator indicates that the maximum soil thrust T_{max} is reached by incrementing P_0, pull load, to P_{max}, setting $s_k = 0$. The denominator T_0 corresponds to the roller operating thrust for $0 < s_k < 1.0$. In this case, when $P_{max} = P_0$, SF = 1 and the roller would stop due to excessive pull.

The second definition of SF corresponds to

$$\overline{SF} = \frac{P_0 + W_{max} \sin\alpha}{P_0 + W_0 \sin\alpha} = \frac{\overline{T}_{max}}{T_0} \tag{259}$$

where, as in Eq. (258), the $\overline{T}_{max}$ corresponds to $s_k = 0$ by incrementing the axle weight W_0 to W_{max}. When $W_{max} = W_0$, SF = 1 and the roller stops due to excessive weight. In essence, both Eqs. (258) and (259) relate to the soil maximum thrust capacity developed for $s_k = 0$.

For the general case of self propulsion; $P_0 = 0$, the roller propels its own weight W_0. Under this condition:

(1) If $\alpha > 0$, Eq. (258) reduces to

$$SF = \frac{P_{max} + W_0 \sin \alpha}{W_0 \sin \alpha} \tag{260}$$

In Eq. (260), if for $s_k = 0$ it is determined that $P_{max} = 0$, then SF = 1. This condition defines a limiting roller slope angle climbing capability, $\alpha = \alpha_{max}$, for self-propulsion.

(2) If $\alpha = 0$, then $\overline{T}_{max} = 0$, and Eq. (259) has no practical significance, since on a level terrain self-propulsion is unrelated to soil thrust. This conclusion derives from the fact that, under the action of a vertical load, there is no net soil thrust mobilized. Under this condition, the leading and trailing soil reactions are balanced (Eq. 153) (Fig. 11):

$$H_k^L + H_k^T = 0$$

Therefore, in this case, the SF refers exclusively to the maximum vertical soil load capacity for $s_k = 0$. Thus, from Eq. (259),

$$\overline{SF} = \frac{W_{max}}{W_0} \tag{261}$$

Equation (261) is the factor of safety versus immobilization valid only for self-propulsion on level terrains ($\alpha = 0$).

For $P_0 > 0$ and $\alpha > 0$, the applicable SF definition corresponds to Eqs. (258) and (259), as specified.

Given $s_k = 0$ and ξ_M, the computer program determines W_{max} connected with an operational pull load P_0. On the same basis, given an operational load W_0, it is possible to determine the corresponding P_{max}, which immobilizes the roller.

E. Applications

The foregoing soil-roller analysis was programmed in Fortran II for use with the IBM 1620 computer. In the following, it is assumed that the soil-roller model developed also applies to a finite-width roller (wheel) as long as the predominant soil failure mode occurs in the fore-aft direction rather than in the lateral direction. The soil-wheel interaction performance (SWIP) program input data is: wheel axle loads (W, P), surface slope α, soil properties (γ, ϕ, c), and wheel dimensions (R, B). Two additional input parameters, ξ_M and slip factor s_k, are also required and are entered by means of the computer's teleprinter. The user, with a minimum of experience and iterating on ξ_M and s_k values, can determine a number of possible admissible solutions. In this report, results obtained satisfy the equilibrium Eqs. (238) and (239) (active zones) and the limiting conditions stated in V-C-3. It is expected that from all solutions which are found at least one will satisfy Condition (245). (Refer to Section VI-A.) It is also assumed that if more than one solution satisfies Condition (245), then the one with the minimum torque energy (Eq. 254) would represent the actual wheel performance.

Thus far, Condition (245) is not incorporated in the SWIP program. This will be done only after the plastic field is extended into the transition and passive regions, utilizing a program subroutine (Part II).

The SWIP program outputs the following:

(1) Stress parameters p, θ and soil-wheel rim interface normal and tangential (shear) stresses (psi) at points L, M, and N (Fig. 4).

(2) Geometric parameters. Coordinates of the center of instantaneous rotation $\underline{I}$, the leading and trailing spiral poles $\overline{I}_1$ and $\overline{I}_2$, and the radial angular directions ξ_L and ξ_N where the soil detaches from the wheel rim at the leading and trailing edges, respectively.

(3) The total and partial, vertical and horizontal soil reaction forces considering the effect of soil weight on both the leading and trailing regions (to an accuracy of 0.5%). The partial moments and total required driving torque. The specific energy input E_M (Eq. 254) and specific thrust energy E_P ($=E_T$) (Eq. 255).

The program outputs the nature of any incompatibility which may arise from either the equilibrium Eqs. (238) and (239) or from the limiting conditions stated in Section V-C-3. By this means, the user can, on an interactive basis, select appropriate new ξ_M, s_k values to bring about a solution.

In what follows, the SWIP program is applied to estimate:

(1) Driven rigid wheel performance tests carried out on horizontal terrains under controlled slip. The wheel axle is subjected to a vertical load W_0 and a pull force P_0 parallel to the undisturbed soil surface.

(2) Driven rigid wheel slope climbing performance. The wheel axis is subjected to a total vertical load $W = (W_0^2 + P_0^2)^{1/2}$ acting on a slope angle defined by $\alpha = \tan^{-1}(P_0/W_0)$, where W_0 and P_0 are loads corresponding to the horizontal test conditions defined in (1), above. The purpose of this slope climbing calculation is to verify if there is theoretically any performance difference when equivalent

wheel normal and pull loads act either on a horizontal or a sloping terrain.[2]

(3) Lunar roving vehicles (LRVs) on the assumption of driven rigid wheels rolling on a level lunar surface. This is applied particularly to the Apollo and Lunokhod-1 vehicles.

Table 1.0 provides a summary of the above-mentioned applications indicating typical wheel loads, dimensions, and soil properties to be used in connection with the given application.

Test case 1, Table 1.0, was performed by the Waterways Experiment Station (WES), Vicksburg, Mississippi, under controlled 25% slip ($s_k = 0.75$) (Ref. 18). The SWIP program applied to this test condition produced the results shown in Tables 1.1 through 1.3a, which correspond to $\xi_M = 99$, 101, and 102 deg. For intermediate values of ξ_M, such as 99 deg $\leq \xi_M \leq 102$ deg, there exists an infinity of solutions satisfying Eqs. (238) and (239). The indicated results correspond only to the bounding values pertaining to a given set of ξ_M and $s_k = 0.75$. Intermediate solutions were also obtained but unfortunately lack of space precludes their inclusion. As mentioned, these results have to also satisfy Condition (245). This condition will eliminate all those cases which do not meet the boundary requirements referred to in Section VI-A. It was also found that for $s_k = 0.75$ and $\xi_M = 98$ deg and $\xi_M = 107$ deg, there are no other compatible solutions, thus indicating the fact that the operational range on ξ_M is bounded and if a solution exists satisfying Condition (245), it must lie within the results given in Tables 1.1 through 1.3a.

The measured torque was $M = 600$ lb-in. and the results indicate that this value is appropriately bounded by the program output as shown. Additional rigid soil wheel tests were also checked using the SWIP program. Particularly, in the case of $W = 108$ lb, $P = 30$ lb, and 25% slip (Ref. 18), the measured torque was $M = 720$ lb-in. and also was satisfactorily approximated and bounded.

In general, concerning the mobilizable soil strength, it is typically assumed that the same c, ϕsoil parameters apply to both the trailing and leading regions. Any divergency between the leading and trailing limiting values of c and ϕ to be used is concerned with the question of how the soil parameters c and ϕ are modified due to the disturbance produced by the passage of the wheel's leading edge or by other wheels along the same track. For instance, with reference to the total torque, a difference in ϕ values does not appear to be very sensitive, as seen in Tables 1.1 – 1.3a for $\phi = 42.3$ deg and Tables 1.4 – 1.4a for $\phi = 35$ deg. However, in order to satisfy Condition (245) and thereby arriving at a complete solution, it may be necessary to resort to different c, ϕ values for the leading and trailing zones.

Regarding the wheel slope performance, Table 1.0, case 2, the computer results are shown in Tables 2.1 through 2.4a. First, it was found that there are no compatible slope solutions for a 25% slip as it occurs for $\alpha = 0$ test. This indicates that there is no analogy which relates equivalent loading between horizontal and sloping tests. Second, the slip performance for self-propulsion ($P = 0$) is a minimum when $\alpha = 0$ and slip increases for increasing slope angle. When both ξ_M and s_k are varied, as shown, solutions will be found between the values indicated. For self-propulsion conditions, the horizontal leading and trailing soil reactions are equal and of opposite direction. The slope climbing energy requirements are generally higher than for $\alpha = 0$ due to the combination of larger torques and wheel slippage.

A hypothetical application of the SWIP program to the Apollo LRV flexible wheels is given in case 3, Table 1.0, on the assumption of rigid wheel behavior. Results shown in Tables 3.1 to 3.2a represent self-propulsion conditions on a level lunar soil surface. Results indicate that the wheel operating range for this case is within 10% to 15% slip ($s_k = 0.90$ to 0.85). Calculations also indicate that the wheels could not operate at 20% slip for $\alpha = 0$. The soil-wheel rim interface stress level is rather low (<3/4 psi), and energy requirements are not unlike the expected mobility performance for on-earth operation.

Case 4 (Table 1.0) represents an application of the SWIP program to the Lunokhod-1 to investigate its mobility performance for $\alpha = 0$. To this effect, lunar soil properties similar to those applied to the Apollo LRV (case 3, Table 1.0) are considered. Under self-propulsion, it is assumed the wheel load is approximately $W = 35$ lb (15.6 kg) (Ref. 25). The wheel radius scales roughly $R = 10.0$ in. (25.4 cm) and width $B = 6\ 1/2$ in. (15.35 cm). The wheel is assumed to operate as a rigid finite-width roller. A pattern of grousers and a metal mesh covers the wheel rim which, on ground contact, confines a soil layer of an approximate thickness equivalent to the projecting grouser lugs. This condition insures the soil-wheel interface mechanical properties are at least equivalent to the lunar soil strength, thus eliminating any uncertainty connected with the soil-wheel interface adhesion. Since the Lunokhod-1 mobility performance is independent of the wheel's surface material, appropriate correlations of lunar soil properties can be made utilizing its mobility performance records in a lunar traverse.

The operational performance of the Lunokhod-1 is shown in Tables 4.1 and 4.1a. Results refer to $\xi_M = 112$ deg for 20% slip ($s_k = 0.80$). It is noted that no compatible solutions were found for $\xi_M = 110$ deg and $s_k = 0.80$.

A review of the results shown for the Apollo and Lunokhod-1 vehicles indicates that after extending the plastic field up to the traction-free surfaces, Condition (245) may be satisfied and a complete solution defined. Further applications of this program are planned to estimate the limiting wheel slope climbing performance conditions after incorporating Condition (245) (Part II).

[2]In this connection, vehicle mobility tests on slopes indicate that the vehicle performance degrades with increasing slope angles. Test results indicate that slope tests cannot strictly be simulated by equivalent wheel axle loading performed on horizontal terrains (Ref. 4).

VII. CONCLUSIONS

(1) A comprehensive theory for the solution of the soil-roller interaction problem has been presented. This solution is applicable to power-driven rollers moving on horizontal or sloping soft soil surfaces under quite general conditions of terrain slope angles, soil properties (cohesion, friction), and loading conditions including gravitational effects.

(2) In this study, Part I, the method of solution satisfies both the roller velocity (slip conditions) and equilibrium requirements within the active zones (Fig. 4). The solution was programmed for computer use. The nature of the developed soil-wheel interaction performance (SWIP) program is that it only outputs bounding values of wheel performance parameters. In Part II, it will be shown that these bounds can be narrowed further and that, from the point of view of the theory of plasticity, complete solutions can be obtained which satisfy overall equilibrium, velocity, and boundary conditions, which include both the transition and passive zones (Fig. 4).

(3) It is considered that a finite-width roller also represents, on a first approximation, the performance of a rigid wheel, which must be verified by tests. Limited application of the theory to rigid wheel tests on level terrains indicates that experimental results compare favorably with theoretical predictions. Experiments have to be performed considering mobility on level and sloping soil surfaces, taking into consideration the underlying concepts of the theory, as formulated, particularly with regard to (Fig. 4):

(a) Soil-wheel failure pattern on slopes.

(b) The existence and shifting of the bifurcation point M separating the leading from the trailing plastic zone along the soil-wheel interface.

(c) The position of the leading and trailing edge detachment points L and N, respectively.

(d) Laboratory determination and practical use of the soil parameters c and ϕ as related to potential soil disturbance affecting wheel performance.

These are just a few of the many items which must be considered before accepting this or any other theory.

(4) The limiting soil-roller interface radial and tangential (shear) stresses were defined and it was found that the obliquity angle of the resultant interface stresses with respect to the radial directions varies along the roller rim.

(5) A general normalized energy Expression (252) was derived which is of practical use for evaluating and correlating wheel (vehicle) test results for slopes ($\alpha \geq 0$). The nature of Expression (252) and limited application of the theory (Tables 1.1 – 1.3a and Tables 2.1 – 2.4a) indicate that the wheel thrust, torque, and efficiency performances relate to the particular slope α. This result points to the fact that wheel tests using equivalent normal and pull forces on horizontal and sloping terrains do not represent similar loading systems since the state of stress and limiting equilibrium conditions of a soil slope and a level terrain are different. Thus, horizontal wheel tests based on equivalent loadings cannot be used to predict wheel slope climbing performance.

(6) A safety factor (SF) concept against wheel immobilization is introduced which is applicable to any driven rigid or flexible wheel for varying loads and slopes. This SF concept sets the framework for the study of mobility as a basic mechanical process whereby a safety number can be assigned to each of the commonly used wheel efficiency performance parameters.

(7) Regarding the validity of the theory, particularly its reliability, the proposed method of solution has to be more extensively evaluated by applying the computer program to a wider range of mobility conditions, slope angles, load combinations, soil properties, and wheel slip values.

VIII. RECOMMENDATIONS

It is recommended that:

(1) The theory and computer program developed for driven rigid rollers (wheels) on soil slopes be extended to also include towed rigid rollers (wheels).

(2) Both the driven and towed rigid wheel solutions, referred to in (1) above, be generalized to consider flexible driven and towed wheels on soil slopes, thus covering the whole spectrum of potential wheel operations as may be applicable to different mobility modes on planetary surfaces.

(3) The solutions mentioned in (1) and (2) above for single wheels be coupled to consider the mechanical interaction between the wheels of a vehicle. Since each wheel of a vehicle system is subjected to varying loads, wheel slips, torque, terrain slopes, and soil properties, prediction of vehicle performance requires knowledge of coupled wheel mechanical behavior. This program will assist in (a) modeling vehicle-terrain interaction: vehicle design configuration, safety factor against immobilization, and power requirements; (b) defining planetary vehicle operation modes: route selection, decision risks, and data rate requirements; and (c) interpreting mobility operations and test results.

(4) The results of the theory be verified and validated by implementing a comprehensive soil-wheel interaction testing program.

APPENDIX

POSITIVE RATE OF DILATION

A. Introduction

Drucker and Prager (Ref. 13) applied the concept of plastic potential to Eq. (56) and derived the stress-strain laws connected with the rigid perfectly plastic material. On this basis, the axial plane strain rates are

$$\dot{\epsilon}_x = \frac{\partial u_x}{\partial x} = \frac{\lambda}{2}\left[\sin\phi - \sin(2\theta + \phi)\right] \qquad (A\text{-}1)$$

$$\dot{\epsilon}_z = \frac{\partial u_z}{\partial z} = \frac{\lambda}{2}\left[\sin\phi + \sin(2\theta + \phi)\right] \qquad (A\text{-}2)$$

where λ is a positive factor of proportionability, in general a function of time and position. For steady state $\lambda = \lambda(x, z)$. The rate of dilation based on Eqs. (A-1) and (A-2) is

$$\dot{\Delta} = \dot{\epsilon}_x + \dot{\epsilon}_z = \lambda \sin\phi \geq 0 \qquad (A\text{-}3)$$

From Eq. (A-3), for $\phi > 0$, $\dot{\Delta} > 0$. Shield (Ref. 7) expressed the velocity components u_x, u_z of a point at failure in terms of the slipline velocity components V^* and V' as follows:

$$u_x = \frac{V^* \cos(\theta + \phi) - V' \sin\theta}{\cos\phi} \qquad (A\text{-}4)$$

$$u_z = \frac{V^* \sin(\theta + \phi) + V' \cos\theta}{\cos\phi} \qquad (A\text{-}5)$$

Next Eq. (A-2) will be determined in connection with the strain rates derived from Eqs. (A-4) and (A-5).

B. Trailing Zone ($\xi_i \leq \pi/2$)

For a generic trailing point (ij) (Fig. 10), setting $\theta_{ij} = \theta$ in Eqs. (42) and (43),

$$V'_{ij} = V' = V'_i \exp\left[(\theta_i - \theta)\tan\phi\right] \qquad (A\text{-}6)$$

$$V^*_{ij} = V^* = 0 \qquad (A\text{-}7)$$

and substituting Eqs. (A-6) and (A-7) in Eqs. (A-4) and (A-5) results in

$$u_x = -V' \frac{\sin\theta}{\cos\phi} = -V_i \frac{\sin\theta}{\cos\phi} \exp\left[(\theta_i - \theta)\tan\phi\right] \qquad (A\text{-}8)$$

$$u_z = V' \frac{\cos\theta}{\cos\phi} = V'_i \frac{\cos\theta}{\cos\phi} \exp\left[(\theta_i - \theta)\tan\phi\right] \qquad (A\text{-}9)$$

With x, z coordinates of point (ij), $\theta_{ij} = \theta_j = \theta$:

$$\theta = \tan^{-1}\left(\frac{z - \bar{z}_1}{x - \bar{x}_1}\right) \qquad (A\text{-}10)$$

$$\frac{\partial u_x}{\partial x} = \dot{\epsilon}_x =$$

$$\frac{V_i'}{\cos \phi} \exp \left[(\theta_i - \theta) \tan \phi\right] (\tan \phi \sin \theta - \cos \theta) \frac{\partial \theta}{\partial x} \quad \text{(A-11)}$$

$$\frac{\partial u_z}{\partial z} = \dot{\epsilon}_z =$$

$$- \frac{V_i'}{\cos \phi} \exp \left[(\theta_i - \theta) \tan \phi\right] (\tan \phi \cos \theta + \sin \theta) \frac{\partial \theta}{\partial z} \quad \text{(A-12)}$$

From Eq. (A-10), with $x - \bar{x}_1 = r_i \exp [(\theta_i - \theta) \tan \phi] \cos \theta$,

$$\frac{\partial \theta}{\partial x} = - \frac{\sin \theta}{r_i} \exp \left[(\theta - \theta_i) \tan \phi\right] \quad \text{(A-13)}$$

$$\frac{\partial \theta}{\partial z} = \frac{\cos \theta}{r_i} \exp \left[(\theta - \theta_i) \tan \phi\right] \quad \text{(A-14)}$$

Substituting Eqs. (A-13) and (A-14) in Eqs. (A-11) and (A-12), respectively, Eq. (A-2) reduces to

$$\dot{\Delta}_{ij} = - \frac{V_i'}{r_i \cos \phi} \tan \phi \quad . \quad \text{(A-15)}$$

Introducing Eq. (38) in Eq. (A-10), and with Eq. (40),

$$\dot{\Delta}_{ij} = \frac{V_i}{r_i \cos \beta_i} \tan \phi = \frac{V_i \tan \phi}{r_i \cos (\bar{\rho}_i - \theta_i' + \phi)} = \dot{\Delta}_i \quad \text{(A-16)}$$

or

$$\dot{\Delta}_i = \frac{V_i \tan \phi}{r_i \sin (\theta_i - \bar{\rho}_i)} \geq 0 \quad \text{(A-17)}$$

Equations (A-15), (A-16), and (A-17) indicate that under steady state conditions the dilation rate $\dot{\Delta}_{ij}$ at a point (ij) reduces to the dilation $\dot{\Delta}_i$ of a point i on the soil-roller interface. Also for $\phi = 0$, $\dot{\Delta}_{ij} = 0$, representing the incompressibility condition of a Tresca material with c = shear yield stress.

To satisfy Eq. (A-17), $\sin (\theta_i - \bar{\rho}_i)$ must be greater than zero; this condition in general holds true as may be verified graphically or analytically in most practical cases.

C. Leading Zone ($\xi_i \geq \xi_M$)

For a generic leading point (ij) (Fig. 10), setting $\theta_{ij} = \theta$ in Eqs. (48) and (49),

$$V_{ij}^* = V^* = V_i^* \exp \left[(\theta - \theta_i) \tan \phi\right] \quad \text{(A-18)}$$

$$V_{ij}' = V' = 0 \quad \text{(A-19)}$$

Replacing Eqs. (A-18) and (A-19) in Eqs. (A-4) and (A-5), with $\theta + \phi = \theta' + \pi/2$,

$$u_x = \frac{V^*}{\cos \phi} \cos (\theta + \phi) =$$

$$- \frac{V_i^* \sin \theta'}{\cos \phi} \exp \left[(\theta - \theta_i) \tan \phi\right] \quad \text{(A-20)}$$

$$u_z = \frac{V^*}{\cos \phi} \sin (\theta + \phi) =$$

$$\frac{V_i^* \cos \theta'}{\cos \phi} \exp \left[(\theta - \theta_i) \tan \phi\right] \quad \text{(A-21)}$$

With (x, z) coordinates of (ij),

$$\theta_i = \tan^{-1} \left(\frac{z - \bar{z}_2}{x - \bar{x}_2}\right) \quad \text{(A-22)}$$

$$\frac{\partial u_x}{\partial x} = \dot{\epsilon}_x =$$

$$\frac{V_i^* \exp \left[(\theta - \theta_i) \tan \phi\right]}{\cos \phi} \left[- \tan \phi \sin \theta' - \cos \theta'\right] \frac{\partial \theta}{\partial x} \quad \text{(A-23)}$$

$$\frac{\partial u_z}{\partial z} = \dot{\epsilon}_z =$$

$$\frac{V_i^* \exp \left[(\theta - \theta_i) \tan \phi\right]}{\cos \phi} \left[\tan \phi \cos \theta' - \sin \theta'\right] \frac{\partial \theta}{\partial z} \quad \text{(A-24)}$$

From Eqs. (A-23) and (A-24) with $x - \bar{x}_2 = \bar{r}_i \exp [(\theta - \theta_i) \tan \phi] \cos \theta'$,

$$\frac{\partial \theta}{\partial x} = - \frac{\sin \theta'}{\bar{r}_i} \exp \left[(\theta_i - \theta) \tan \phi\right] \quad \text{(A-25)}$$

$$\frac{\partial\theta}{\partial z} = \frac{\cos\theta'}{\bar{r}_i} \exp\left[(\theta_i - \theta)\tan\phi\right] \qquad \text{(A-26)}$$

After substituting Eqs. (A-25) and (A-26) in Eqs. (A-23) and (A-24), respectively, Eq. (A-2) reduces to

$$\dot{\Delta}_{ij} = \frac{V_i^*}{\bar{r}_i \cos\phi} \tan\phi \qquad \text{(A-27)}$$

and with Eq. (46),

$$\dot{\Delta}_{ij} = \frac{V_i}{\bar{r}_i} \frac{\cos(\alpha + \xi_i - \bar{\rho}_i)}{\sin(\alpha + \xi_i - \theta_i')} \tan\phi = \dot{\Delta}_i \qquad \text{(A-28)}$$

To satisfy Eq. (A-2), $|\alpha + \xi_i - \bar{\rho}_i| \leq \pi/2$, which is satisfied for $0 \leq s_k \leq 1.0$.

As for the trailing zone, Eqs. (A-27) and (A-28) also indicate that the dilation rate $\dot{\Delta}_{ij}$ at point (ij) reduces to the dilation rate $\dot{\Delta}_i$ at point i on the soil-roller rim interface.

In particular, for rim point i = M, $\theta_M' = \bar{\rho}_M$ and Eqs. (A-16) and (A-28) yield, with Eqs. (20) and (23),

$$\dot{\Delta}_M^T = \frac{V_M}{r_M} \frac{\tan\phi}{\cos\phi} = \frac{V_M}{a_M} \tan\phi \qquad \text{(A-29)}$$

$$\dot{\Delta}_M^L = \frac{V_M}{\bar{r}_M} \cot\Delta \tan\phi = \frac{V_M}{a_M} \tan\phi \qquad \text{(A-30)}$$

or

$$\dot{\Delta}_M = \Delta_M^L = \Delta_M^T$$

Consequently, as expected, since the state of stress along the soil-roller interface is uniform and continuous, the soil dilation rate at point M is the same when approaching M along (ML)M or along (MN)M (Fig. 4). Also, since $\dot{\Delta}_i$ is proportional to ω (rad/s), it would be of interest to verify to what extent the theory of plastic potential (Ref. 13) is applicable to the prediction of soil deformation under conditions of steady-state motion. It is known that for continued straining under unsteady conditions the dilation predictions far exceed the measured increments (Ref. 23).

NOMENCLATURE

a_M	velocity arm
B or b	roller width
C	roller center
c	cohesion
ds, ds'	elemental arc lengths along first and second sliplines
E	soil-roller specific energy dissipation coefficient
E_M	energy input per unit time due to moment M at roller axis
$E_{S/R}$	soil-roller energy dissipation
E_P or E_T	specific thrust force energy output
H	horizontal force soil reaction
I	center of instantaneous rotation
$\bar{I}_1, \bar{I}_2$	leading and trailing spiral poles
i	point on roller rim
ij	point of intersection of i and j
j	point along slipline
L	distance parallel to slope α
M	moment
N	normal load
P*	roller load per unit width
P	pull force on roller axle, parallel to slope (P = bP*)
P_w	power consumption per kilometer
p	stress parameter
q_r	stress resultant (soil-roller interface)
R	roller radius
R_e	effective rolling radius
R_ϕ	radius of "ϕ circle" (Fig. 13)
$\bar{r}_i, r_i$	leading and trailing spiral radial vectors of point i
SF	safety factor related to P_{max}
$\overline{SF}$	safety factor related to W_{max}
s	slip %
s, s'	first and second slipline curvilinear coordinates
s_k	slip factor = 1 - s
T	thrust force
$u_{x,i}, u_{z,i}$	velocity components of point i in x and z directions
V_C	translational velocity of roller center C
V_i	absolute velocity of point i
V_i^*, V_i'	velocity components of point i along first and second sliplines
W	roller axle weight, vertical reaction
x, z	Cartesian coordinates
z	roller sinkage
α	terrain slope
$\bar{\beta}_T, \bar{\beta}_L$	angular orientation of $\bar{I}_1$, $\bar{I}_2$ with reference to x-axis (Fig. 5)
γ	soil unit volume weight
Δ	increment
$\dot{\Delta}$	rate of dilation
Δ_M	angle as defined in Eq. (15)
δ	obliquity angle of q_r with respect to a radial roller direction
$\dot{\epsilon}_x, \dot{\epsilon}_z$	axial strain rates, x and z directions
θ	stress parameter

θ_i, θ_i' angular orientations of first and second sliplines at point i

λ positive factor of proportionability

μ $= \pi/4 - \phi/2$

ξ_i angular orientation of rim point i (Fig. 2)

ξ_M angular orientation of rim point M (Bifurcation point) (Fig. 4), deg

ρ, ρ' spiral radii of curvature for first and second sliplines

$\bar{\rho}_i$ angular orientation of velocity V_i of rim point i

σ normal stress

τ shear stress

ϕ soil friction angle

$\eta\%$ thrust efficiency

Ω angular orientation of a vector normal to a surface

ω angular velocity, rad/s

Superscripts

L leading

T trailing

Subscripts

k see Section V-D

p passive

s spiral

T transition

REFERENCES

1. Brereton, R. G., Burke, J. D., Coryell, R. B., and Jaffe, L. D., "Lunar Traverse Missions," in JPL Quarterly Technical Review, Vol. 1, No. 1, pp. 125-137. Jet Propulsion Laboratory, Pasadena, Calif., Apr. 1971.

2. Bekker, M. G., Introduction to Terrain-Vehicle Systems. The University of Michigan Press, Ann Arbor, Mich., 1969.

3. Costes, N. C., Carrier, W. D., Mitchell, J. K., and Scott, R. F., "Apollo 11 Soil Mechanics Investigations," Science, Vol. 16, pp. 739-741, Jan. 30, 1970.

4. Kloc, I., Vehicle Mobility Tests — Soft Soil Slopes," JPL Internal Document 760-51. Jet Propulsion Laboratory, Pasadena, Calif., June 25, 1970.

5. "Tass Presents Detail Description of Lunokhod-1," Supplement. Soviet-Block Research in Geophysics, Astronomy, and Space, No. 248, pp. 59-74. JPRS 52634, U. S. Department of Commerce, Mar. 16, 1971.

6. Kötter, F., "Die Bestimmung des Druckes an Gekrumten Gleitflächen, eine Aufgabe aus der Lehre vom Erddruck," Ber. Akad. Wiss., pp. 229-233, 1903.

7. Shield, R. T., "Mixed Boundary Value Problems in Soil Mechanics," Quart. Appl. Math., Vol. 11, pp. 61-75, 1953.

8. Marshall, E. A., "Rolling Contact With Plastic Deformation," J. Mech. Phys. Solids, Vol. 16, pp. 243-254, 1968.

9. Dagan, C., and Tulin, M. P., "A Study of the Steady Flow of a Rigid-Plastic Clay Beneath a Driven Wheel," J. Terramech., Vol. 6, No. 2, pp. 9-27, 1969.

10. Boucherie, M., Étude de la Locomotion Sous Terrains — Evolution de Roues Rigides en Milieux Pulverulents a Deux et Trois Dimensions, Thesis. Faculté de Sciences, Grenoble, France, 1964.

11. Wong, J. Y., and Reece, A. R., "Soil Failure Beneath Rigid Wheels," in Proceedings of the Second International Conference on Terrain Vehicle Systems, pp. 425-445, University of Toronto Press, Toronto, Canada, 1966.

12. Hill, R., The Mathematical Theory of Plasticity, pp. 161-163, Oxford University Press, Oxford, England, 1950.

13. Drucker, D. C., and Prager, W., "Soil Mechanics and Plastic Analysis or Limit Design," Quart. Appl. Math., Vol. 10, pp. 157-165, 1952.

14. Poletayev, A. F., "The Compaction of Soil Under a Rolling Wheel," J. Terramech., Vol. 1, No. 3, p. 7, 1964.

15. Onafeko, O., and Reece, A. R., "Soil Stresses and Deformations Beneath Rigid Wheels," J. Terramech., Vol. 4, No. 1, pp. 59-80, 1967.

16. Wong, J. Y., "Some Problems in the Mechanics of Soil-Wheel Interaction," in Proceedings of the Third Conference on Terrain Vehicle Systems, pp. 305-317. Haus der Technik, Essen, West Germany, 1969.

17. Terzaghi, K., Theoretical Soil Mechanics, John Wiley & Sons, Inc., New York, N. Y., 1943.

18. Leflaive, E. M., Mechanics of Wheels on Soft Soils, Report 2, Effect of Width on Rigid Wheel Performance, Technical Report 3-729. U. S. Army Engineer Waterways Experiment Station, Vicksburg, Miss., Nov. 1967.

19. Nadai, A., Theory of Flow and Fracture of Solids, Vol. II, pp. 454-456, McGraw-Hill Book Co., Inc., New York, N. Y., 1963.

20. Shield, R. T., "On the Plastic Flow of Metals Under Conditions of Axial Symmetry," Proc. Royal Soc. London, Ser. A, Vol. 233, pp. 267-287, 1955.

21. Cox, A. D., Eason, G., and Hopkins, H. G., "Axially Symmetric Plastic Deformation in Soils," Phil. Trans. Royal Soc. A, Vol. 254, pp. 1-45, 1961.

22. Leflaive, E. M., Mechanics of Wheels on Soft Soils, A Method of Analyzing Test Results, Technical Report 3-729, pp. 3-4, U. S. Army Engineer Waterways Experiment Station, Vicksburg, Miss., Jun. 1966.

23. Haythornthwaite, R. M., "Stress and Strain in Soils," in Plasticity, Proceedings of the Second Symposium on Naval Structural Mechanics, pp. 185-193, Pergamon Press, London, England, 1960.

24. Private communication from D. R. Freitag, Waterways Experiment Station (WES), Vicksburg, Mississippi, Nov. 9, 1969.

25. Photographs of Lunokhod from Tass from Sovfoto - Pravada, The New York Times, New York, Feb. 13, 1971.

Table 1.0. Soil-wheel input data for SWIP program application

Case	Application	Loads		Wheel		Soil				Slip s, %	Torque M, lb-in.	Remarks
		W, lb	P, lb	R, in.	B, in.	α, deg	γ, lb/in.^{3}	ϕ, deg	c, psi			
1	Horizontal test[a]	94.0	35.0	13.95	12.0	0	0.0584[b]	42.3[b]	0.06[b]	25	600	Tables 1.1-1.3a
		94.0	35.0	13.95	12.0	0	0.0584	35.0	0.06	See remarks	See remarks	Tables 1.4-1.4a
2	Slope	100.3	0	13.95	12.0	20.4	0.0584	42.3	0.06	See remarks	See remarks	Tables 2.1-2.4a
3	Apollo LRV	60.0	0	16.00	10.0	0	0.01	33.0	0.05	See remarks	See remarks	Tables 3.1-3.2a
4	Lunokhod-1	35.0	0	10.00	6.5	0	0.01	33.0	0.05	See remarks	See remarks	Tables 4.1 and 4.1a

[a]Reference 18.

[b]Reference 24.

Table I.1. Horizontal test for ξ_M = 99 and s_k = 0.75 (upper bound)

```
                         ***INPUT PARAMETERS***

W,P,XI(M),SK =             94.0000    35.0000    98.9999       .7500
ALPHA,GAMMA,PHI,C =         0.0000      .0584    43.1999       .0600
R,B =                                 13.9500    12.0000


                         ***STRESS PARAMETERS***

THETA(LOP)=   138.8836    THETA(LLP)=  100.9219    THETA(MP)=    33.3508
THETA(M)   =   80.1508    THETA(NM)  =   32.7970   THETA(NO)=     7.2770

PL  =       .2025    PLL  =       .7029    PML  =      1.0277
PM  =       .9936    PMN  =       .6941    PNM  =       .4675

NORMAL STRESSES AT L,M,N      =       .2214        .9949        .2219
TANGENTIAL STRESSES AT L,M,N=        .2390        .6770        .2634


                       ***GEOMETRIC PARAMETERS***

CENTER OF INSTANTANEOUS ROTATION---  XB  =    0.0000    ZB  =    10.4625
TRAILING SPIRAL POLE---              XP1=   -3.1136    ZP1=      8.4132
LEADING SPIRAL POLE---               XP2=   -3.6829    ZP2=     12.7905
BIFORCATION POINT---                 XM  =   -2.1822    ZM  =    13.7782
LEADING EDGE---                      XL  =   -3.8046    ZL  =    13.4211
LEADING SPIRAL COORDINATES---        XML=   -4.7131    ZML=     18.1296
TRAILING EDGE---                     XN  =    4.3825    ZN  =    13.2436
TRAILING SPIRAL COORDINATES---       XMN=    6.8327    ZMN=     14.8225

XI(L)=   105.8268         XI(N)=    71.6897

                        ***VERTICAL REACTION***


WKPL= -20.0822 WKGL=    4.5211 WKSL= -39.9925 TOTAL LEADING =  -55.5535
WKPT=    1.7050 WKGT=    6.8574 WKST= -47.0518 TOTAL TRAILING=  -38.4894

                       ***HORIZONTAL REACTION***


HKPL=  27.0809 HKL  =  -9.0225                      TOTAL LEADING =   18.0583
HKPT= -13.1595 HKT  = -39.8988                      TOTAL TRAILING=  -53.0583


                             ***MOMENTS***

MGL  = -18.2792 MSL  = 276.7167 MPL  =-345.1012 TOTAL LEADING =  -86.6636
MGT  =  19.5666 MST  = 423.4217 MPT  = 195.0420 TOTAL TRAILING=  638.0304


TOTAL TORQUE =    551.3667 LB-INCHES =     76.2293 KG-METERS

EM,EP,                   =        .5606        .3723
```

Table 1.1a. Horizontal test for ξ_M = 99 and s_k = 0.75 (lower bound)

```
                    ***INPUT PARAMETERS***

H,P,XI(0),SK =            94.0000    35.0000    98.9999      .7500
ALPHA,GAMMA,PHI,C =        0.0000      .0586    43.1999      .0600
R,K =                                13.9500    17.0000


                    ***STRESS PARAMETERS***

THETA(LOP)=   142.1724   THETA(LLP)=  110.2319   THETA(MP)=    33.3508
THETA(M)  =    80.1508   THETA(NM) =   20.4582   THETA(NO)=    18.8118

PO  =      .2025    PLL  =     .5770    PML  =      .9969
PM  =      .9300    PMN  =     .4883    PNM  =      .2137

NORMAL STRESSES AT L,M,N     =      .2465      .9271      .0621
TANGENTIAL STRESSES AT L,M,N=       .2914      .6337      .1171


                    ***GEOMETRIC PARAMETERS***

CENTER OF INSTANTANEOUS ROTATION--- XB  =   0.0000   ZB  =   1[illegible].[illegible]25
TRAILING SPIRAL POLE---             XP1=   -3.1136   ZP1=     8.4132
LEADING SPIRAL POLE---              XP2=   -3.6829   ZP2=    12.7905
BIFURCATION POINT---                XM  =  -2.1822   ZM  =   13.7782
LEADING EDGE---                     XL  =  -3.9047   ZL  =   13.3923
LEADING SPIRAL COORDINATES---       XML=   -5.8733   ZML=    18.7336
TRAILING EDGE---                    XN  =   6.8736   ZN  =   12.1390
TRAILING SPIRAL COORDINATES---      XMN=   10.4574   ZMN=    13.4759

XI(L)=   106.2547        XI(N)=    60.4796

                    ***VERTICAL REACTION***


WKPL=  -16.8019 WKGL=    6.4663 WKSL= -47.2141 TOTAL LEADING =   -57.5497
WKPT=    2.4648 WKGT=   12.6762 WKST= -52.0350 TOTAL TRAILING=   -36.8939

                    ***HORIZONTAL REACTION***


HKPL=  31.9877 HKL  =  -4.7201                  TOTAL LEADING =    27.2675
HKPT=  -9.5026 HKT  = -52.7648                  TOTAL TRAILING=   -62.2675


                    ***MOMENTS***

MGL  = -23.3186 MSL  = 253.9022 MPL  =-437.7999 TOTAL LEADING = -207.2164
MGT  =  62.0401 MST  = 510.0199 MPT  = 144.4692 TOTAL TRAILING=  716.5293


TOTAL TORQUE =    509.3129 LB-INCHES =     70.4151 KG-METERS

FM,FP,                  =         .5178        .3723
```

Table 1.2. Horizontal test for $\xi_M = 101$ and $s_k = 0.75$ (upper bound)

```
                    ***INPUT PARAMETERS***

W,P,XI(M),SK =             94.0000    35.0000   100.9999      .7500
ALPHA,GAMMA,PHI,C =         0.0000      .0584    43.1999      .0600
R,B =                                 13.9500    12.0000


                    ***STRESS PARAMETERS***

THETA(LOP)=   130.6559   THETA(LLP)=    87.8879   THETA(MP)=    39.4808
THETA(M)  =    86.2808   THETA(NM)  =   47.0870   THETA(NO)=    14.9337

PO  =      .2025   PLL  =      .8229   PML  =     1.0496
PM  =     1.0393   PMN  =      .8225   PNN  =      .5811

NORMAL STRESSES AT L,M,N      =       .1958     1.1446      .3601
TANGENTIAL STRESSES AT L,M,N=      -.0118      .6910      .3654


                  ***GEOMETRIC PARAMETERS***

CENTER OF INSTANTANEOUS ROTATION--- XR  =   0.0000   ZR  =   10.4625
TRAILING SPIRAL POLE---             XP1=  -3.0342   ZP1=    7.9629
LEADING SPIRAL POLE---              XP2=  -4.4147   ZP2=   12.2496
BIFURCATION POINT---                XM  =  -2.6617   ZM  =   13.6936
LEADING EDGE---                     XL  =  -4.3780   ZL  =   13.2451
LEADING SPIRAL COORDINATES---       XML=  -4.2297   ZML=   17.2675
TRAILING EDGE---                    XN  =   2.3469   ZN  =   13.7511
TRAILING SPIRAL COORDINATES---      XMN=   4.3990   ZMN=   15.9585

XI(L)=   108.2908        XI(N)=    80.3146

                   ***VERTICAL REACTION***


WKPL= -23.3242 WKGL=   3.1253 WKSL= -31.2873 TOTAL LEADING =  -51.4862
WKPT=  -1.6661 WKGT=   5.5013 WKST= -46.4165 TOTAL TRAILING=  -42.5812

                  ***HORIZONTAL REACTION***


HKPL=  20.1000 HKL  = -11.0983                 TOTAL LEADING =    9.0017
HKPT= -16.8108 HKT  = -27.1908                 TOTAL TRAILING=  -44.0017


                      ***MOMENTS***

MGL  = -16.9624 MSL  = 284.7550 MPL  =-207.9697 TOTAL LEADING =   59.8229
MGT  =   6.8709 MST  = 311.4613 MPT  = 245.0691 TOTAL TRAILING=  563.4014


TOTAL TORQUE =   623.2243 LB-INCHES =    86.1640 KG-METERS

EM,EP                  =       .6336       .3723
```

Table 1.2a. Horizontal test for ξ_M = 101 and s_k = 0.75 (lower bound)

```
                        ***INPUT PARAMETERS***

W,P,XI(M),SK =            94.0000    35.0000   100.9999       .7500
ALPHA,GAMMA,PHI,C =        0.0000      .0584    43.1999       .0600
R,B =                                13.9500    12.0000


                        ***STRESS PARAMETERS***

THETA(LOP)=  133.6438   THETA(LLP)=    99.0599   THETA(MP)=    39.4808
THETA(M)   =   86.2808   THETA(NN) =    34.6336   THETA(NO)=    27.6457

PO  =       .2025    PLL  =        .6292    PML  =        .9665
PM  =       .9283    PMN  =        .5826    PNN  =        .2546

NORMAL STRESSES AT L,M,N     =        .1594      1.0156       .1047
TANGENTIAL STRESSES AT L,M,N=        .1440       .6172       .1516


                      ***GEOMETRIC PARAMETERS***

CENTER OF INSTANTANEOUS ROTATION--- XR =    0.0000    ZR =    10.4625
TRAILING SPIRAL POLE---             XP1=   -3.0342    ZP1=     7.9629
LEADING SPIRAL POLE---              XP2=   -4.4147    ZP2=    12.2496
BIFURCATION POINT---                XM =   -2.6617    ZM =    13.6936
LEADING EDGE---                     XL =   -4.5635    ZL =    13.1824
LEADING SPIRAL COORDINATES---       XML=   -5.3643    ZML=    18.2046
TRAILING EDGE---                    XN =    4.5360    ZN =    13.1919
TRAILING SPIRAL COORDINATES---      XMN=    7.9823    ZMN=    15.5723

XI(L)=  109.0949          XI(N)=    71.0244

                        ***VERTICAL REACTION***


WKPL= -20.5356 WKGL=   5.1418 WKSL= -39.1615 TOTAL LEADING =  -54.5553
WKPT=     .5906 WKGT=  11.1683 WKST= -51.2684 TOTAL TRAILING=  -39.5094

                      ***HORIZONTAL REACTION***


HKPL=  25.5291 HKL  =  -8.1080                    TOTAL LEADING =   17.4211
HKPT= -13.1707 HKT  = -39.2503                    TOTAL TRAILING=  -52.4211


                           ***MOMENTS***

MGL  = -25.3294 MSL  = 288.8261 MPL  =-302.6423 TOTAL LEADING =  -39.1456
MGT  =  35.0876 MST  = 390.2206 MPT  = 195.3001 TOTAL TRAILING=  620.6084


TOTAL TORQUE =    581.4627 LB-INCHES =     80.3902 KG-METERS

EM,EP                   =         .5912        .3723
```

Table 1.3. Horizontal test for $\xi_M = 102$ and $s_k = 0.75$ (upper bound)

```
                     ***INPUT PARAMETERS***

W,P,XI(M),SK =          94.0000    35.0000  101.9999      .7500
ALPHA,GAMMA,PHI,C =      0.0000      .0584   43.1999      .0600
R,B =                              13.9500   12.0000


                     ***STRESS PARAMETERS***

THETA(LOP)=   127.6682   THETA(LLP)=    82.3019   THETA(MP)=    42.3430
THETA(M)  =    89.1430   THETA(NN) =    52.9346   THETA(NO)=    17.5547

PO =      .2025   PLL  =      .8960   PML  =     1.0786
PM =     1.0751   PMN  =      .8871   PNN  =      .6459

NORMAL STRESSES AT L,M,N     =      .2377     1.2323      .4490
TANGENTIAL STRESSES AT L,M,N=     -.1513      .7019      .4216


                   ***GEOMETRIC PARAMETERS***

CENTER OF INSTANTANEOUS ROTATION--- XB =   0.0000   ZB =   10.4625
TRAILING SPIRAL POLE---             XP1=  -2.9887   ZP1=    7.7388
LEADING SPIRAL POLE---              XP2=  -4.7633   ZP2=   11.9474
BIFURCATION POINT---                XM =  -2.9003   ZM =   13.6451
LEADING EDGE---                     XL =  -4.5980   ZL =   13.1704
LEADING SPIRAL COORDINATES---       XML=  -4.1134   ZML=   16.7556
TRAILING EDGE---                    XN =   1.6305   ZN =   13.8543
TRAILING SPIRAL COORDINATES---      XMN=   3.4561   ZMN=   16.2712

XI(L)=   109.2450          XI(N)=    83.2874

                     ***VERTICAL REACTION***


WKPL= -23.8804 WKGL=   2.4838 WKSL= -27.2761 TOTAL LEADING =  -48.6727
WKPT=  -3.5701 WKGT=   5.0575 WKST= -46.8998 TOTAL TRAILING=  -45.4124

                   ***HORIZONTAL REACTION***


HKPL=  16.9616 HKL = -11.0585                  TOTAL LEADING =    5.9030
HKPT= -18.3406 HKT = -22.5624                  TOTAL TRAILING=  -40.9030


                       ***MOMENTS***

MGL = -15.2603 MSL = 271.1994 MPL =-150.8970 TOTAL LEADING =  105.0420
MGT =   3.1780 MST = 272.4780 MPT = 268.1729 TOTAL TRAILING=  543.8289


TOTAL TORQUE =   648.8710 LB-INCHES =    89.7098 KG-METERS

FM,FP             =       .6597        .3723
```

Table 1.3a. Horizontal test for ξ_M = 102 and s_k = 0.75 (lower bound)

```
                    ***INPUT PARAMETERS***

W,P,XI(M),SK =            94.0000    35.0000   101.9999      .7500
ALPHA,GAMMA,PHI,C =        0.0000      .0584    43.1999      .0600
P,R =                                13.9500    12.0000


                    ***STRESS PARAMETERS***

THETA(LPP)=   130.8651    THETA(LLP)=    95.3359    THETA(MP)=    42.3430
THETA(M)  =    89.1430    THETA(NM)  =    38.9915    THETA(MO)=    33.4347

PLL =       .2025    PLL  =      .6491    PML  =      .9575
PM  =       .9263    PMM  =      .5989    PNM  =      .2430

NORMAL STRESSES AT L,M,N     =      .1468      1.0529      .1068
TANGENTIAL STRESSES AT L,M,N=       .0727       .6048      .1498


                    ***GEOMETRIC PARAMETERS***

CENTER OF INSTANTANEOUS ROTATION--- XB  =    0.0000    ZB  =    10.4625
TRAILING SPIRAL POLE---             XP1=   -2.9887    ZP1=      7.7388
LEADING SPIRAL POLE---              XP2=   -4.7633    ZP2=     11.9474
BIFURCATION POINT---                XM  =  -2.9003    ZM  =    13.6451
LEADING EDGE---                     XL  =  -4.8684    ZL  =    13.0728
LEADING SPIRAL COORDINATES---       XML=   -5.3220    ZML=     17.9289
TRAILING EDGE---                    XN  =    3.9708    ZN  =    13.3729
TRAILING SPIRAL COORDINATES---      XMN=     7.4559    ZMN=     16.1942

XI(L)=   110.4258          XI(N)=    73.4621

                    ***VERTICAL REACTION***


WKPL= -21.3843 WKGL=    4.7147 WKSL= -36.3175 TOTAL LEADING =  -52.9872
WKPT=    -.4287 WKGT=   11.5658 WKST= -52.2253 TOTAL TRAILING=  -41.0883

                    ***HORIZONTAL REACTION***


HKPL=  23.3345 HKL  =  -8.5112                  TOTAL LEADING =   14.8232
HKPT= -14.1953 HKT  = -35.6279                  TOTAL TRAILING=  -49.8232


                    ***MOMENTS***

MGL  = -25.9613 MSL  = 290.5152 MPL  =-256.0629 TOTAL LEADING =    8.4909
MGT  =  31.2519 MST  = 354.2337 MPT  = 210.1242 TOTAL TRAILING=  595.6100


TOTAL TORQUE =    604.1009 LB-INCHES =     83.5201 KG-METERS

SM,SP                =         .6142         .3723
```

Table 1.4. Horizontal test for ξ_M = 104 and s_k = 0.75 (upper bound)

```
                         ***INPUT PARAMETERS***

W,P,XI(M),SK =           94.0000     35.0000  103.9999      .7500
ALPHA,GAMMA,PHI,C =       0.0000      .0584    34.9999      .0600
R,B =                                13.9500   12.0000

                        ***STRESS PARAMETERS***

THETA(LOP)=  147.0000   THETA(LLP)=   92.4864   THETA(MP)=   47.6787
THETA(M)  =  102.6787   THETA(NN) =   38.3496   THETA(NO)=   14.7468

PO =      .2009   PLL =      .7616   PML =      .9852
PM =      .9567   PMN =      .6260   PNN =      .3577

NORMAL STRESSES AT L,M,N    =      .2845     1.1647      .1637
TANGENTIAL STRESSES AT L,M,N=    -.1940      .4635      .1742

                      ***GEOMETRIC PARAMETERS***

CENTER OF INSTANTANEOUS ROTATION--- XB =   0.0000    ZB =   10.4625
TRAILING SPIRAL POLE---             XP1=  -2.1518    ZP1=    8.0994
LEADING SPIRAL POLE---              XP2=  -5.4226    ZP2=   11.2867
BIFURCATION POINT---                XM =  -3.3748    ZM =   13.5356
LEADING EDGE---                     XL =  -5.4894    ZL =   12.8245
LEADING SPIRAL COORDINATES---       XML=  -5.6508    ZML=   16.5409
TRAILING EDGE---                    XN =   4.3598    ZN =   13.2512
TRAILING SPIRAL COORDINATES---      XMN=   7.4397    ZMN=   15.6879

XI(L)=  113.1730        XI(N)=   71.7880

                        ***VERTICAL REACTION***

WKPL= -17.3331 WKGL=   3.4031 WKSL= -31.6086 TOTAL LEADING =  -45.5386
WKPT=   2.2742 WKGT=  13.0597 WKST= -63.6575 TOTAL TRAILING=  -48.3235

                       ***HORIZONTAL REACTION***

HKPL=  23.1116 HKL =  -7.7770                TOTAL LEADING =   15.3346
HKPT= -15.6881 HKT = -34.6464                TOTAL TRAILING=  -50.3346

                            ***MOMENTS***

MGL = -22.3480 MSL = 272.3250 MPL =-244.5668 TOTAL LEADING =    5.4101
MGT =  32.6770 MST = 332.9537 MPT = 242.4732 TOTAL TRAILING=  608.1040

TOTAL TORQUE =   613.5141 LB-INCHES =    84.8215 KG-METERS

EM,ET,THRUST EFFICIENCY=       .6238        .3723        .5968
```

Table 1.4a. Horizontal test for ξ_M = 104 and s_k = 0.75 (lower bound)

```
                  ***INPUT PARAMETERS***

W,P,XI(M),SK =            94.0000    35.0000  103.9999      .7500
ALPHA,GAMMA,PHI,C =        0.0000      .0584   34.9999      .0600
R,B =                                13.9500   12.0000


                 ***STRESS PARAMETERS***

THETA(LOP)=  148.4617   THETA(LLP)=   96.3393   THETA(MP)=   47.6787
THETA(M)  =  102.6787   THETA(NN) =   32.7638   THETA(NO)=   21.2900

PO =      .2009   PLL =      .7183   PML =      .9691
PM =      .9313   PMN =      .5446   PNN =      .2659

NORMAL STRESSES AT L,M,N     =      .2444     1.1315      .0933
TANGENTIAL STRESSES AT L,M,N=     -.1379      .4512      .1253


               ***GEOMETRIC PARAMETERS***

CENTER OF INSTANTANEOUS ROTATION--- XB =   0.0000   ZB =   10.4625
TRAILING SPIRAL POLE---             XP1=  -2.1518   ZP1=    8.0994
LEADING SPIRAL POLE---              XP2=  -5.4226   ZP2=   11.2867
BIFURCATION POINT---                XM =  -3.3748   ZM =   13.5356
LEADING EDGE---                     XL =  -5.5887   ZL =   12.7815
LEADING SPIRAL COORDINATES---       XML=  -6.0313   ZML=   16.7657
TRAILING EDGE---                    XN =   5.3083   ZN =   12.9005
TRAILING SPIRAL COORDINATES---      XMN=   8.8594   ZMN=   15.1858

XI(L)=  113.6174        XI(N)=   67.6336

                 ***VERTICAL REACTION***


WKPL= -16.4021 WKGL=   4.0320 WKSL= -34.5012 TOTAL LEADING =  -46.8713
WKPT=   2.7157 WKGT=  16.0181 WKST= -65.5958 TOTAL TRAILING=  -46.8619

               ***HORIZONTAL REACTION***


HKPL=  25.0784 HKL =  -6.9340                TOTAL LEADING =   18.1443
HKPT= -13.2243 HKT =  -39.9200               TOTAL TRAILING=  -53.1443


                    ***MOMENTS***

MGL = -25.5632 MSL = 280.4473 MPL =-277.4984 TOTAL LEADING =  -22.6143
MGT =  52.2253 MST = 364.2121 MPT = 207.2344 TOTAL TRAILING=  623.6719


TOTAL TORQUE =    601.0575 LB-INCHES =     83.0993 KG-METERS

FM,FT,THRUST EFFICIENCY=        .6111        .3723        .6092
```

Table 2.1. Wheel performance on slope for ξ_M = 110 and s_k = 0.55 (upper bound)

```
                    ***INPUT PARAMETERS***

W,P,XI(M),SK =          100.3000    0.0000  109.9999      .5500
ALPHA,GAMMA,PHI,C =      20.4159     .0584   43.1999      .0600
R,B =                              13.9500   12.0000

                    ***STRESS PARAMETERS***

THETA(LOP)=  135.4994   THETA(LLP)=   91.8329   THETA(MP)=    61.6883
THETA(M)  =  108.4883   THETA(NN) =   81.2609   THETA(NO)=    43.3803

PO =      .2025   PLL =      .8475   PML =     1.0565
PM =     1.0314   PMN =      .9135   PNN =      .7011

NORMAL STRESSES AT L,M,N     =      .4372      .9594      .5715
TANGENTIAL STRESSES AT L,M,N=     -.4654      .7060      .4754

                    ***GEOMETRIC PARAMETERS***

CENTER OF INSTANTANEOUS ROTATION--- XB =   -2.6764    ZB =     7.1905
TRAILING SPIRAL POLE---             XP1=   -5.8977    ZP1=     1.2107
LEADING SPIRAL POLE---              XP2=  -10.3797    ZP2=     8.1417
BIFURCATION POINT---                XM =   -9.0442    ZM =    10.6209
LEADING EDGE---                     XL =  -10.4161    ZL =     9.2793
LEADING SPIRAL COORDINATES---       XML=  -10.5274    ZML=    12.7547
TRAILING EDGE---                    XN =   -4.0309    ZN =    13.3549
TRAILING SPIRAL COORDINATES---      XMN=   -3.5423    ZMN=    16.5337

XI(L)=  117.8875        XI(N)=    86.3796

                    ***VERTICAL REACTION***

WKPL= -19.2240 WKGL=    1.9010 WKSL= -21.9923 TOTAL LEADING =  -39.3153
WKPT= -13.2269 WKGT=    6.1382 WKST= -54.3763 TOTAL TRAILING=  -61.4650

                    ***HORIZONTAL REACTION***

HKPL=  19.0691 HKL =  -3.2536                 TOTAL LEADING =   15.8154
HKPT= -16.2901 HKT =    .4747                 TOTAL TRAILING=  -15.8154

                    ***MOMENTS***

MGL = -21.1603 MSL = 261.8861 MPL =   -9.9489 TOTAL LEADING =  230.7768
MGT = -38.5212 MST = 244.5758 MPT = 294.5256 TOTAL TRAILING=  500.5803

TOTAL TORQUE =    731.3572 LB-INCHES =    101.1139 KG-METERS

EM,ET,THRUST EFFICIENCY=       1.0140        .3722        .3670
```

Table 2.1a. Wheel performance on slope for $\xi_M = 110$ and $s_k = 0.55$ (lower bound)

```
                    ***INPUT PARAMETERS***

W,P,XI(M),SK =          100.3000      0.0000  109.9999       .5500
ALPHA,GAMMA,PHI,C =      20.4159       .0584   43.1999       .0600
R,B =                                13.9500   12.0000

                    ***STRESS PARAMETERS***

THETA(LOP)=  137.2509   THETA(LLP)=  100.7263   THETA(MP)=   61.6883
THETA(M)  =  108.4883   THETA(NN) =   74.0657   THETA(NO)=   51.7660

PO  =      .2025    PLL  =      .6706    PML  =      .9648
PM  =      .9181    PMN  =      .7337    PNN  =      .4207

NORMAL STRESSES AT L,M,N     =      .2419       .8470       .3178
TANGENTIAL STRESSES AT L,M,N=     -.2787       .6284       .2853

                  ***GEOMETRIC PARAMETERS***

CENTER OF INSTANTANEOUS ROTATION--- XB =  -2.6764    ZB =     7.1905
TRAILING SPIRAL POLE---             XP1=  -5.8977    ZP1=     1.2107
LEADING SPIRAL POLE---              XP2= -10.3797    ZP2=     8.1417
BIFURCATION POINT---                XM  =  -9.0442    ZM  =   10.6209
LEADING EDGE---                     XL  = -10.5634    ZL  =    9.1113
LEADING SPIRAL COORDINATES---       XML= -11.3735    ZML=    13.3880
TRAILING EDGE---                    XN  =  -2.3159    ZN  =   13.7564
TRAILING SPIRAL COORDINATES---      XMN=  -1.1089    ZMN=    17.9838

XI(L)=   118.8051          XI(N)=    79.1403

                    ***VERTICAL REACTION***


WKPL= -17.3385 WKGL=    3.1853 WKSL= -27.5860 TOTAL LEADING =  -41.7393
WKPT= -11.0954 WKGT=   11.0070 WKST= -58.5678 TOTAL TRAILING=  -58.6563

                  ***HORIZONTAL REACTION***


HKPL=  22.9885 HKL  =  -1.2492                     TOTAL LEADING =   21.7393
HKPT= -16.4917 HKT  =  -5.2475                     TOTAL TRAILING=  -21.7393

                         ***MOMENTS***

MGL  = -34.0184 MSL  = 307.4669 MPL  = -70.9631 TOTAL LEADING =  202.4853
MGT  = -56.1329 MST  = 242.1864 MPT  = 283.2736 TOTAL TRAILING=  469.3271


TOTAL TORQUE  =    671.8124 LB-INCHES =     92.8815 KG-METERS

EM,ET,THRUST EFFICIENCY=         .9315         .3722         .3995
```

Table 2.2. Wheel performance on slope for ξ_M = 110 and s_k = 0.65 (upper bound)

```
                              ***INPUT PARAMETERS***

W,P,XI(M),SK =           100.3000     0.0000  109.9999      .6500
ALPHA,GAMMA,PHI,C =       20.4159      .0584   43.1999      .0600
R,B =                                13.9500   12.0000

                              ***STRESS PARAMETERS***

THETA(LOP)=  134.7457    THETA(LLP)=    85.0939   THETA(MP)=    70.1512
THETA(M)   =  116.9512    THETA(NN) =    88.2381   THETA(NO)=    44.8502

PO =      .2025    PLL  =    1.0312    PML  =     1.1457
PM =     1.1318    PMN  =    1.0572    PNN  =      .8398

NORMAL STRESSES AT L,M,N      =     .6401     1.2850      .7661
TANGENTIAL STRESSES AT L,M,N=    -.6255      .7437      .5748

                              ***GEOMETRIC PARAMETERS***

CENTER OF INSTANTANEOUS ROTATION--- XB =  -3.1630    ZB =     8.4979
TRAILING SPIRAL POLE---             XP1=  -5.1566    ZP1=     2.9751
LEADING SPIRAL POLE---              XP2= -10.2569    ZP2=     7.2615
BIFURCATION POINT---                XM =  -9.0442    ZM =    10.6209
LEADING EDGE---                     XL = -10.0497    ZL =     9.6749
LEADING SPIRAL COORDINATES---       XML=  -9.8667    ZML=    11.8075
TRAILING EDGE---                    XN =  -4.8458    ZN =    13.0812
TRAILING SPIRAL COORDINATES---      XMN=  -4.7345    ZMN=    16.7006

XI(L)=  115.6725         XI(N)=    89.9106

                              ***VERTICAL REACTION***

WKPL= -15.0300 WKGL=     .7114 WKSL= -13.4206 TOTAL LEADING =   -27.7392
WKPT= -19.9701 WKGT=    6.3684 WKST= -59.1700 TOTAL TRAILING=   -72.7717

                              ***HORIZONTAL REACTION***

HKPL=  11.9736 HKL =   -2.0915                 TOTAL LEADING =     9.8821
HKPT= -19.7495 HKT =    9.8674                 TOTAL TRAILING=    -9.8821

                              ***MOMENTS***

MGL =   -8.5330 MSL = 157.1346 MPL =  20.8128 TOTAL LEADING =  169.4144
MGT = -42.8072 MST = 214.5360 MPT = 391.0730 TOTAL TRAILING=  562.8018

TOTAL TORQUE =    732.2163 LB-INCHES =    101.2327 KG-METERS

EM,ET,THRUST EFFICIENCY=        .8590        .3722        .4332
```

Table 2.2a. Wheel performance on slope for ξ_M = 110 and s_k = 0.65 (lower bound)

```
                         ***INPUT PARAMETERS***

W,P,XI(M),SK =          100.3000      0.0000   109.9999      .6500
ALPHA,GAMMA,PHI,C =      20.4159       .0584    43.1999      .0600
R,B =                                13.9500    12.0000


                        ***STRESS PARAMETERS***

THETA(LOP)=  134.5818   THETA(LLP)=    89.0328   THETA(MP)=    70.1512
THETA(M)  =  116.9512   THETA(NN) =    84.9370   THETA(NO)=    48.1827

PO =      .2025    PLL =      .9014    PML =      1.0527
PM =     1.0320    PMN =      .9366    PNN =       .6756

NORMAL STRESSES AT L,M,N     =      .4973      1.1661      .5929
TANGENTIAL STRESSES AT L,M,N=     -.5148       .6782      .4621


                       ***GEOMETRIC PARAMETERS***

CENTER OF INSTANTANEOUS ROTATION--- XB =   -3.1630    ZB =      8.4979
TRAILING SPIRAL POLE---             XP1=   -5.1566    ZP1=      2.9751
LEADING SPIRAL POLE---              XP2= -10.2569     ZP2=      7.2615
BIFURCATION POINT---                XM =   -9.0442    ZM =     10.6209
LEADING EDGE---                     XL = -10.2191     ZL =      9.4958
LEADING SPIRAL COORDINATES---       XML= -10.1747     ZML=     12.1278
TRAILING EDGE---                    XN =   -4.2429    ZN =     13.2891
TRAILING SPIRAL COORDINATES---      XMN=   -3.8774    ZMN=     17.4139

XI(L)=  116.6853         XI(N)=   87.2911

                        ***VERTICAL REACTION***


WKPL= -15.6411 WKGL=   1.1163 WKSL= -16.0262 TOTAL LEADING =  -30.5510
WKPT= -18.3141 WKGT=   8.2754 WKST= -59.6836 TOTAL TRAILING=  -69.7223

                       ***HORIZONTAL REACTION***


HKPL=  14.1199 HKL =  -1.7898                  TOTAL LEADING =   12.3300
HKPT= -19.8063 HKT =   7.4762                  TOTAL TRAILING=  -12.3300


                            ***MOMENTS***

MGL = -12.8101 MSL = 183.1972 MPL =   6.3445 TOTAL LEADING =  176.7316
MGT = -52.2301 MST = 212.8244 MPT = 380.4392 TOTAL TRAILING=  541.0335


TOTAL TORQUE =    717.7651 LB-INCHES =     99.2347 KG-METERS

FM,ET,THRUST EFFICIENCY=        .8421        .3722        .4420
```

Table 2.3. Wheel performance on slope for ξ_M = 105 and s_k = 0.65 (upper bound)

```
                         ***INPUT PARAMETERS***

W,P,XI(M),SK =          100.3000     0.0000  104.9999      .6500
ALPHA,GAMMA,PHI,C =      20.4159      .0584   43.1999      .0600
R,B =                               13.9500   12.0000

                         ***STRESS PARAMETERS***

THETA(LOP)=  140.6762   THETA(LLP)=    96.7495   THETA(MP)=    59.7416
THETA(M)   = 106.5416   THETA(NN) =    76.6502   THETA(NU)=    37.2337

PO =      .2025    PLL =      .8547    PML =      1.0901
PM =     1.0562    PMN =      .9376    PNN =       .7373

NORMAL STRESSES AT L,M,N      =       .2992      1.0610      .5578
TANGENTIAL STRESSES AT L,M,N=      -.3172       .7198      .4913

                       ***GEOMETRIC PARAMETERS***

CENTER OF INSTANTANEOUS ROTATION--- XB =  -3.1630    ZB =     8.4979
TRAILING SPIRAL POLE---             XP1=  -5.8589    ZP1=     3.8767
LEADING SPIRAL POLE---              XP2=  -9.3819    ZP2=     9.1441
BIFURCATION POINT---                XM =  -8.0841    ZM =    11.3687
LEADING EDGE---                     XL =  -9.5078    ZL =    10.2080
LEADING SPIRAL COORDINATES---       XML=  -9.9371    ZML=    13.8351
TRAILING EDGE---                    XN =  -3.5793    ZN =    13.4829
TRAILING SPIRAL COORDINATES---      XMN=  -2.9136    ZMN=    16.2883

XI(L)=  112.5501         XI(N)=   84.4513

                         ***VERTICAL REACTION***


WKPL= -18.7890 WKGL=   2.3175 WKSL= -26.9640 TOTAL LEADING =  -43.4354
WKPT= -11.0238 WKGT=   4.9675 WKST= -51.2681 TOTAL TRAILING=  -57.3245

                       ***HORIZONTAL REACTION***


HKPL=  22.2113 HKL =  -3.0039                    TOTAL LEADING =   19.2073
HKPT= -16.1693 HKT =  -3.0380                    TOTAL TRAILING=  -19.2073


                            ***MOMENTS***

MGL = -22.9015 MSL = 288.7918 MPL = -85.8012 TOTAL LEADING =  180.0890
MGT = -27.3353 MST = 258.0377 MPT = 277.2376 TOTAL TRAILING=  507.9399


TOTAL TORQUE =    688.0289 LB-INCHES =     95.1235 KG-METERS

FM,ET,THRUST EFFICIENCY=       .8072         .3722         .4611
```

Table 2.3a. Wheel performance on slope for ξ_M = 105 and s_k = 0.65 (lower bound)

```
                    ***INPUT PARAMETERS***

W,P,XI(M),SK =          100.3000     0.0000  104.9999      .6500
ALPHA,GAMMA,PHI,C =      20.4159      .0584   43.1999      .0600
R,B =                              13.9500   12.0000


                    ***STRESS PARAMETERS***

THETA(LOP)=  144.6045    THETA(LLP)=  111.9612   THETA(MP)=    59.7416
THETA(M)  =  106.5416    THETA(NN) =   60.8132   THETA(NO)=    56.5732

PO  =      .2025    PLL  =      .5905    PML  =      .9742
PM  =      .8925    PMN  =      .6214    PNN  =      .2327

NORMAL STRESSES AT L,M,N     =      .1238      .8866      .1220
TANGENTIAL STRESSES AT L,M,N=     -.0344      .6082      .1522


                    ***GEOMETRIC PARAMETERS***

CENTER OF INSTANTANEOUS ROTATION--- XB =  -3.1630    ZB =     8.4979
TRAILING SPIRAL POLE---             XP1=  -5.8589    ZP1=     3.8767
LEADING SPIRAL POLE---              XP2=  -9.3819    ZP2=     9.1441
BIFURCATION POINT---                XM =  -8.0841    ZM =    11.3687
LEADING EDGE---                     XL =  -9.7268    ZL =     9.9995
LEADING SPIRAL COORDINATES---       XML= -11.6486    ZML=    14.7655
TRAILING EDGE---                    XN =   -.2333    ZN =    13.9480
TRAILING SPIRAL COORDINATES---      XMN=   2.2053    ZMN=    18.3139

XI(L)=  113.7920          XI(N)=    70.5424

                    ***VERTICAL REACTION***


WKPL= -14.2141 WKGL=   4.9177 WKSL= -36.9407 TOTAL LEADING =  -46.2371
WKPT=  -6.3939 WKGT=  14.5754 WKST= -62.3644 TOTAL TRAILING=  -54.1829

                    ***HORIZONTAL REACTION***


HKPL=  29.1273 HKL  =   2.5820                TOTAL LEADING =   31.7094
HKPT= -14.7801 HKT  = -16.9292                TOTAL TRAILING=  -31.7094


                    ***MOMENTS***

MGL = -44.7884 MSL = 338.9945 MPL =-213.3103 TOTAL LEADING =   80.8957
MGT = -45.3722 MST = 317.9378 MPT = 235.8248 TOTAL TRAILING=  508.3904


TOTAL TORQUE =    589.2861 LB-INCHES =    81.4718 KG-METERS

FM,ET,THRUST EFFICIENCY=       .6913        .3722        .5383
```

Table 2.4. Wheel performance on slope for ξ_M = 105 and s_k = 0.70 (upper bound)

```
                        ***INPUT PARAMETERS***

W,P,XI(M),SK =          100.3000     0.0000  104.9999       .7000
ALPHA,GAMMA,PHI,C =      20.4159      .0584   43.1999       .0600
R,B =                               13.9500   12.0000


                        ***STRESS PARAMETERS***

THETA(LOP)=  140.1015    THETA(LLP)=    95.0272    THETA(MP)=    64.6400
THETA(M)  =  111.4400    THETA(NN) =    79.0130    THETA(NO)=    39.6779

PO =       .2025    PLL =       .8875    PML =      1.0926
PM =      1.0613    PMN =       .9562    PNN =       .7353

NORMAL STRESSES AT L,M,N      =      .3302      1.1885       .5801
TANGENTIAL STRESSES AT L,M,N=      -.3545       .7009       .4950


                       ***GEOMETRIC PARAMETERS***

CENTER OF INSTANTANEOUS ROTATION--- XB =  -3.4063     ZB =     9.1516
TRAILING SPIRAL POLE---             XP1=  -5.4884     ZP1=     4.7588
LEADING SPIRAL POLE---              XP2=  -9.3245     ZP2=     8.7518
BIFURCATION POINT---                XM =  -8.0841     ZM =    11.3687
LEADING EDGE---                     XL =  -9.4567     ZL =    10.2553
LEADING SPIRAL COORDINATES---       XML=  -9.7420     ZML=    13.4988
TRAILING EDGE---                    XN =  -3.8068     ZN =    13.4205
TRAILING SPIRAL COORDINATES---      XMN=  -3.1856     ZMN=    16.6198

XI(L)=  112.2640         XI(N)=    85.4203

                        ***VERTICAL REACTION***


WKPL= -17.6474 WKGL=    1.8740 WKSL= -23.7603 TOTAL LEADING =   -39.5337
WKPT= -13.3298 WKGT=    5.6038 WKST= -53.0616 TOTAL TRAILING=   -60.7876

                      ***HORIZONTAL REACTION***


HKPL=  19.6827 HKL =   -2.2556                  TOTAL LEADING =    17.4271
HKPT= -17.9479 HKT =     .5208                  TOTAL TRAILING=   -17.4271


                            ***MOMENTS***

MGL = -18.6533 MSL = 248.9197 MPL = -65.3835 TOTAL LEADING =  164.8829
MGT = -31.2311 MST = 237.8679 MPT = 317.2553 TOTAL TRAILING=  523.8920


TOTAL TORQUE =    688.7750 LB-INCHES =     95.2267 KG-METERS

EM,ET,THRUST EFFICIENCY=        .7503        .3722        .4960
```

Table 2.4a. Wheel performance on slope for ξ_M = 105 and s_k = 0.70 (lower bound)

```
                    ***INPUT PARAMETERS***

W,P,XI(M),SK =          100.3000      0.0000  104.9999      .7000
ALPHA,GAMMA,PHI,C =      20.4159       .0584   43.1999      .0600
R,B =                                13.9500   12.0000

                    ***STRESS PARAMETERS***

THETA(LOP)=  142.3620   THETA(LLP)=  106.4128   THETA(MP)=   64.6400
THETA(M)  =  111.4400   THETA(NN) =   67.2308   THETA(NO)=   50.6741

PO =      .2025   PLL =      .6581   PML =      .9738
PM =      .9102   PMN =      .7086   PNN =      .3485

NORMAL STRESSES AT L,M,N     =      .1604     1.0101      .2184
TANGENTIAL STRESSES AT L,M,N=     -.1217      .6011      .2292

                  ***GEOMETRIC PARAMETERS***

CENTER OF INSTANTANEOUS ROTATION--- XB =  -3.4063   ZB =    9.1516
TRAILING SPIRAL POLE---             XP1=  -5.4884   ZP1=    4.7588
LEADING SPIRAL POLE---              XP2=  -9.3245   ZP2=    8.7518
BIFURCATION POINT---                XM =  -8.0841   ZM =   11.3687
LEADING EDGE---                     XL =  -9.6997   ZL =   10.0258
LEADING SPIRAL COORDINATES---       XML= -10.9471   ZML=   14.2607
TRAILING EDGE---                    XN =  -1.6729   ZN =   13.8493
TRAILING SPIRAL COORDINATES---      XMN=    .1837   ZMN=   18.2728

XI(L)=  113.6369        XI(N)=    76.4715

                    ***VERTICAL REACTION***

WKPL= -15.1582 WKGL=   3.6518 WKSL= -31.0287 TOTAL LEADING =  -42.5350
WKPT=  -9.1669 WKGT=  12.1758 WKST= -60.4015 TOTAL TRAILING=  -57.3926

                  ***HORIZONTAL REACTION***

HKPL=  24.8834 HKL =   1.1439                TOTAL LEADING =   26.0273
HKPT= -17.3956 HKT =  -8.6317                TOTAL TRAILING=  -26.0273

                        ***MOMENTS***

MGL = -33.9626 MSL = 292.4108 MPL =-148.4692 TOTAL LEADING =  109.9789
MGT = -48.9456 MST = 285.0673 MPT = 289.6205 TOTAL TRAILING=  525.7422

TOTAL TORQUE =   635.7212 LB-INCHES =    87.8917 KG-METERS

EM,ET,THRUST EFFICIENCY=       .6925       .3722       .5374
```

Table 3.1. Wheel performance for Apollo LRV for $\xi_M = 105$ and $s_k = 0.85$ (upper bound)

```
                      ***INPUT PARAMETERS***

W,P,XI(M),SK =           60.0000     0.0000  104.9999      .8500
ALPHA,GAMMA,PHI,C =       0.0000      .0100   32.9999      .0500
R,B =                                16.0000   10.0000


                      ***STRESS PARAMETERS***

THETA(LOP)=  152.0047   THETA(LLP)=  107.2372   THETA(MP)=    65.8722
THETA(M)  =  122.8722   THETA(NN) =   64.4247   THETA(NO)=    24.3706

PO  =      .1690   PLL  =      .4664   PML  =      .5239
PM  =      .5057   PMN  =      .4771   PNN  =      .4192

NORMAL STRESSES AT L,M,N     =     .1419       .6853       .3045
TANGENTIAL STRESSES AT L,M,N=    -.0574       .0998       .2251


                    ***GEOMETRIC PARAMETERS***

CENTER OF INSTANTANEOUS ROTATION--- XB =    0.0000    ZB =    13.6000
TRAILING SPIRAL POLE---             XP1=   -1.2045    ZP1=    10.9107
LEADING SPIRAL POLE---              XP2=   -6.4211    ZP2=    10.3642
BIFURCATION POINT---                XM =   -4.1411    ZM =    15.4548
LEADING EDGE---                     XL =   -7.5777    ZL =    14.0917
LEADING SPIRAL COORDINATES---       XML=   -9.0627    ZML=    18.8781
TRAILING EDGE---                    XN =    1.2092    ZN =    15.9542
TRAILING SPIRAL COORDINATES---      XMN=    3.3255    ZMN=    20.3762

XI(L)=  118.2687         XI(N)=    85.6656

                      ***VERTICAL REACTION***


WKPL=  -6.7976 WKGL=    1.1156 WKSL= -21.9803 TOTAL LEADING =  -27.6623
WKPT=  -4.0106 WKGT=    1.7418 WKST= -29.8765 TOTAL TRAILING=  -32.1453

                    ***HORIZONTAL REACTION***


HKPL=  16.3462 HKL  =   1.8722                 TOTAL LEADING =   18.2184
HKPT= -14.8678 HKT  =  -3.3506                 TOTAL TRAILING=  -18.2184


                          ***MOMENTS***

MGL  =  -7.2459 MSL  = 158.9629 MPL =-213.5682 TOTAL LEADING =  -61.8512
MGT  =   -.2526 MST  =  10.2989 MPT = 261.6018 TOTAL TRAILING=  271.6481


TOTAL TORQUE =    209.7969 LB-INCHES =     29.0055 KG-METERS

FM,FP                 =       .2571      0.0000
```

Table 3.1a. Wheel performance for Apollo LRV for ξ_M = 105 and s_k = 0.85 (lower bound)

```
                    ***INPUT PARAMETERS***

W,P,XI(M),SK =            60.0000     0.0000  104.9999      .8500
ALPHA,GAMMA,PHI,C =        0.0000      .0100   32.9999      .0500
R,B =                                16.0000   10.0000

                    ***STRESS PARAMETERS***

THETA(LOP)=  160.8913   THETA(LLP)=  122.4615   THETA(MP)=    65.8722
THETA(M)   =  122.8722   THETA(NN)  =   44.2667   THETA(NO)=    16.5041

PO  =      .1690    PLL  =      .4040    PML  =      .4849
PM  =      .4503    PMN  =      .3926    PNN  =      .3172

NORMAL STRESSES AT L,M,N      =      .1103      .6019      .1474
TANGENTIAL STRESSES AT L,M,N=      .0383      .0889      .1457

                    ***GEOMETRIC PARAMETERS***

CENTER OF INSTANTANEOUS ROTATION--- XB =     0.0000    ZB =    13.6000
TRAILING SPIRAL POLE---             XP1=    -1.2045    ZP1=    10.9107
LEADING SPIRAL POLE---              XP2=    -6.4211    ZP2=    10.3642
BIFURCATION POINT---                XM =    -4.1411    ZM =    15.4548
LEADING EDGE---                     XL =    -8.4650    ZL =    13.5772
LEADING SPIRAL COORDINATES---       XML=   -12.1069    ZML=    19.3022
TRAILING EDGE---                    XN =     3.5966    ZN =    15.5905
TRAILING SPIRAL COORDINATES---      XMN=     8.2388    ZMN=    20.1154

XI(L)=  121.9425          XI(N)=    77.0096

                    ***VERTICAL REACTION***

WKPL=  -3.0416 WKGL=    2.1807 WKSL= -27.9771 TOTAL LEADING =  -28.8380
WKPT=     .6794 WKGT=    3.5441 WKST= -35.1432 TOTAL TRAILING=  -30.9196

                    ***HORIZONTAL REACTION***

HKPL=  20.8851 HKL =    7.5002                 TOTAL LEADING =   28.3854
HKPT= -15.3401 HKT =  -13.0452                 TOTAL TRAILING=  -28.3854

                    ***MOMENTS***

MGL = -10.3476 MSL = 164.3556 MPL =-313.7059 TOTAL LEADING = -159.6979
MGT =   7.5987 MST =  73.3065 MPT = 279.1733 TOTAL TRAILING=  360.0787

TOTAL TORQUE =    200.3807 LB-INCHES =     27.7036 KG-METERS

FM,FP                  =        .2455       0.0000
```

Table 3.2. Wheel performance for Apollo LRV for ξ_M = 105 and s_k = 0.90 (upper bound)

```
                         ***INPUT PARAMETERS***

W,P,XI(M),SK =            60.0000      0.0000  104.9999      .9000
ALPHA,GAMMA,PHI,C =        0.0000       .0100   32.9999      .0500
R,B =                                 16.0000   10.0000

                         ***STRESS PARAMETERS***

THETA(LOP)=  149.3241   THETA(LLP)=   97.2966   THETA(MP)=   75.7096
THETA(M)  =  132.7096   THETA(NN) =   79.7521   THETA(NO)=   31.3747

PO  =     .1690   PLL =      .5499   PML  =      .5852
PM  =     .5739   PMN =      .5604   PNN  =      .5062

NORMAL STRESSES AT L,M,N     =     .2061      .8094      .4919
TANGENTIAL STRESSES AT L,M,N=    -.1360      .0086      .2684

                        ***GEOMETRIC PARAMETERS***

CENTER OF INSTANTANEOUS ROTATION--- XB =    0.0000    ZB =   14.4000
TRAILING SPIRAL POLE---             XP1=    -.6850    ZP1=   11.7107
LEADING SPIRAL POLE---              XP2=   -6.0214    ZP2=    8.0725
BIFURCATION POINT---                XM =   -4.1411    ZM =   15.4548
LEADING EDGE---                     XL =   -6.8399    ZL =   14.4642
LEADING SPIRAL COORDINATES---       XML=   -7.2572    ZML=   17.7234
TRAILING EDGE---                    XN =     .0904    ZN =   15.9997
TRAILING SPIRAL COORDINATES---      XMN=     .9671    ZMN=   20.8491

XI(L)=  115.3086        XI(N)=   89.6762

                         ***VERTICAL REACTION***

WKPL=  -7.1048 WKGL=     .4948 WKSL= -16.2880 TOTAL LEADING =  -22.8980
WKPT=  -9.2000 WKGT=    1.3934 WKST= -29.5081 TOTAL TRAILING=  -37.3146

                        ***HORIZONTAL REACTION***

HKPL=  11.5836 HKL =     .7605                TOTAL LEADING =   12.3441
HKPT= -16.5940 HKT =    4.2498                TOTAL TRAILING=  -12.3441

                              ***MOMENTS***

MGL =  -3.6164 MSL = 120.1449 MPL =-136.5276 TOTAL LEADING =  -19.9991
MGT =  -1.7654 MST = -75.9649 MPT = 301.4836 TOTAL TRAILING=  223.7532

TOTAL TORQUE =    203.7541 LB-INCHES =    28.1700 KG-METERS

FM,EP,                =         .2358       0.0000
```

Table 3.2a. Wheel performance for Apollo LRV for ξ_M = 105 and s_k = 0.90 (lower bound)

```
                    ***INPUT PARAMETERS***

W,P,XI(M),SK =           60.0000     0.0000   104.9999      .9000
ALPHA,GAMMA,PHI,C =       0.0000      .0100    32.9999      .0500
R,B =                                16.0000   10.0000

                    ***STRESS PARAMETERS***

THETA(LOP)=  156.1713   THETA(LLP)=  119.7895   THETA(MP)=    75.7096
THETA(M)   =  132.7096   THETA(NN) =   46.2387   THETA(NO)=    24.4482

PO =      .1690    PLL  =      .3857    PML  =      .4642
PM =      .4278    PMN  =      .3715    PNN  =      .2770

NORMAL STRESSES AT L,M,N      =       .0986       .5837      .1201
TANGENTIAL STRESSES AT L,M,N=       .0010       .0064      .1280

                  ***GEOMETRIC PARAMETERS***

CENTER OF INSTANTANEOUS ROTATION--- XB =     0.0000    ZB =    14.4000
TRAILING SPIRAL POLE---             XP1=     -.6850    ZP1=    11.7107
LEADING SPIRAL POLE---              XP2=    -6.0214    ZP2=     8.0725
BIFURCATION POINT---                XM =    -4.1411    ZM =    15.4548
LEADING EDGE---                     XL =    -8.9807    ZL =    13.2418
LEADING SPIRAL COORDINATES--        XML=   -12.2590    ZML=    18.9685
TRAILING EDGE---                    XN =     3.1271    ZN =    15.6914
TRAILING SPIRAL COORDINATES---      XMN=     8.7059    ZMN=    21.5168

XI(L)=   124.1454          XI(N)=    78.7290

                    ***VERTICAL REACTION***

WKPL=  -3.8413 WKGL=    2.1765 WKSL= -26.1374 TOTAL LEADING =   -27.8020
WKPT=   -.1987 WKGT=    4.4923 WKST= -36.3118 TOTAL TRAILING=   -32.0182

                  ***HORIZONTAL REACTION***

HKPL=  19.0737 HKL =    8.3584                TOTAL LEADING =    27.4322
HKPT= -17.0687 HKT =  -10.3634                TOTAL TRAILING=   -27.4322

                        ***MOMENTS***

MGL =   -6.6617 MSL = 166.5952 MPL =-267.8815 TOTAL LEADING = -107.9480
MGT =    9.4905 MST =  24.2904 MPT = 318.7603 TOTAL TRAILING=  352.5412

TOTAL TORQUE =    244.5932 LB-INCHES =      33.8162 KG-METERS

EM,EP,                =           .2830        0.0000
```

Table 4.1. Wheel performance for Lunokhod-1 for ξ_M = 112 and s_k = 0.80 (upper bound)

```
                          ***INPUT PARAMETERS***

W,P,XI(M),SK =            35.0000    0.0000  111.9999      .8000
ALPHA,GAMMA,PHI,C =        0.0000     .0100   32.9999      .0500
R,B =                                10.0000    6.5000

                          ***STRESS PARAMETERS***

THETA(LOP)=  155.8434   THETA(LLP)=  107.6283   THETA(MP)=   71.2469
THETA(M)  =  128.2469   THETA(NN) =   68.5672   THETA(NO)=   24.4682

PO =      .1690    PLL =     .5043    PML =      .5484
PM =      .5345    PMN =     .5127    PNN =      .4594

NORMAL STRESSES AT L,M,N     =      .1939       .7224       .3843
TANGENTIAL STRESSES AT L,M,N=     -.1447       .1207       .2502

                         ***GEOMETRIC PARAMETERS***

CENTER OF INSTANTANEOUS ROTATION--- XB =    0.0000    ZB =     8.0000
TRAILING SPIRAL POLE---             XP1=    -.8259    ZP1=     5.5672
LEADING SPIRAL POLE---              XP2=   -5.2719    ZP2=     4.9247
BIFURCATION POINT---                XM =   -3.7460    ZM =     9.2718
LEADING EDGE---                     XL =   -6.1601    ZL =     7.8773
LEADING SPIRAL COORDINATES---       XML=   -7.3217    ZML=    11.5329
TRAILING EDGE---                    XN =     .8982    ZN =     9.9595
TRAILING SPIRAL COORDINATES---      XMN=    2.5642    ZMN=    14.2034

XI(L)=  128.0258         XI(N)=     84.8463

                          ***VERTICAL REACTION***

WKPL=  -3.4992 WKGL=     .3896 WKSL= -10.6691 TOTAL LEADING =   -13.7787
WKPT=  -3.2561 WKGT=     .9156 WKST= -18.9917 TOTAL TRAILING=   -21.3323

                         ***HORIZONTAL REACTION***

HKPL=   8.7846 HKL =    1.2993                TOTAL LEADING =    10.0839
HKPT=  -9.7117 HKT =    -.3722                TOTAL TRAILING=   -10.0839

                              ***MOMENTS***

MGL =  -1.9460 MSL =  70.1045 MPL = -61.8630 TOTAL LEADING =     6.2953
MGT =   -.3179 MST = -31.3827 MPT = 112.0215 TOTAL TRAILING=    80.3208

TOTAL TORQUE =     86.6161 LB-INCHES =     11.9751 KG-METERS

EM,FT,                =       .3093       0.0000
```

Table 4.1a. Wheel performance for Lunokhod-1 for ξ_M = 112 and s_k = 0.80 (lower bound)

```
                    ***INPUT PARAMETERS***

W,P,XI(M),SK =          35.0000     0.0000  111.9999      .8000
ALPHA,GAMMA,PHI,C =      0.0000      .0100   32.9999      .0500
R,B =                              10.0000    6.5000

                   ***STRESS PARAMETERS***

THETA(LOP)=  188.0952   THETA(LLP)=  145.0048   THETA(MP)=    71.2469
THETA(M)  =  128.2469   THETA(NN) =   23.3997   THETA(NO)=    -2.5815

PO =      .1690    PLL =      .4490    PML =       .5347
PM =      .4812    PMN =      .3895    PNN =       .3047

NORMAL STRESSES AT L,M,N    =      .1436      .6426      .1376
TANGENTIAL STRESSES AT L,M,N=      .0873      .1087      .1393

                 ***GEOMETRIC PARAMETERS***

CENTER OF INSTANTANEOUS ROTATION--- XB =    0.0000    ZB =     8.0000
TRAILING SPIRAL POLE---             XP1=    -.8259    ZP1=     5.5672
LEADING SPIRAL POLE---              XP2=   -5.2219    ZP2=     4.9247
BIFURCATION POINT---                XM =   -3.7460    ZM =     9.2718
LEADING EDGE---                     XL =   -7.5514    ZL =     6.5556
LEADING SPIRAL COORDINATES---       XML=  -13.8984    ZML=    10.9990
TRAILING EDGE---                    XN =    5.5428    ZN =     8.3232
TRAILING SPIRAL COORDINATES---      XMN=   13.3810    ZMN=    11.7151

XI(L)=  139.0378        XI(N)=    56.3384

                   ***VERTICAL REACTION***

WKPL=    4.6079 WKGL=    1.8160 WKSL= -20.7413 TOTAL LEADING =   -14.3173
WKPT=    5.0207 WKGT=    3.9375 WKST= -29.5777 TOTAL TRAILING=   -20.6194

                 ***HORIZONTAL REACTION***

HKPL=  17.0385 HKL =  12.3711                  TOTAL LEADING =    29.4096
HKPT= -11.7633 HKT = -17.6463                  TOTAL TRAILING=   -29.4096

                       ***MOMENTS***

MGL =   -3.1632 MSL = 117.5277 MPL =-200.4959 TOTAL LEADING =   -86.1314
MGT =   18.9818 MST = -44.7006 MPT = 166.9795 TOTAL TRAILING=   141.2607

TOTAL TORQUE =     55.1293 LB-INCHES =      7.6219 KG-METERS

FM,FT,                   =          .1968       0.0000
```

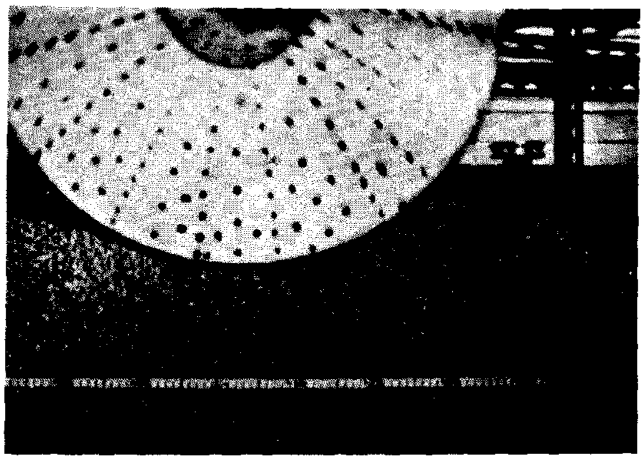

Fig. 1. Typical failure pattern for driven rigid wheel on a pack of aluminum rolls

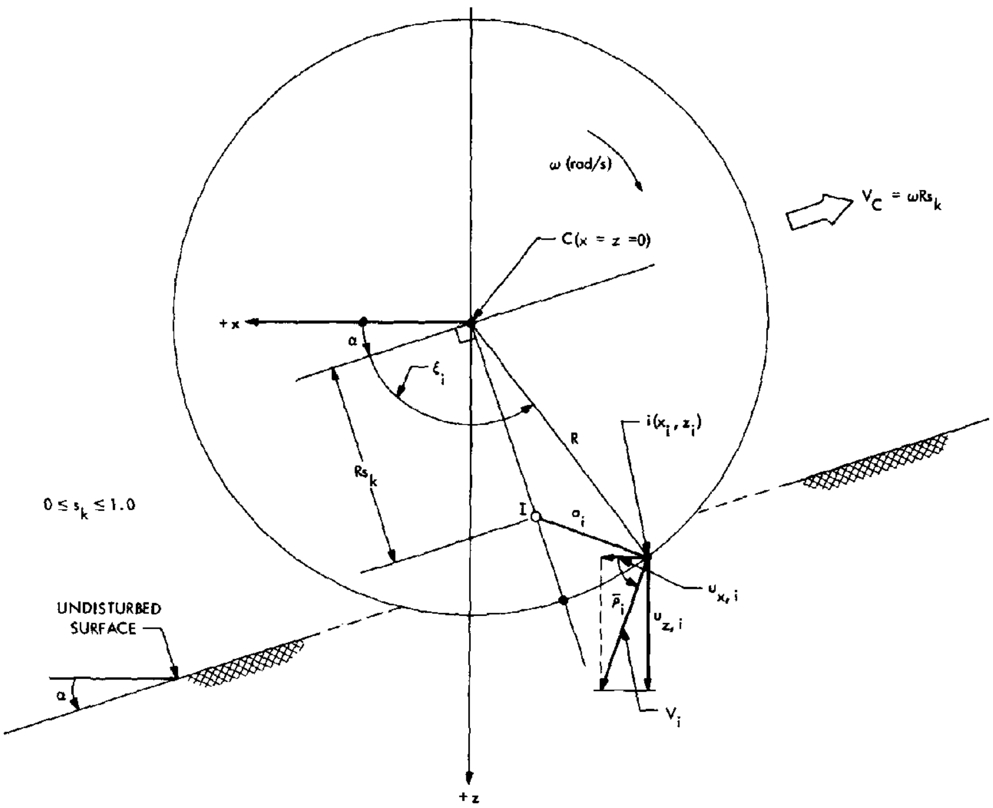

Fig. 2. Roller motion on sloping soil

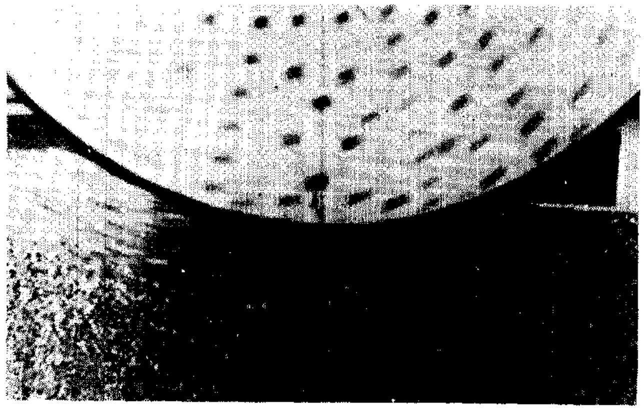

Fig. 3. Driven rigid roller 100% slip (s_k = 0, V_C = 0) on a pack of aluminum rolls

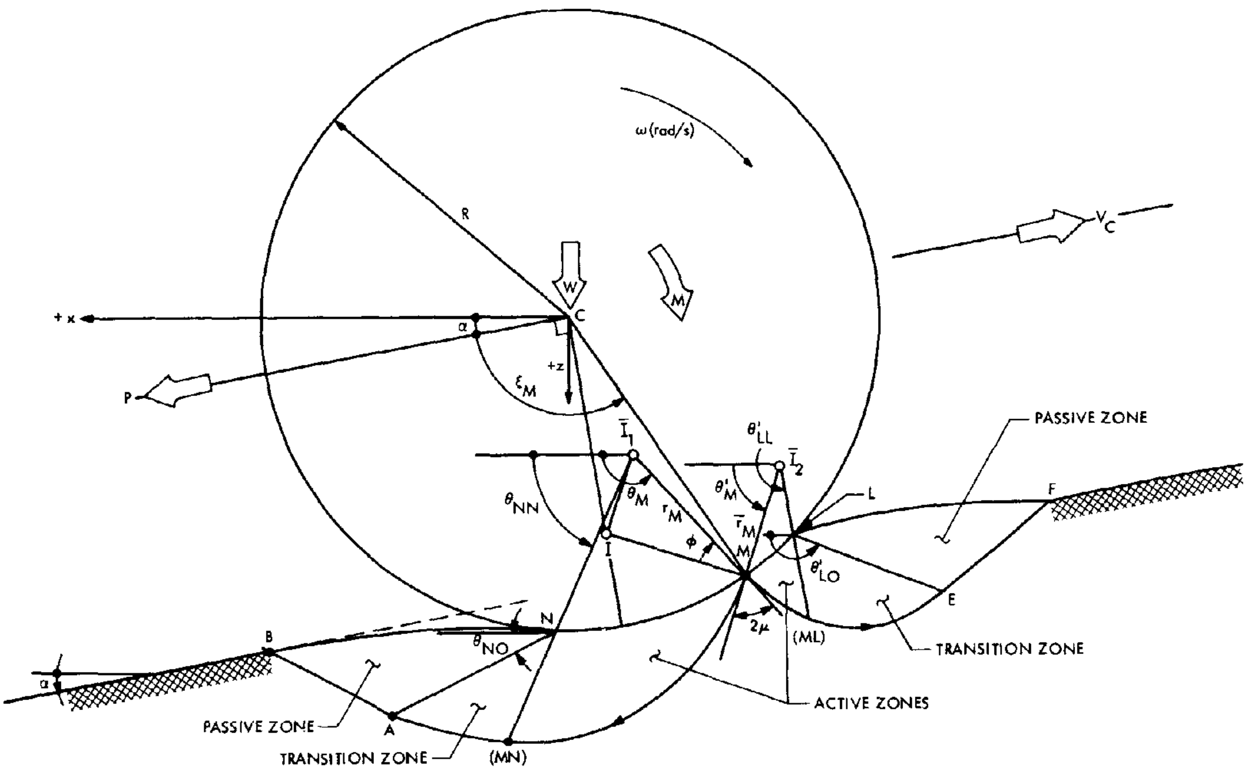

Fig. 4. Soil-roller plastic flow configuration

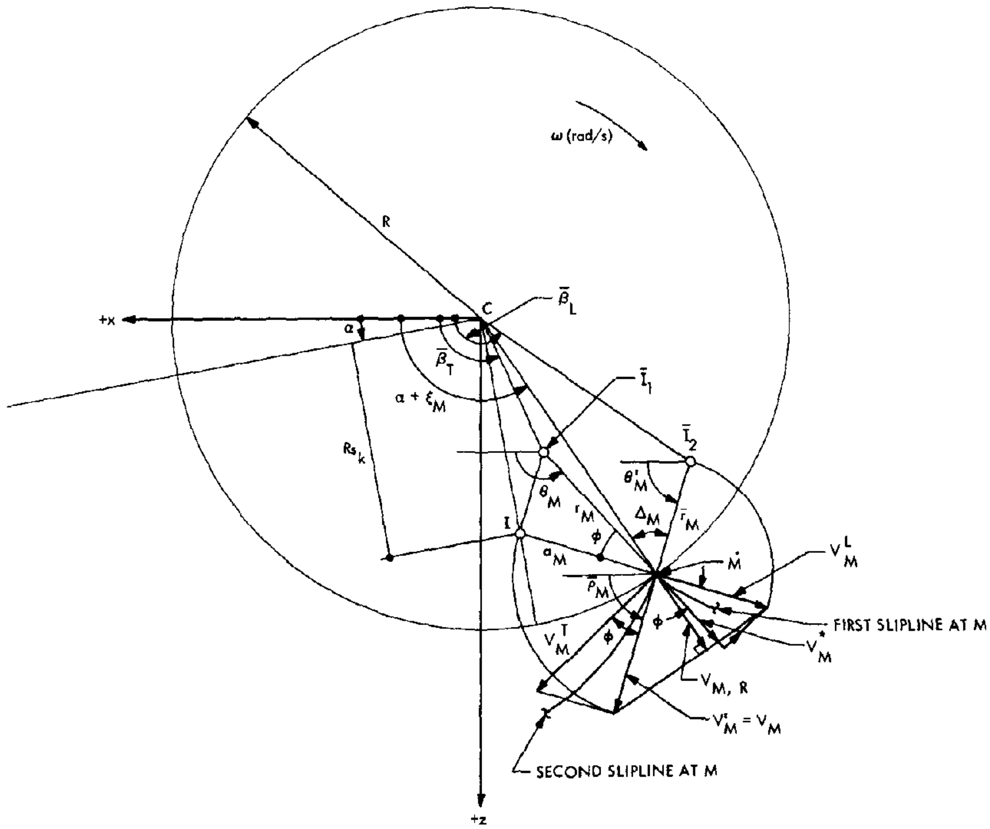

Fig. 5. Soil-roller rim-velocity boundary conditions (bifurcation of plastic zones)

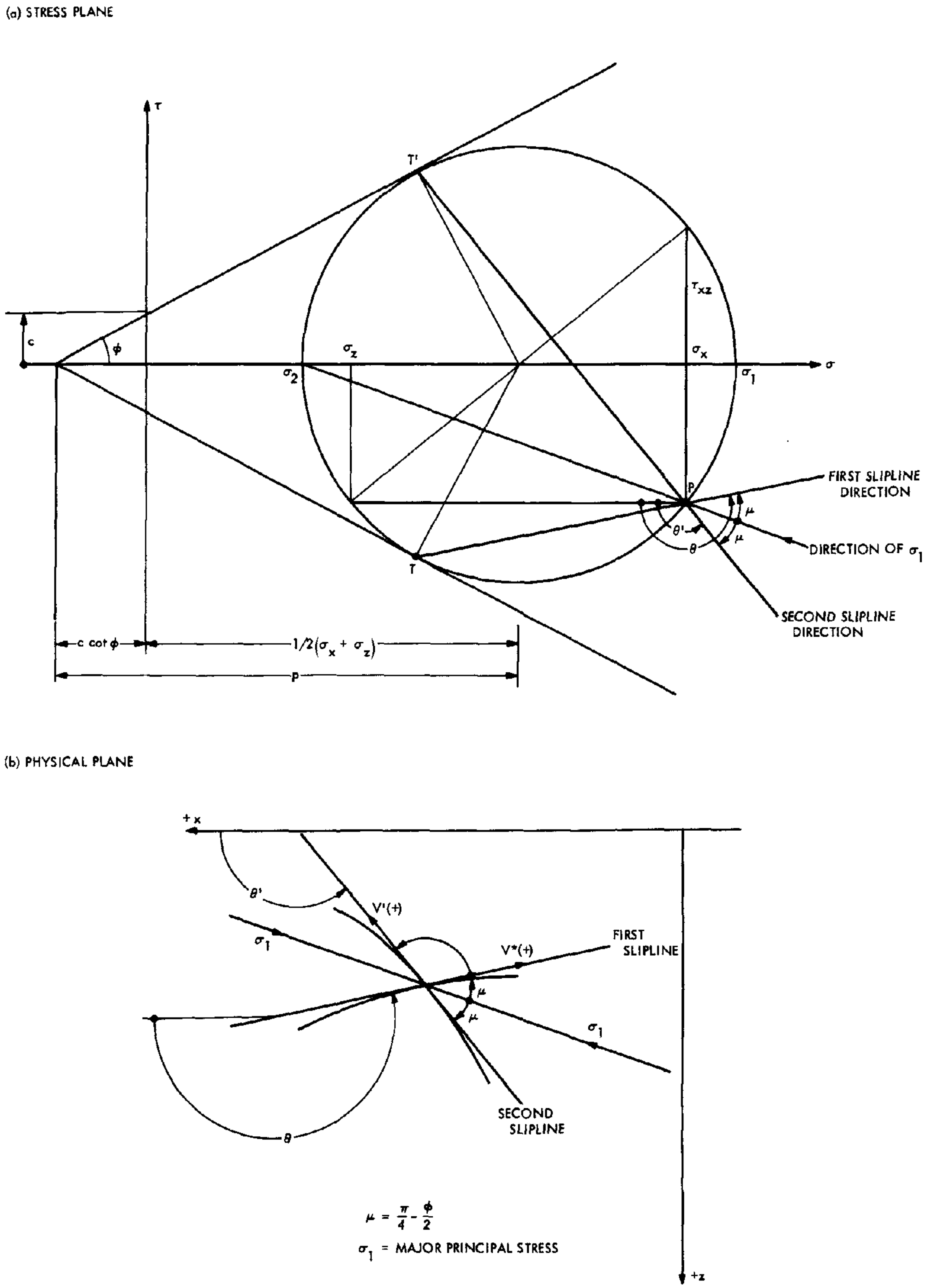

Fig. 6. Limiting stress state

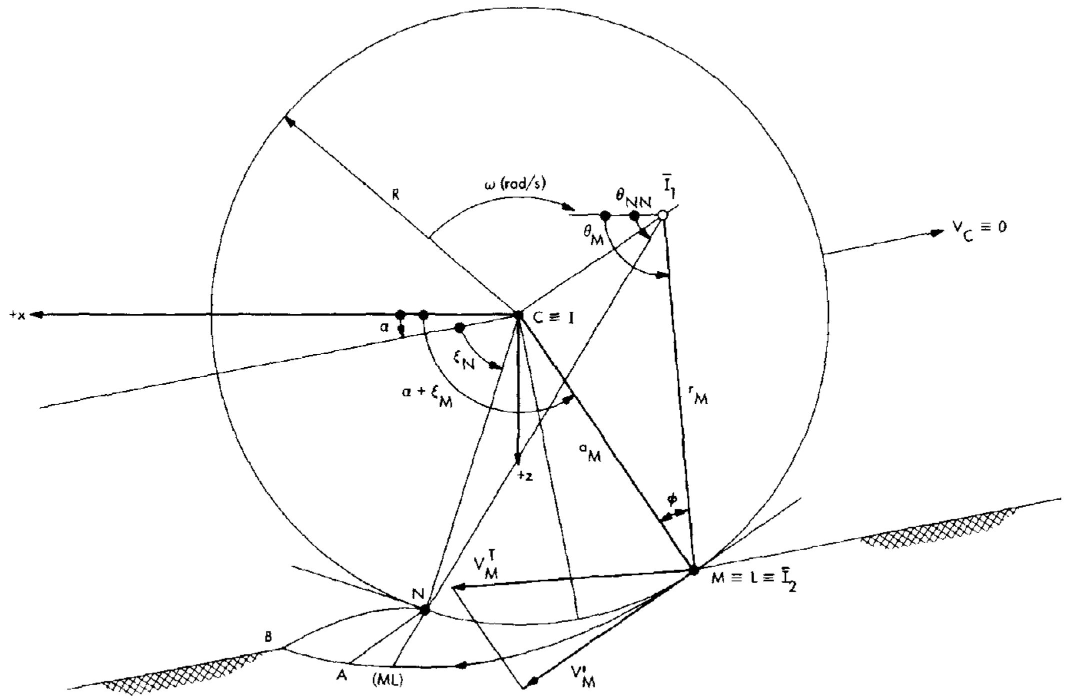

Fig. 7. Limit position of leading pole ($s_k = 0$)

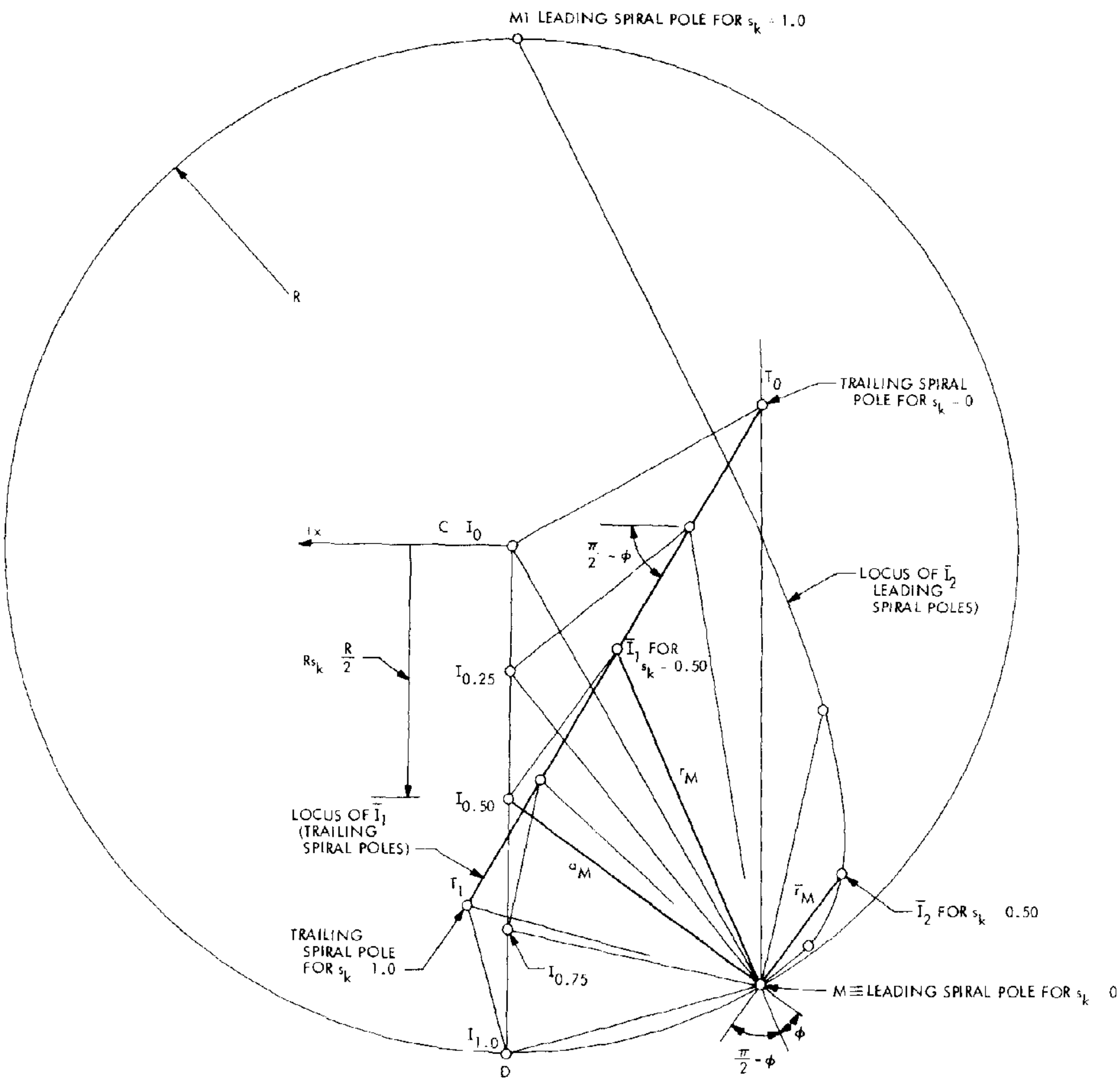

Fig. 8. Locus of leading and trailing spiral poles

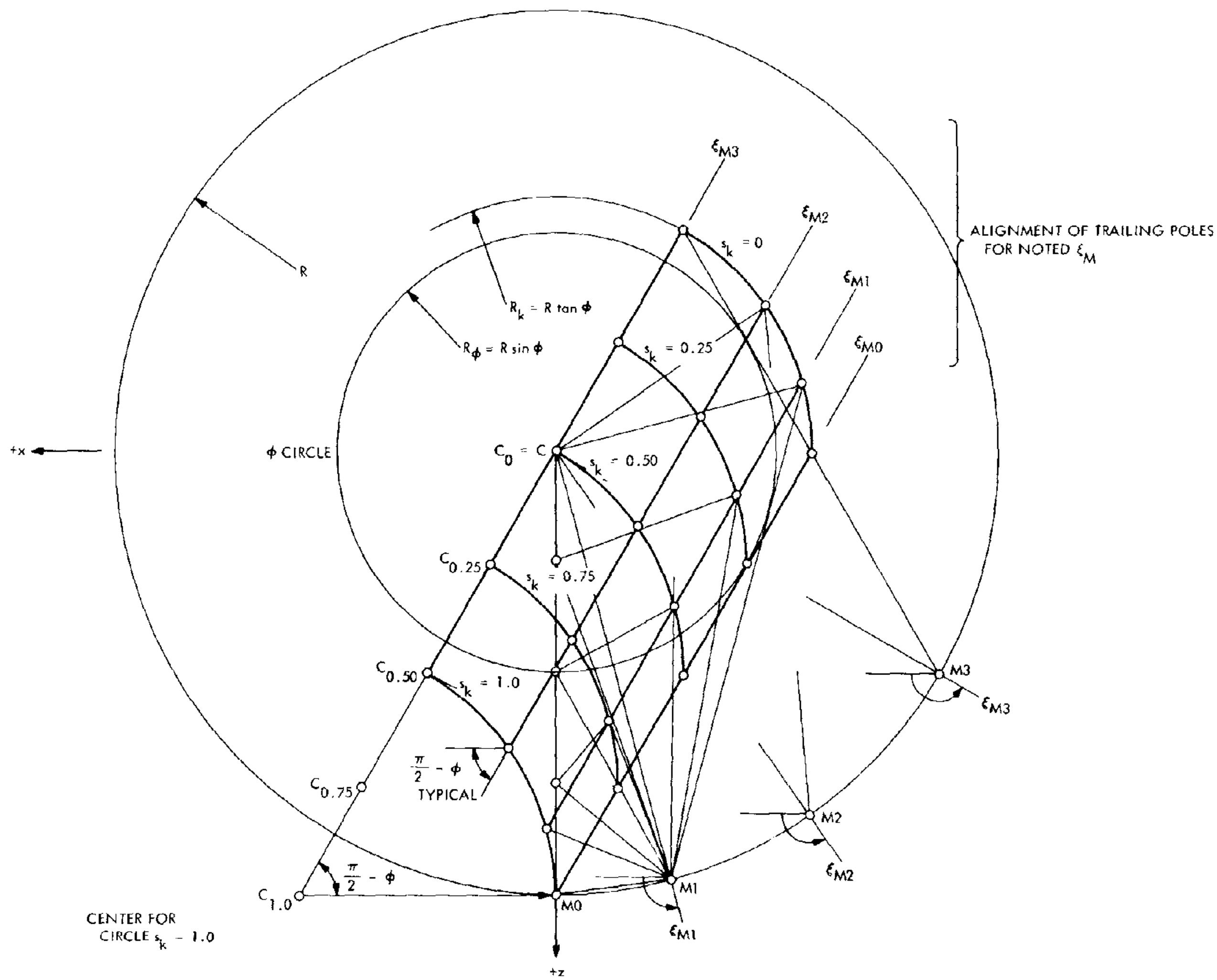

Fig. 9. Locus of trailing poles $\bar{I}_l$ for varying ξ_M and s_k

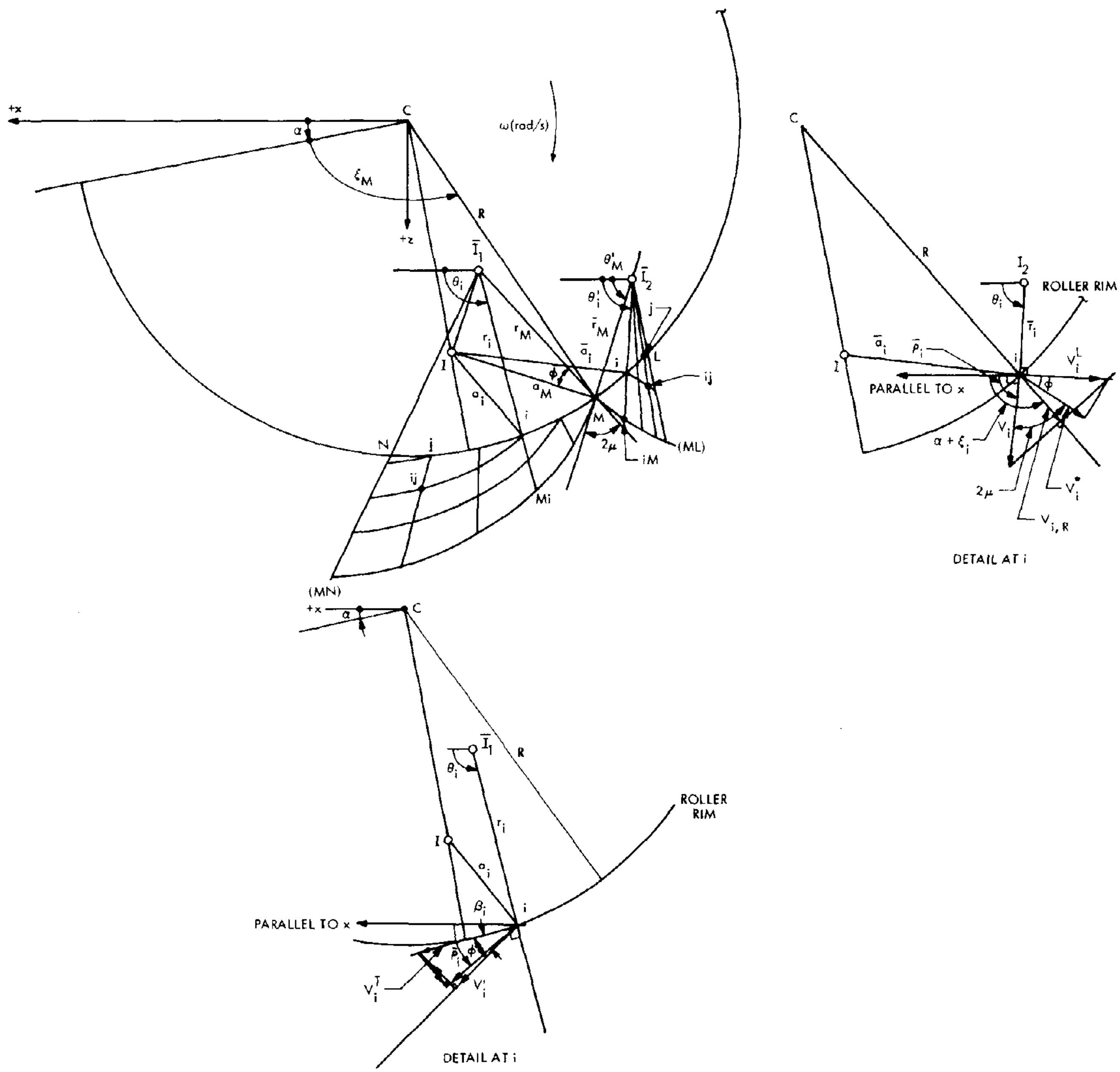

Fig. 10. Soil-roller interface velocities

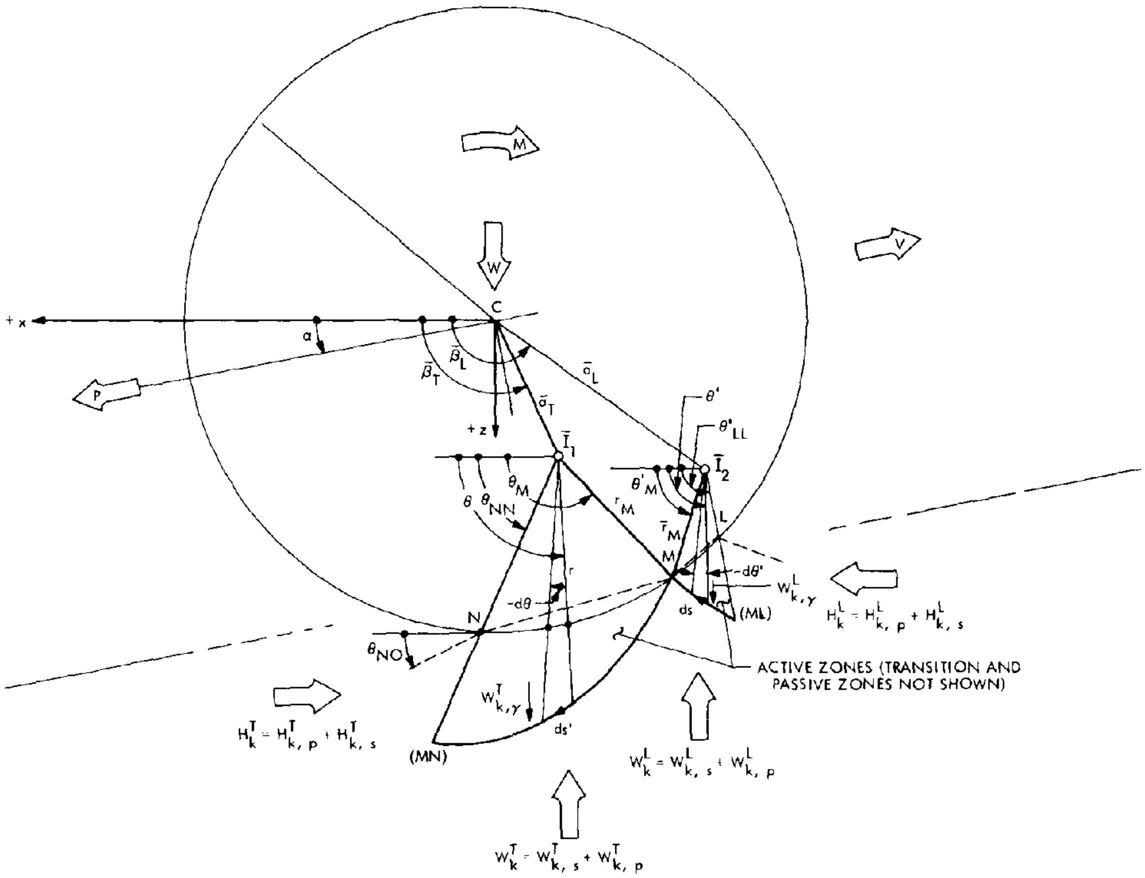

Fig. 11. Soil-roller free body equilibrium

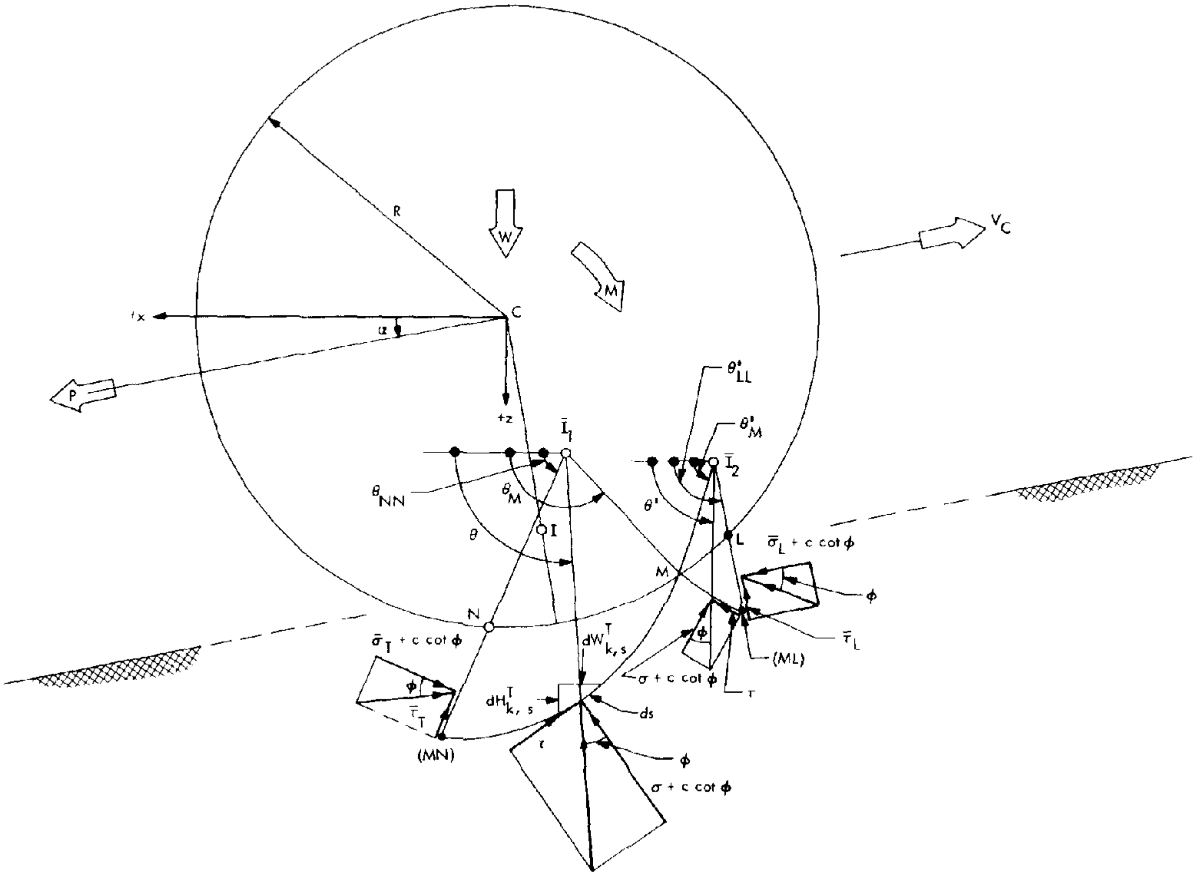

Fig. 12. Stresses along sliplines (active zones)

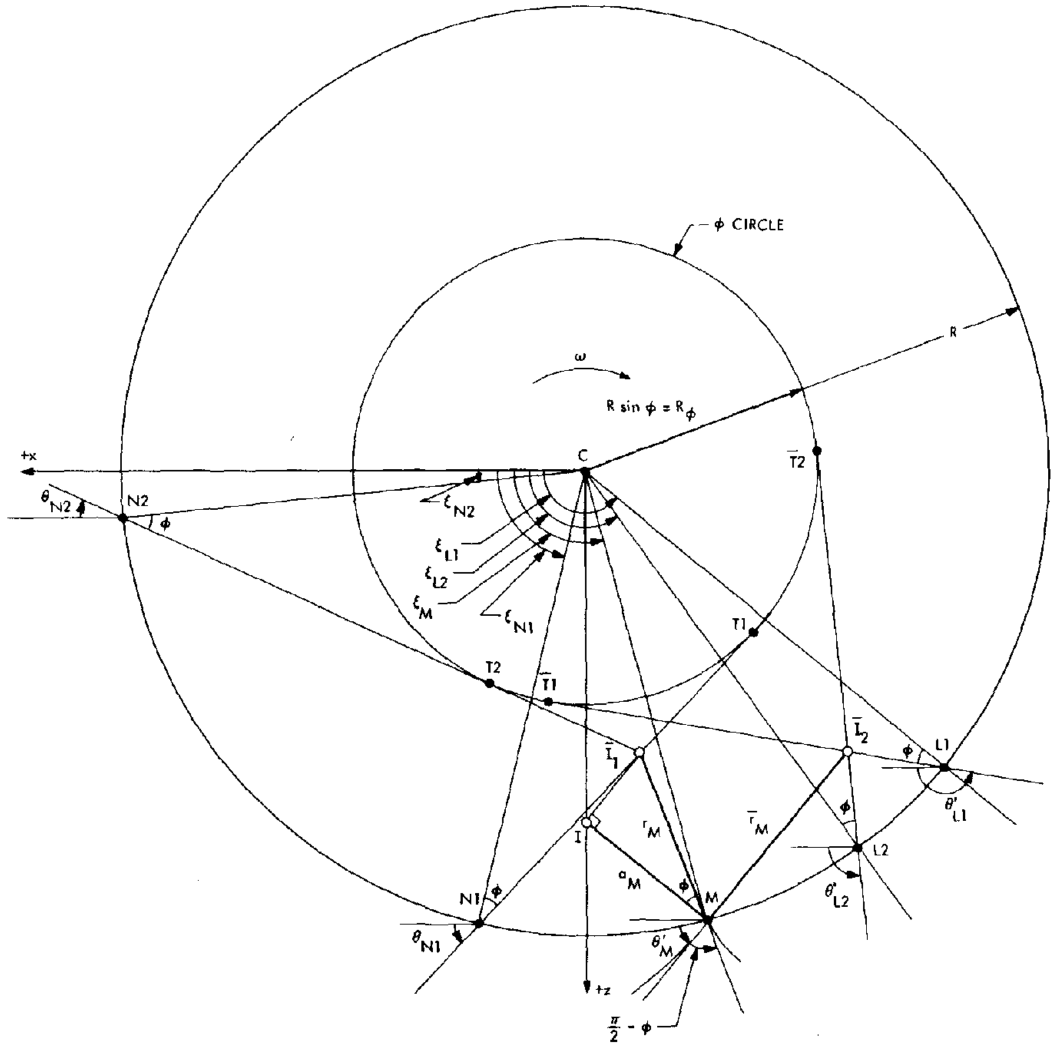

Fig. 13. Limiting slipline directions at leading and trailing zones

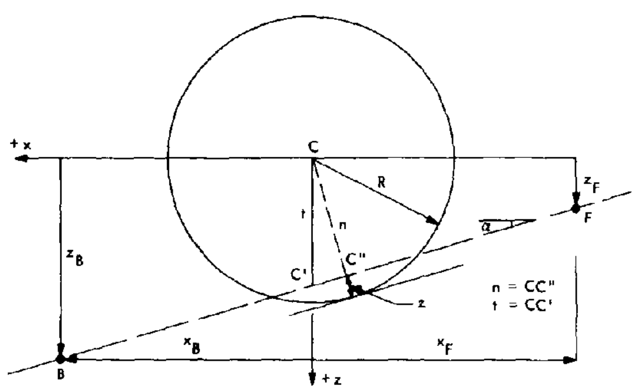

Fig. 14. Roller sinkage

NASA — JPL — Coml., L.A., Calif.